EVALUATION OF SURFACE PROPERTIES OF ROLLER COMPACTED PAVEMENTS USING 3D PHOTOGRAMMETRY METHOD

A THESIS SUBMITTED TO
THE GRADUATE SCHOOL OF NATURAL AND APPLIED SCIENCES
OF
MIDDLE EAST TECHNICAL UNIVERSITY

BY

EMİNE BİLGE TAN

IN PARTIAL FULFILLMENT OF THE REQUIREMENTS
FOR
THE DEGREE OF MASTER OF SCIENCE
IN
CIVIL ENGINEERING

APRIL 2023

Approval of the thesis:

EVALUATION OF SURFACE PROPERTIES OF ROLLER COMPACTED PAVEMENTS USING 3D PHOTOGRAMMETRY METHOD

submitted by **EMİNE BİLGE TAN** in partial fulfillment of the requirements for the degree of **Master of Science** i**n Civil Engineering, Middle East Technical University** by,

Prof. Dr. Halil Kalıpçılar
Dean, Graduate School of **Natural and Applied Sciences** _____

Prof. Dr. Erdem Canbay
Head of the Department, **Civil Engineering** _____

Prof. Dr. İsmail Özgür Yaman
Supervisor, **Civil Engineering, METU** _____

Assoc. Prof. Dr. Hande Işık Öztürk
Co-Supervisor, **Civil Engineering, METU** _____

Examining Committee Members:

Prof. Dr. Murat Güler
Civil Engineering, METU _____

Prof. Dr. İsmail Özgür Yaman
Civil Engineering, METU _____

Assoc. Prof. Dr. Hande Işık Öztürk
Civil Engineering, METU _____

Assoc. Prof. Dr. Çağla Meral Akgül
Civil Engineering, METU. _____

Prof. Dr. Mustafa Şahmaran
Civil Engineering., Hacettepe University _____

Date: 25.04.2023

I hereby declare that all information in this document has been obtained and presented in accordance with academic rules and ethical conduct. I also declare that, as required by these rules and conduct, I have fully cited and referenced all material and results that are not original to this work.

Name Last name : Emine Bilge Tan

Signature :

ABSTRACT

EVALUATION OF SURFACE PROPERTIES OF ROLLER COMPACTED CONCRETE PAVEMENTS USING 3D PHOTOGRAMMETRY METHOD

Tan, Emine Bilge
Master of Science, Civil Engineering
Supervisor : Prof. Dr. İsmail Özgür Yaman
Co-Supervisor: Assoc. Prof. Dr. Hande Işık Öztürk

April 2023, 156 pages

Owing to their cost-effectiveness and longevity, the popularity and the use of roller-compacted concrete (RCC) pavements have grown in Turkey both on urban and rural roads in recent years. Despite the vast amount of research on the mechanical and durability properties of RCC pavements, few studies have been conducted to examine the surface texture characterization, which impacts driving comfort, fuel economy, and safety. This study aims to investigate the effects of the RCC mixture proportions on the macro- and micro-texture characterization of RCC pavements. Therefore, RCC samples were prepared using various cement dosages, aggregate gradations, water contents, and compaction degrees. The British Pendulum Test and sand-patch test, two conventional indirect methods, were initially used to assess micro- and macro-texture properties. The surface characteristics of the RCC pavements were then measured using a novel 3D photogrammetry technique that was created and utilized for the first time. The most significant result of this study shows that both smaller and larger aggregate sizes, in combination with an ideal water content of 5%, significantly enhance the macrotexture and skid resistance in RCC pavements, offering crucial information for pavement designers. Strong correlations between the important texture parameters were observed in these ideal

mixtures, which also exhibited smoother surface textures and more uniform mixtures. The results of this study will help to improve RCC pavement mix designs, which will ultimately improve driving comfort and road safety.

Keywords: Roller-Compacted Concrete, Pavement Surface Properties, Mixture Parameters, British Pendulum Test, Sand-Patch Test, 3D Photogrammetry

ÖZ

SİLİNDİRLE SIKIŞTIRILMIŞ BETON YOLLARIN YÜZEY ÖZELLİKLERİNİN 3D FOTOGRAMETRİ YÖNTEMİ İLE DEĞERLENDİRİLMESİ

Tan, Emine Bilge
Yüksek Lisans, İnşaat Mühendisliği
Tez Yöneticisi: Prof. Dr. İsmail Özgür Yaman
Ortak Tez Yöneticisi: Doç. Dr. Hande Işık Öztürk

Nisan 2023, 156 sayfa

Son yıllarda, Türkiye'de şehir ve kırsal yollarda kullanılmak üzere dayanıklılığı ve maliyet etkinliği nedeniyle silindirle sıkıştırılmış beton (RCC) kaplamalar popülerlik kazanmıştır. RCC kaplamaların kullanımı artmasına rağmen, literatürde karışım parametreleri ve sürüş konforu ve güvenliği üzerinde etkili olan yüzey özellikleri arasındaki ilişkiyi araştıran çalışmalar eksiktir. Bu çalışmada, farklı çimento dozajları, agrega gradasyonları ve su oranları ile hazırlanan RCC numuneleri üzerinde çalışılmıştır. Mikro ve makro doku özellikleri öncelikle İngiliz pandülü testi ve kum-yama testi gibi geleneksel indirek yöntemlerle değerlendirilmiştir. Daha sonra, literatürde ilk kez kullanılan 3D fotogrametri yöntemi ile RCC kaplamalarının yüzey özellikleri ölçülmüştür. Son olarak, iki yöntem arasındaki ilişki kurulmuştur. Bu çalışmanın en önemli sonucu, hem daha küçük hem de daha büyük agrega boyutlarının, ideal bir su içeriği olan %5 ile birleştiğinde, RCC kaplamalarında makro doku ve kayma direncini önemli ölçüde artırdığını göstermektedir. Bu, kaplama tasarımcıları için kritik bilgiler sunmaktadır. Bu ideal karışımlarda önemli doku parametreleri arasında güçlü korelasyonlar gözlemlenmiştir ve aynı zamanda

daha düzgün yüzey dokuları ve daha homojen karışımlar sergilemiştir. Bu çalışmanın bulguları, RCC kaplama karışım tasarımlarının optimizasyonuna katkıda bulunarak yol güvenliği ve sürüş konforunu artırmaktadır.

Anahtar Kelimeler: Silindirle Sıkıştırılmış Beton, Kaplama Yüzey Özellikleri, Karışım Parametreleri, İngiliz Pandülü Testi, Kum-Yama Testi, 3D Fotogrametri

To my late grandmother, Emine Tan, and my late cousin, Tayyar Balkaya, who left us unexpectedly and too soon.

ACKNOWLEDGMENTS

My heartfelt appreciation goes to my supervisor, Prof. Dr. İsmail Özgür Yaman, for his invaluable guidance and support in this study. His expertise was crucial to its success. I also thank my co-supervisor, Assoc. Prof. Dr. Hande Işık Öztürk, for her valuable input and mentorship since 2016, enriching both my work and learning experience.

I would like to express my gratitude to the respected members of the examining committee, Prof. Dr. Murat Güler, Assoc. Prof. Dr. Çağla Meral Akgül, and Prof. Dr. Mustafa Şahmaran for their insightful observations and constructive criticisms.

The success of this study hinged on the invaluable support of key individuals. My deepest gratitude goes to Semiha Uhde Yıldırım for her unwavering assistance and heartfelt thanks to Ahmet Sağlam and Reza Shabani for their crucial contributions to the project.

Throughout this journey, my cherished friends Seher Dilek, S. Selin Aktaş, Gönç Berk Güneş, Asena Melisa Sarıcı, Gülçin Dalkıç Melek, Yakup Betüs, Müge Özgenoğlu, Başak Çakmak, Akın Batuhan Ünnü, Berkay Akçören, and Geran Özdeş Çelik have consistently provided me with inspiration, support, and camaraderie. I cannot express my gratitude to them for everything they have done for me. Their support and presence were priceless.

I sincerely thank my family, particularly my siblings Bahar Tan and Hasan Tuğtigin Tan, for their unwavering love and support. Gratitude also goes to my aunt, Prof. Dr. Türkan Akbayrak, whose guidance and mentorship have been crucial to my personal growth and success throughout this journey. To all my dear friends and family who never lost faith in me, your unwavering belief has been a source of strength and motivation throughout this journey. Thank you for your support.

TABLE OF CONTENTS

LIST OF TABLES

TABLES

LIST OF FIGURES

FIGURES

LIST OF ABBREVIATIONS

ABBREVIATIONS

AC	:	Asphalt concrete
ACF	:	Autocorrelation Function
ACPA	:	American Concrete Pavement Association
ANOVA	:	Analysis of Variance
ANSI/ASME	:	American National Standards Institute/American Society of Mechanical Engineers
ASCE	:	The American Society of Civil Engineers
ASCII	:	American Standard Code for Information Interchange
ASTM	:	American Society for Testing and Materials
BPN	:	British Pendulum Number
BPT	:	British Pendulum Tester
BrD	:	Brush Drag
CA	:	Coarse Aggregate
CRCP	:	Continuously Reinforced Concrete Pavements
DFT	:	Dynamic Friction Test
DSR	:	Drive Scene Recorder
EAC	:	Exposed Aggregate Concrete
FA	:	Fine Aggregate
FHWA	:	United States Federal Highway Administration
GB	:	Gigabyte
GDH	:	Turkish General Directorate of Highways
HMA	:	Hot Mix Asphalt
HS	:	Height of Sand
ICE	:	Institution of Civil Engineers Highway Design and Management Guide
IQR	:	The Interquartile Range

ISO	:	International Organization for Standardization
JCP	:	Joined Concrete Pavements
JPCP	:	Jointed Plain Concrete Pavements
JPEG	:	Joint Photographic Experts Group
JRCP	:	Jointed Reinforced Concrete Pavements
LSPL	:	Least-squares Plane
LT	:	Longitudinal Tining
MG	:	Megabyte
MPD	:	Mean Profile Dept
OD	:	Specific Gravity
OFT	:	Outflow Time
OGFC	:	Open-graded Friction Course
PCC	:	Portland Cement Concrete
PFT	:	Portable Friction Tester
PIARC	:	The Permanent International Association of Road Congresses
PLY	:	Polygon File Format
PNG	:	Portable Network Graphics
PV	:	Peak-to-valley Height
RCC	:	The Roller Compacted Concrete
RCCP	:	Roller Compacted Concrete Pavements
RMS	:	Root Mean Square
ROSAN	:	Laser-based Road Surface Analyzer
SFC	:	Side-way Force Coefficient
SGC	:	Superpave Gyratory Compaction
SRV	:	Skid Resistance Value
SSD	:	Specific Gravity
STL	:	Stereolithography
TT	:	Transverse Tining

LIST OF SYMBOLS

SYMBOLS

CD	:	Cement Dosage
DF	:	Degree of Freedom
D_{max}	:	Maximum Aggregate Size
F_A	:	Adhesion Coefficient
F_H	:	The Hysteresis Coefficient
GN	:	Gyration Number
MS	:	Mean Square
S_a	:	Arithmetical Mean Height
S_{al}	:	The Autocorrelation Length
S_{da}	:	Mean Dale Area
S_{dq}	:	Root Mean Square Gradient
S_{dr}	:	Developed Interfacial Area Ratio
S_{dv}	:	Mean Dale Volume
S_{ha}	:	Mean Hill Area
S_{hv}	:	Mean Hill Volume
S_{ku}	:	Kurtosis
S_{pc}	:	Arithmetic Mean Peak Curvature
S_{pd}	:	Peak Density
S_q	:	Root Mean Square Height
SS	:	Sum of Square
S_{sk}	:	Skewness
S_{tr}	:	Texture Aspect Ratio
S_{5p}	:	Five Point Peak Height
S_{5v}	:	Five Point Pit Height
S_{10z}	:	Ten-Point Height
$V_m(mr)$	:	Material Volume

$V_{mc}(p,q)$	:	Core Material Volume
$V_{mp}(p)$	:	Peak Material Volume
$V_{v}(mr)$	:	Void Volume
$V_{vv}(p)$	:	Dale Void Volume
$V_{vc}(p,q)$	:	Core Void Volume
W (%)	:	Water Content

CHAPTER 1

INTRODUCTION

Rigid pavements, also known as concrete pavements, are a type of pavement commonly used for roads, highways, and other high-traffic areas. They are made of concrete, a durable and long-lasting material that can withstand heavy loads and harsh weather conditions. Rigid pavements are typically constructed from a series of concrete slabs poured onto a compacted base course and subgrade. As roads continue to deteriorate, new methods have been developed to improve the application of rigid pavements. The various types of rigid pavements that have been developed over time include joined concrete pavements (JCP), continuously reinforced concrete pavements (CRCP), roller compacted concrete pavements (RCCP), concrete overlays, and precast concrete pavements.

Increasing traffic loads and the subsequent maintenance and repair costs of urban and rural roads have led to the search for more economical and durable alternatives to asphalt and surface coatings. One of these alternatives is the roller compacted concrete (RCC) pavement technology which is considered as a special type of rigid pavement. RCC pavements are similar to conventional concrete pavements in that they are also designed to withstand heavy loads and harsh weather conditions, but they are typically manufactured using a different paving process. Instead of being cast with special pavers, RCC pavements are typically constructed by the use of conventional asphalt equipment. When compared to conventional concrete pavements, a drier mix is paved by an asphalt paver and compacted with vibratory rollers. This paving process makes RCC pavements faster and less expensive to produce than conventional concrete pavements. RCC pavements are the preferred

choice in many countries, particularly in the United States, for industrial facilities, ports, and parking lots that are subject to heavy loads and travel at low speeds.

The main advantages of RCC pavements are their high strength and durability, as well as the possibility to produce them with conventional asphalt paving equipment. In addition, RCC pavements can be opened to traffic quickly due to their dry consistency compared to conventional concrete mixes. These characteristics of RCC pavements have made them an important alternative. However, as described in the literature, RCC pavements are not suitable for use on high-speed roads due to their surface texture and roughness. The effect of the mix design of RCCP on surface texture needs further research. In addition to the effects of the mix design, the measurement of surface texture is another topic that is heavily debated in the literature. Therefore, there is a need to investigate the surface texture characteristics of RCC pavements to improve their surface quality.

1.1 The motivation for the research

Pavement texturing refers to the surface characteristics of pavement, including its roughness, texture, and skid resistance. Pavement texturing is important because it affects the ride quality of pavement and can have a significant impact on safety. Smooth pavements may be more comfortable to drive on, but they may also be more prone to accidents due to skidding or slipping. On the other hand, rough or textured pavements may be less comfortable to drive on, but they may also provide better traction and be less prone to accidents. Therefore, it is important to consider pavement texturing when designing and constructing pavements to ensure that they are safe and comfortable for drivers.

The measurement of surface texture for rigid pavements has evolved as technology and understanding of pavement surfaces have advanced. One of the earliest methods of surface texture measurement was the sand patch test, which was developed in the 1940s. This method involves applying a uniform layer of sand to a pavement surface

and measuring the amount of sand retained after it has been subjected to a known load. The sand patch test was widely used for many years, but it had several limitations, including the fact that it was time-consuming and required the use of a large amount of sand. In the 1960s, the British Pendulum Tester (BPT) was developed as a more efficient and accurate method for measuring surface texture. The BPT uses a pendulum to apply a known load to a pavement surface and measures the friction between the pavement and a rubber slider. The BPT was widely adopted and is still in use today. In the 1980s, the Portable Friction Tester (PFT) was developed as a further improvement on the BPT. The PFT uses a similar principle to the BPT, but it is more portable and easier to use. The PFT has become one of the most widely used methods for measuring surface texture in the field.

More recently, there has been a push towards developing contactless methods for measuring surface texture, such as laser-based systems that can measure the reflection of the pavement surface. While these methods show promise, they are still in the early stages of development and have not yet been widely adopted.

1.2 Objective of the study

The objective of this study is to investigate the effects of the mixture proportions of concrete on the macro- and micro-texture characterization of RCCP using photogrammetry techniques. For this purpose, 12 different RCC mixes with two different cement dosages (200 and 400 kg/m3), two different maximum aggregate grain sizes (12 and 19 mm), and three different water contents (4%, 5%, and 6%) were cast. Using these mixtures, specimens were prepared using the Superpave Gyratory Compaction (SGC) method with three different gyration numbers (50, 60, and 75). In this study, a novel 3D photogrammetry method was developed to evaluate the surface properties of these specimens. In addition, the proposed method was validated using standardized experimental data. The British pendulum test (BPT) for evaluating the friction and microtexture properties of the prepared specimens and the

sand patch test for evaluating the macrotexture were preferred because they are the most commonly used methods available in the literature.

1.3 Outline of the thesis

This thesis includes six chapters: The Introduction, Literature Review, Materials and Methods, Results and Discussion, and Conclusion. In the Introduction, the background and significance of the research topic, research objectives, thesis outline, and organization are discussed. The Literature Review consists of an overview of the existing research on the topic, identical to the gaps in current knowledge. Additionally, a theoretical framework and its evolution are presented. In the Materials and Methods section, a description of the research design and methodology is presented. Details of the materials and equipment used, data collection, and analysis procedures are described in this chapter. The Discussion and Results section presents data and findings. It also includes a comparison of the results within the study and literature review. Finally, in the Conclusion chapter, a summary of the main findings, limitations, future directions of the study, and suggestions for future research are provided.

CHAPTER 2

LITERATURE REVIEW

Road surfaces need constant repair and replacement due to wear and tear. Under the influence of traffic and the weight of heavy vehicles, pavement deteriorates. In addition, environmental factors such as temperature, sunlight, and water penetrating pavement layers cause pavements to deteriorate over time. The proactive, preventive maintenance strategy known as "pavement preservation" should be employed to manage the gradual and progressive deterioration of pavements. A pavement preservation strategy reduces the cost of maintaining the road network over the life of a facility by minimizing the need for more expensive and disruptive road resurfacing work, resulting in longer, smoother pavements and adequately addressing traffic safety.

The extent of cracking on the road surface is an indicator of the durability of the road surface. Pavement is critical to providing both a safe roadway for traffic and a waterproof layer to protect the underlying pavement from moisture, which can significantly weaken and shorten the life of the road. To ensure safe roads, national regulations specify design criteria, such as minimum curve radii or grades and minimum sight distances. However, braking distance and speed on curves, which are directly related to surface parameters, are critical for road users. Texturing is a critical phase in the production of PCC. To achieve the desired appearance and friction, the surface must be finished, textured, and tined after the PCC is applied and consolidated. Texturing and tinning increase friction and skid resistance, as the surface would be too smooth for traffic without additional work. This work is done while the concrete is still sufficiently workable to add texture to the surface.

Pavement surface characteristics affect several aspects of a road's operation, including safety, comfort, travel times, operating costs, noise, and the dynamics of moving vehicles. The quality of pavement construction, materials used, wear caused by vehicles, and deterioration caused by environmental variables, among other factors, affect the life of the pavement. Thus, there are various standardized experimental methods and novel 2D and 3D techniques to characterize the surface characteristics of the pavements.

The literature review chapter of this thesis is divided into three subsections which mainly focus on the pavement surface properties, RCC pavement surface performance, and surface texture measurement methods.

2.1 Rigid Pavements

Since the construction of the first concrete pavement in 1865, it has been widely utilized to pave highways and airports, as well as business and residential streets, in line with the requirements for durability and sustainability (First Concrete Pavement ASCE). As roads deteriorate, new methods have been developed to enhance their application. As pavement design has improved, conventionally reinforced PCC pavements have been introduced. There are several types of conventionally reinforced PCC pavements, including continuously reinforced concrete pavements (CRCP), jointed plain concrete pavements (JPCP), jointed reinforced concrete pavements (JRCP), and full-depth concrete pavements. Some of these pavements have contraction joints with dowels and steel reinforcements.

Pavement surface characteristics have a significant effect on durability and sustainability. It is anticipated of pavements to be safe, quiet, and smooth. Therefore, several studies have examined pavement surface characteristics considering different aspects, such as their relation to the mixture design or how to predict wear considering climatic effects.

In addition to the traditional methods of concrete pavement construction mentioned above, several alternative paving technologies have been developed that challenge conventional methods while providing specific design options. These options were described by Van Dam et al. (2011) in a guide entitled "Sustainable Concrete Pavements: A Manual of Practice". One of these is roller-compacted concrete (RCC). The stiff concrete mixtures used for RCC pavements are laid and compacted using tools typically used for hot mix asphalt (HMA) construction. RCC is beginning to be used on roads and local roadways, where it has traditionally been used in hydraulic engineering, industrial facilities, and cargo handling zones.

2.1.1 Importance of Surface Properties for Safety and Durability of Rigid Pavements

Concrete pavements are commonly used in modern infrastructure projects owing to their durability and long-term performance. However, the surface properties of concrete pavements play a crucial role in ensuring their safety and long-term durability. In this section, some of the latest studies on the safety and durability of concrete pavement surfaces are reviewed.

Santero et al. (2011) conducted a study on the sustainability of concrete pavements and suggested that organizations seeking to increase vehicle fuel efficiency should minimize rolling resistance, which is the energy loss associated with the pavement-vehicle interaction. Pavement irregularities are a significant cause of rolling resistance, as they activate vehicle suspension systems, consume energy, and lead to a significant increase in fuel consumption. Therefore, it is critical to ensure that concrete pavements have a good surface texture, slip resistance, and long-term friction performance to minimize rolling resistance and increase sustainability. In addition to sustainability, durability is an essential aspect of concrete pavement surface properties. A good surface texture, slip resistance, and long-term friction performance are crucial for ensuring durability, as they enhance the overall performance of concrete pavements. In another study, an optimization method for all

surface textures was recommended by Chen et al. (2013) in combination with the Fujikawa-Koike tire/pavement contact model for the design and construction of particularly slip-resistant and noise-absorbing permeable concrete pavements. The focus of this research also included the analysis of the abrasion process and attenuating the weakening of surface textures on concrete pavement slabs using an accelerated abrasion test. The results demonstrate that the surface textures of permeable concrete pavement slabs are exceptionally durable compared to typical grooved or exposed concrete pavements.

Ahammed and Tighe (2008) analyzed 197 concrete pavement sections from a Long-Term Pavement Performance (LTPP) database for their long-term friction performance. The analysis found that the surface friction of concrete pavements was less responsive to ambient temperatures and consistently maintained a higher level of skid resistance with a tinned or grooved texture. Compared to cumulative axle weights, cumulative traffic passes are more sensitive to friction longevity. Five other models were successfully constructed to forecast the long-term skid resistance of concrete pavements as a function of texture type, cumulative traffic passes, speed, and compressive strength of concrete. With reasonable prediction accuracy, these models were statistically significant at the 95% confidence level.

Last but not least, safety is also amongst the most important aspects of concrete pavements as well as sustainability and durability. The top priority of any transportation agency should be to improve safe infrastructure for the community and its users. For the safety of drivers and pedestrians, the pavement surface must, among other things, provide adequate surface friction while reducing splash and spray, be free of potentially hazardous distresses (such as potholes, faulting, and blowups), and provide better visibility at night-time and in inclement weather (Van Dam and Taylor, 2009). Having said that; there are many studies in the field of safety as well as talking about sustainability, durability, and even noise and driving comfort at the same time. Therefore, there are various studies on the enhanced surface properties of rigid pavements, thus some of which are summarized as follows.

Yu et al. (2021) studied the groove parameters to optimize these parameters considering driving stability and skid-resistance performance into account. According to the results, groove depth had the greatest influence on texture depth. In contrast, groove spacing had the greatest influence on stress concentration coefficient and steady-state steering resistance torque. In addition, maximizing the width of the groove group can balance the driving stability and the durability of the skid resistance.

As mentioned earlier, one of the most important elements affecting road safety, especially in skidding accidents in wet weather, is the skid resistance of the pavement surface. Countermeasures are required to improve the skid resistance of concrete pavements in tunnels. Guo et al. (2009) investigated porous concrete surfaces and open-graded friction course (OGFC) surfaces as potential pavement surfaces that could provide durable skid resistance. Porous concrete was applied directly to the normal concrete pavement to provide adequate skid resistance. The skid resistance of the porous concrete was tested using an accelerated abrasion equipment. According to the results, porous concrete has a higher content of coarse aggregate, which results in long-lasting skid resistance.

On the matter of noise and driving comfort: Wei et al. (2018) investigated the surface texture, including roughness, macrotexture, and microtexture, in various pavements to fully analyze the relationship between the texture characteristics of the concrete pavement and the tire/pavement noise of grooved concrete pavements. The results show that tire and pavement noise are significantly affected by pavement roughness, while noise levels on flat pavements are insufficient. Tire/pavement noise was also significantly affected by macrotexture depth. However, there is no direct relationship between the side-way force coefficient (SFC) and tire/pavement noise. Another factor that could contribute to high tire/pavement noise levels is concrete pavements with deep grooves.

Another example is that Kuemmel et al. (2000) studied 57 different PCC pavement textures, including different transverse and longitudinal tining patterns. Explaining

noise differences within and between different textures as well as documenting noise and texture differences were some of the objectives of their study. Surface texture measurements were made using a laser-based road surface analyzer (ROSAN) developed in collaboration between the Turner Fairbanks Research Center and private industry. Different PCC pavement sections constructed using the same tining standards showed significant differences in surface texture, including tine spacing, width, and depth. Significant variation was found within a test section in all states. The relationship between noise and texture depth estimated by ROSAN was found to be low. Using the ROSAN results, a stronger correlation was detected between the depth and width of tining.

The durability also varies depending on the different types of texturing method. As the last example, Gierasimiuk et al. (2021) compared the skid resistance of textured concrete pavements using different approaches to simulate conditions encountered on actual roads. Five different concrete pavement texturing techniques-burlap drag (BuD), brush drag (BrD), transverse tining (TT), longitudinal tining (LT), and exposed aggregate concrete (EAC)-were tested. Before and during the simulation of abrasion (1st phase of the test) and polishing (2nd phase of the test) of the specimens with a slab polisher, the changes in skid resistance were measured using a British pendulum tester and a circular texture meter. The EAC pavement would be a durable solution, which was confirmed by the high value of the MPD coefficient after the test and the correct values of the coefficient of friction, as the skid resistance on high-speed roads is guaranteed throughout the service life.

As roads deteriorate, new methods have been developed to enhance the applications of PCC pavements. Concrete pavement surface characteristics have a significant effect on durability and sustainability. Some pavements have contraction joints with dowels and steel reinforcements. It is anticipated that pavements will be safe, quiet, and smooth in the future.

2.2 Roller Compacted Concrete

Roller-compacted concrete (RCC) is a viable and fast construction alternative for many pavement applications. Using vibratory rollers or plate compaction machinery, roller-compacted concrete (RCC) is a zero-slump mixture of aggregates, cementitious materials, water, and admixtures. The mixture is placed by a paver using the same easily accessible tools used for asphalt pavement construction and compacted by a roller. Compared to conventional Portland cement pavements, RCC pavements feature faster construction time, better load-bearing capacity, resistance to freeze-thaw cycles, durability, lower initial cost, less maintenance, and longer service life. In addition, RCC pavements can be constructed with little impact on the running traffic.

Because of their relatively coarse surface, compared to other rigid pavements, RCC pavements have typically been used for pavements carrying heavy loads in low-speed regions. Because RCC uses similar aggregate gradations and employs similar placing techniques as asphalt concrete (AC), the typical surface texture is more open than conventional concrete and resembles the open texture of asphalt (Harrington et al., 2010).

According to Zollinger (2016), RCC surfaces may experience some loss of fine aggregate during the initial years of service. However, this loss can be minimized through diamond grinding after construction. Diamond grinding is a common method used to improve surface texture and smoothness, resulting in roads with desirable frictional properties. The surface texture of RCC can be influenced by various factors such as different methods, mixtures, mix designs, and applications, as noted in various studies (Adresi & Lacidogna, 2021; Harrington et al., 2010). By considering these factors and implementing diamond grinding, the loss of fine aggregate can be minimized, and the overall durability and performance of RCC surfaces can be improved.

2.2.1 Studies and Problems on RCC Pavement Surfaces

RCC Pavements (RCCP) have significant differences from traditional rigid pavements. A cost-efficient and long-lasting pavement technique, RCCP is being employed more frequently in various transportation applications. Yet, RCCP's usage as a final surface has been constrained by its rough and uneven surface characteristics. In this regard, many studies have been conducted to enhance the durability and skid resistance of RCCP surface properties. Thus, this section briefly discusses the surface properties of RCCP.

Aghaeipor and Madhkhan (2020) reviewed the literature on the mechanics, mechanical characteristics, and qualities affecting the durability and surface properties of RCCP, as well as its history, benefits, and drawbacks... Surface quality following construction is one of the drawbacks of RCCP. A rough and uneven surface characterizes the RCCP. The size and type of aggregates used to produce the surface texture of concrete play a significant role. The finished surface will have a better and more consistent texture regardless of the size of the largest aggregate applied. On the other hand, the lack of a macrotexture on RCCP which is nearly smooth due to roller vibration during construction, prevents it from being used as the final surface. Therefore, Adresi and Lacidogna (2021) attempted to improve the RCCP by presenting various scenarios to generate new surfaces with micro/macro texture and investigating their durability and skid resistance under traffic abrasion. The results showed that the abrasion resistance of the samples was significantly affected by changes in mix design and skid resistance, resulting in significant changes in macrotexture. For the RCCP specimens, various macrotextures had acceptable skid resistance. Stamping had the highest mean texture depth (MTD) and BPN while seeding had the lowest.

Sufficient skid resistance is necessary to ensure a secure and non-slip pavement surface. Chhorn et al. (2017) investigated the performance of a roller-compacted concrete pavement (RCCP) using five RCCP paved sections in Seokcho, South Korea. For sections with maximum aggregate sizes of 13 and 19 mm, the relationship

between the Vebe time and BPN of RCCP was also investigated in this study. The results of the investigation showed that the skid resistance of RCCP tends to increase as the stiffness of the RCC mix increases. In dry mixes, the mortar is not enough to cover the surface completely, so the aggregate is exposed after compaction, resulting in high skid resistance. In a wet mix, on the other hand, sufficient mortar can cover and fill the space between the aggregates at the surface, resulting in a slippery and low-friction surface. However, skid resistance decreases if the mix becomes too stiff.

Overall, the subject of the importance of mix design and application to surface texture was addressed by Topličić-Ćurčić et al. (2015) as it studied the properties, materials, and durability of roller-compacted concrete pavements. Smoothness was mentioned as a characteristic of RCC. Compared to conventional PCC pavements, RCC pavements are not as smooth. If the smoothness of the pavement is particularly important in an RCC project, some measures should be considered. Countermeasures that can be taken to improve the final result include using a maximum aggregate size of no more than 13 mm, avoiding construction of the pavement in layers thicker than 200 mm (after compaction), using a high-density paver with string-line grade control, and being able to achieve compaction without excessive rolling.

2.3 Surface Properties

According to the United States Federal Highway Administration (FHWA), the smoothness of a pavement surface is a measure of how comfortable it is for travelers. Smoothness and roughness are terms that indicate how far a surface is from a true planar surface, and both are significant indicators of pavement performance (as defined by ASTM E867). The term "pavement roughness" refers to irregularities in the pavement surface that adversely affect a vehicle's ride quality, traffic safety, fuel consumption, vehicle maintenance expenses, and noise pollution.

The Permanent International Association of Road Congresses (PIARC) published a technical study in 1978 that served as the first source for classifying surface

irregularities in terms of their wavelengths (De Los Santos and Gasca, 1978). The length scales (spatial wavelengths) used by PIARC to classify road surface roughness are as follows:

- Microtexture: 0 mm – 0.5 mm
- Macrotexture: 0.5 mm – 50 mm
- Mega texture: 50 mm – 0.5 m
- Unevenness: 0.5 m – 50 m

The different pavement texture groups based on covering wavelength are depicted in Figure 2.1, along with related phenomena and surface characteristics.

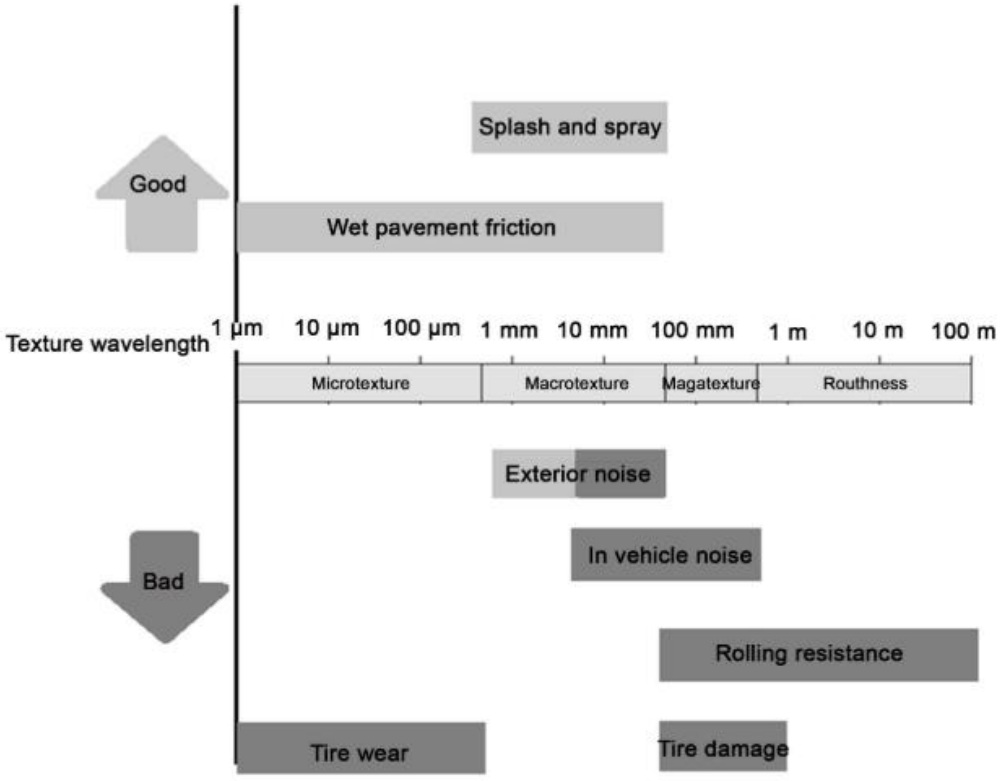

Figure 2.1 Surface characteristics and pavement wavelength (Mataei et al., 2016)

2.3.1 Microtexture

The amplitude of deviations with wavelengths smaller than or equal to 0.5 mm is known as microtexture. This texture scale, assessed on the micron scale, is usually observed on the surfaces of coarse aggregate particles (Figure 2.2), as well as on the texture of fine material and mortar used as a binder (Snyder, 2019).

Dondi et al. (2010) mentioned that since microtexture is frequently observed on aggregate surfaces, it is a result of the mineralogy and petrology of aggregate particles and is influenced by traffic and weather/climatic factors. It is believed that the microtexture of the road influences skid resistance at all speeds in both dry and wet situations. Direct tire-pavement contact is made possible by microtexture, which also helps with the adhesion factor of friction.

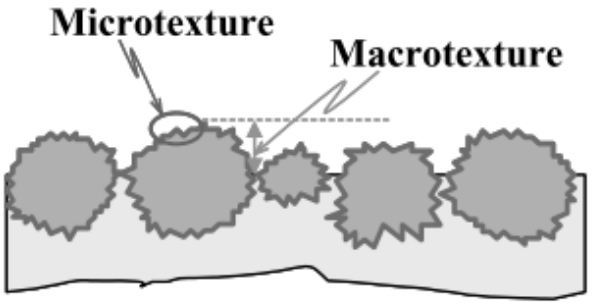

Figure 2.2 Micro and macrotexture (Flintsch et al., 2003)

The majority of the frictional force between pavement surfaces is produced by microtexture. It is frequently determined indirectly using friction, or so-called "skid resistance."

2.3.2 Macrotexture

The size, shape, spacing, and arrangement of the coarse aggregate particles affect macrotexture, which is the amplitude of deviations with wavelengths ranging from 0.5 mm to 50 mm (Figure 2.2). Tire noise and water drainage from the tire footprint are the two main effects of macrotexture. Hysteretic friction is hypothesized to be influenced by this textural scale, especially at high speeds. The hysteresis component of friction is provided by pavement macrotexture, which also enables rapid water drainage from the pavement. Better tire-pavement contact lowers the risk of hydroplaning and is enabled by enhanced drainage (Snyder, 2019).

2.3.3 Unevenness and Mega texture

Longitudinal profiles larger than the tire footprint are linked to the unevenness of the road surface, which has wavelengths ranging from 0.5 m to 50 m. Vehicle dynamics, ride quality, dynamic loads, and drainage are all affected by it. Unevenness is typically caused by either poor initial construction or deformation brought on by loads, and in severe circumstances, it can result in loss of contact with the surface (Snyder, 2019).

Megatexture on the road are deviations with wavelengths ranging from 50 to 500 mm. Ruts, potholes, large joints, and cracks are a few examples of megatexture. It is therefore closely related to noise and rolling resistance since it influences tire wall vibration but not vehicle suspension. Megatexture may have an impact on tire/road contact even though its sizes are often larger than those that effect skid resistance (Snyder, 2019). A comparison of different surface textures mentioned before is shown in Figure 2.3.

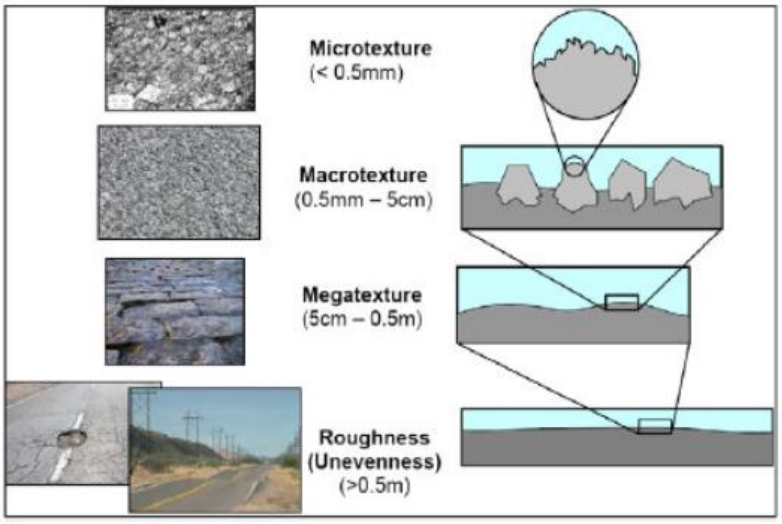

Figure 2.3 Comparison of different surface textures (Aavik et al., 2013)

2.3.4 Road-Tire Friction

The measurement and relationship of road friction to the risks of traffic accidents is a challenge. Thus, the lowest permitted road friction is defined by established threshold values for road friction in many different countries. The probability of accidents may increase if the friction level is below this value. These cutoff points are the outcome of studies investigating the connection between friction on the road and accident risks.

The different friction methods in use and quantitative relationships between road friction and accident risk were discussed in detail by Wallman and Åström (2001). Moreover, a summary of factors affecting road-surface friction is given in Table 2.1. Microtexture, macrotexture, the characteristics of the pavement material, and slip speed are among the variables that are considered to be under the control of transportation agencies.

Table 2.1 Factors affecting tire-road friction (Mataei et al., 2016)

Pavement Surface Characteristics	Vehicle Operating Parameters	Tire Properties	Environment
• Microtexture • Macrotexture • Megatexture • Unevenness • Material properties • Temperature	• Slip speed -Vehicle speed -Braking action • Driving maneuver -Turning -Overtaking	• Foot Print • Tread design and condition • Rubber composition and hardness • Inflation pressure • Load • Temperature	• Climate -Wind -Temperature -Water (rainfall, condensation) -Snow and Ice • Contaminants -Anti-skid material (salt, sand) -Dirt, mud, debris

The resistance that an object meets when moving over another object is known as friction. Tire-pavement friction, as used in the context of pavement surfaces, refers to the grip that a tire develops with a road surface at a specific moment. Tire-pavement friction enables absolute control during acceleration, cornering, and deceleration. It depends on two factors, adhesion, and hysteresis. The hysteresis coefficient (F_H) is a function of the energy losses within the tire/rubber as it is deformed by the textured pavement surface, whereas the adhesion coefficient (F_A) is a function of the shear forces produced at the tire-pavement interface (Figure 2.4).

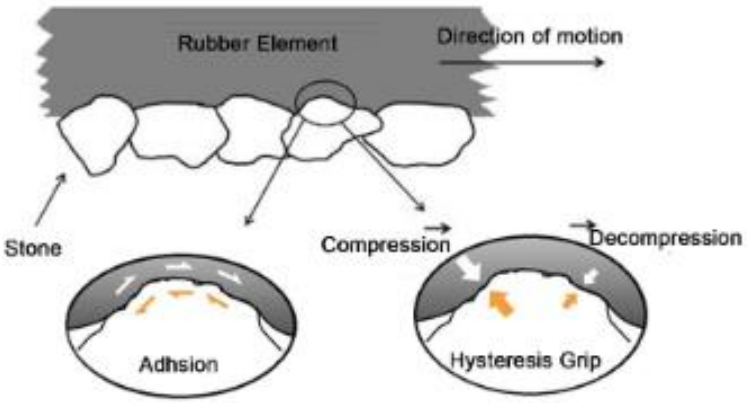

Figure 2.4 Plot of adhesion (F_A) and hysteresis (F_H) (Mataei et al., 2016)

When shear strength and actual contact area are high, there is a high adhesion coefficient; however, when the pavement is wet, a trapped water film weakens the interface shear strength and reduces adhesion. For hysteresis to work, the tire must be compressed against the pavement surface. This causes deformation energy to be stored inside the rubber, and as the tire relaxes, some of the energy is dissipated as

heat. Adhesion is especially sensitive to the micro-level asperities (microtexture) of the aggregate particles present in the pavement surface due to the generation of an adhesion force at the pavement-tire interface. In contrast, the hysteresis force created within the tire is particularly sensitive to the macrolevel asperities (macro-texture) developed in the surface by mix design and/or construction methods. This phenomenon causes the overall friction on smooth-textured and dry pavements to be governed by adhesion at lower speeds. The overall friction on wet, rough-textured pavements are governed by hysteresis at higher speeds (Mataei et al., 2016).

2.3.5 Skid Resistance

The force generated when a tire slides on a pavement surface due to resistance to the rotation is known as skid resistance. There are several test procedures and devices available to measure pavement texture characteristics. Every single one of them has specific attributes, and it's important to understand that they all measure slightly different parameters, making it impossible to directly compare the findings. However, there are various ways to compare these measurement tests, which will be discussed later in this chapter.

2.4 Laboratory Experiments

Several laboratory techniques can be used to measure the surface texture of a pavement. Some common methods include:

- British Pendulum Tester (BPT)
- Sand Patch Test
- Dynamic Friction Test
- Outflow Test
- Profilometer (with and without contact)

2.4.1 British Pendulum Tester (BPT)

The instrument used to measure the skid resistance of a pavement surface is the British Pendulum Tester (BPT). It consists of a pendulum arm with a weight at one end and a rubber slider at the other. In Figure 2.5a and Figure 2.5b, British Pendulum Tester is shown in detail. The pendulum is released from a fixed height while the slider is positioned on the pavement (Figure 2.5c). The deflection of the pendulum arm is used to quantify the force required to cause the slider to skid, and the results are reported as the Skid Resistance Value (SRV).

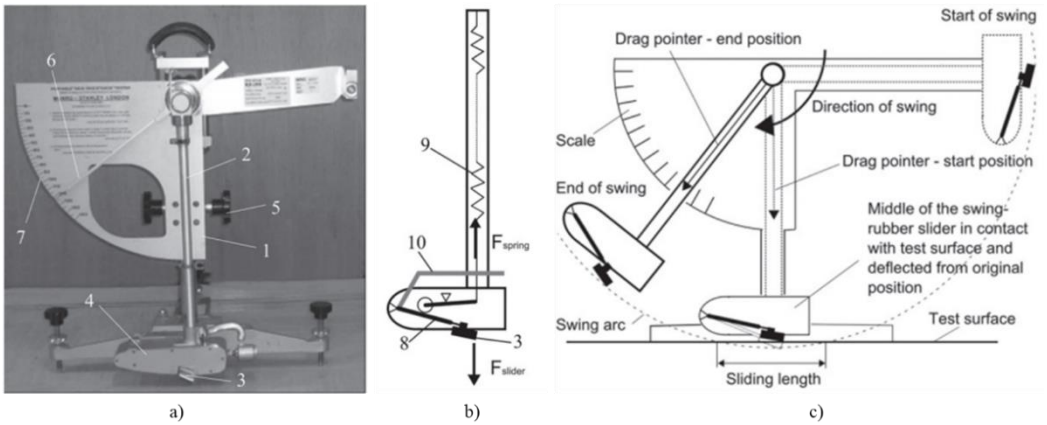

Figure 2.5 (a) Portable skid resistance tester with the pendulum frame (1), pendulum arm (2), rubber slider (3) in the pendulum head (4), knob for height adjustment (5), drag pointer (6) and scale (7). (b) Pendulum arm schematics with rubber slider (3), lever mechanism (8), spring (9), and lifting handle (10). (c) Phases of the swing from the start of the swing, through sliding, to the end of the swing (Hiti and Ducman, 2014)

Because of its ease of use and low cost, BPT is often used to evaluate the skid resistance of pavement surfaces. Owing to its ability to mimic the circumstances that can cause sliding, it is particularly useful for testing wet or slippery surfaces. The SRV can be used to assess whether a surface satisfies the safety requirements or to compare the skid resistance of different pavement surfaces.

Several standards provide guidance on the use of the BPT for skid resistance measurement and can be used to help ensure that the results are accurate and comparable to other test results. Some of these standards are given below:

- EN 13036-4: Skid resistance and friction - Part 4: Pavement type testing devices - Requirements and test methods for the British Pendulum Tester (BPT)
- ASTM E303: Standard Test Method for Measuring Surface Frictional Properties Using the British Pendulum Tester

Although BPT is widely used, it is prone to human error. Hiti and Ducman (2014) discussed the calibration process for BPT, which involved the calibration of the instrument on a reference surface with a specified skid resistance value. They also used a modified calibration method using a reference surface with a known coefficient of friction - a measurement of the resistance to slipping between two surfaces in contact. The accuracy and repeatability of the two calibration techniques were compared and evaluated. It was found that the improved calibration process provided more precise and consistent results.

2.4.2 Sand Patch Test

The most popular volumetric approach to measuring macrotexture is the sand patch method (ASTM E965 and ISO 10844). The apparatus for the sand patch test is given in Figure 2.6. The volumetric mean texture depth (MTD) of pavement macrotexture is determined by forming a circle on the pavement surface with a known volume of spherical sand particles and measuring the diameter of the spread.

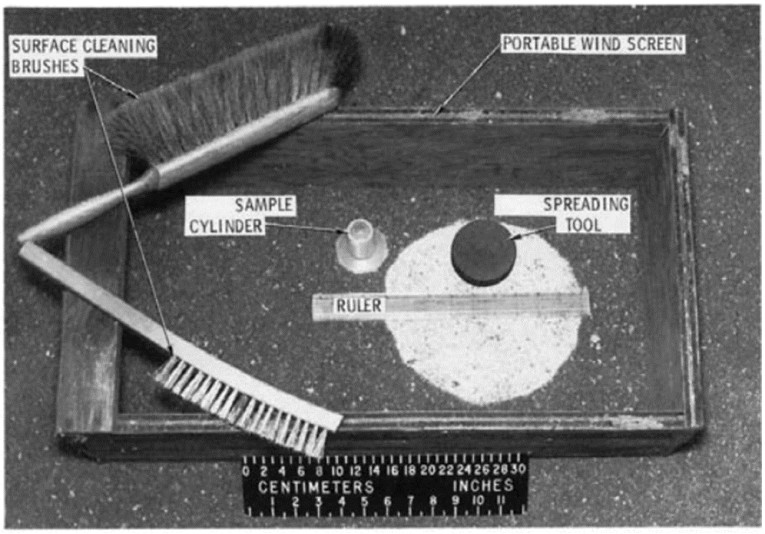

Figure 2.6 Apparatus of Sand Patch Test (ASTM E965)

The sand patch test can be used on a variety of road surfaces, including asphalt and concrete, and is relatively easy and inexpensive to perform. However, it has some drawbacks, such as requiring a clean, dry pavement surface and the possibility that results will vary due to variations in sand and pavement surface. Despite these drawbacks, the sand patch test is still a popular method for evaluating the skid resistance of pavement surfaces.

With the use of a rubber slider, 50 ml of known size and standardized sand is distributed radially across the surface, filling the coating voids while avoiding going over protrusions. The average diameter (D) of each circle is determined. The "height of sand (HS)" is the proportion of the circle's area to the volume of sand (V) (Eq. 2-1).

$$MTD = \frac{40 * V}{\pi * D^2} \qquad \text{Eq. 2-1}$$

The sand patch test, a method for evaluating the skid resistance of pavement surfaces, especially asphalt pavements, is discussed by Chamberlin and Amsler (1982). They discussed the limitations of the sand patch test and possible sources of error after

reviewing the relevant studies. They suggested that the sand patch test is more suitable for assessing the skid resistance of asphalt pavements because asphalt pavements are more porous than concrete pavements.

2.4.3 Dynamic Friction Test

Dynamic friction testing (Figure 2.7) is a technique for evaluating the skid resistance of a pavement surface to skidding using a system that simulates the motion of a moving vehicle. A dynamic friction tester, sometimes called a trailer-mounted skid trailer, consists of a trailer with wheels and brakes. The force required to stop the trailer is measured by sensors as it is pushed across the pavement surface at a constant speed.

The test method is described in ASTM E 1911. Its basic principle is based on Coulomb's law of friction. In this method, three rubber tires are fixed under a horizontally rotating disk (Kaçmaz et al., 2018). When the disk reaches a speed of 80 km/h during the test, it automatically lowers perpendicular to the pavement surface and contacts the road. As shown in Figure 2.8, the rubber tires rotate under a constant load W, acting perpendicular to the road surface and with speed V, with a linear force F. F is the frictional force between the road surface and the rubber tires. The coefficient of friction (μ) can be determined by dividing F by W. Peak friction values can be measured at speeds of 20, 40, 60, and 80 km/h.

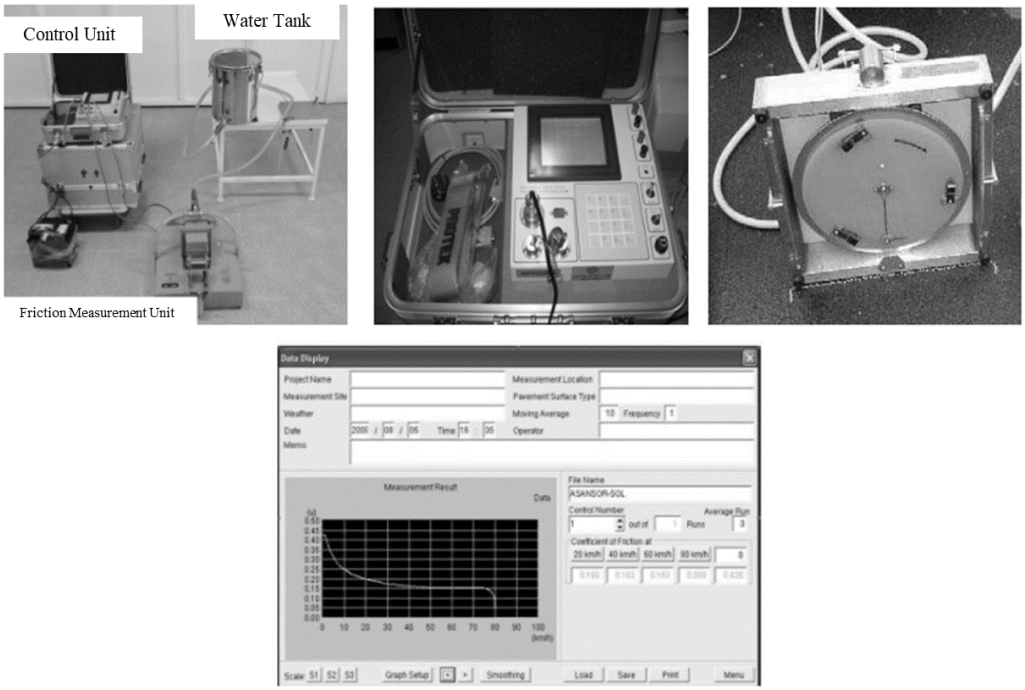

Figure 2.7 Dynamic friction meter tester (Measuring System, Control Unit, Measuring Unit Rotating Disc, Data transfer) (Kaçmaz et al., 2015)

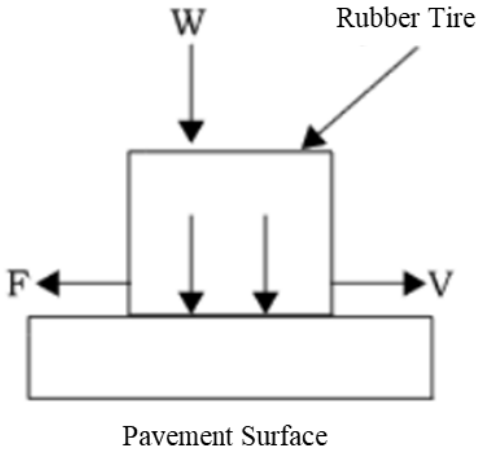

Figure 2.8 Forces acting on the rotating disk in the DFT device (Kaçmaz et al., 2015)

2.4.4 Outflow Test

An indirect approach to determining the volumetric MTD of a macrotexture from the connectivity of the texture is the outflow test (ASTM E2380). A transparent vertical cylinder with a rubber ring on the bottom is placed on the pavement surface for the Outflow Meter test. The time required to allow a given volume of water to pass through the transparent vertical cylinder is then allowed to flow into the pavement, and this time is recorded. This period shows how quickly the water drains from the surface of the pavement and how well it can drain water. The macrotexture of the pavement can be related to this time, called the outflow time. By measuring the escape time of water under a moving tire, this test result indicates a surface's tendency to aquaplaning. The macrotexture of the pavement surface is determined by the measurement parameter outflow time (OFT). Low OFTs are seen on pavement surfaces with rough macrotextures while high OFTs are found on surfaces with smooth macrotextures (Hall et al., 2009).

The outflow test is typically used in conjunction with other methods for measuring surface texture, such as the sand patch test or the British Pendulum Tester (BPT). It is a relatively simple and inexpensive method that can be performed in the field or a laboratory setting.

2.5 Profilometers

Profilometer is used to gauge a surface's profile and surface finish. Surfaces can consist of a series of peaks and valleys of different heights, depths, and spacings on a small scale. The ability of a surface to create a seal, look glossy or matte, feel smooth or rough, or be used as a wear surface depends on subtle variations in these characteristics. Surface roughness or surface finish specifications are frequently stated in technical drawings in industries that manufacture mechanical parts, and profilometers are used to confirm that the specifications are satisfied (GD&T Basics, n.d.).

2.5.1 Contact Profilometer

A contact profilometer is a type of profilometer that uses a physical probe to contact the surface of the material being measured. This probe is typically a diamond-tipped stylus that is dragged across the surface while a sensor measures the vertical movement of the probe. The data collected by the profilometer is then used to create a profile of the surface, which can be used to determine various surface texture parameters (Chappard et al., 2003).

Contact profilometers are commonly used in the manufacturing and metrology industries to evaluate surface texture on a wide range of materials including metals, ceramics, plastics, and composites. They can measure surface roughness, waviness, and form. They are also used in various applications such as quality control, research and development, surface characterization, and more.

One of the oldest studies done by Stout (1997) describes the use of contact profilometry for measuring surface roughness. The paper states that contact profilometry is a well-established method for measuring surface roughness and that it is commonly used in industry. In this study, the principle of operation of the instrument and the various stylus geometries used are discussed. Measurement of the roughness parameters is considered in detail, including the selection of measurement length, sampling intervals, and filtering techniques. The measurement of surface roughness on a wide range of materials is discussed, including metals, ceramics, and plastics.

2.5.2 Non-contact Profilometer

Non-contact profilometers are advanced surface measurement instruments that can measure surface topography without physically touching the surface. The different types of non-contact instruments vary based on the underlying principles used for measurement. They use various technologies like light, laser, or interferometry to scan and create a three-dimensional image of the surface's profile (Keyence, n.d.).

Overall, non-contact profilometers offer many advantages over traditional contact-based profilometers, such as greater accuracy, faster measurement times, and the ability to measure fragile or delicate surfaces without damaging them. A laser profilometer is a type of non-contact surface profilometry device that uses a laser beam to scan a surface and measure its topography. It is used to evaluate the surface texture of a wide range of materials, including metals, plastics, ceramics, and pavements (Corrosionpedia, n.d.). The device works by emitting a laser beam onto the surface being measured, and a sensor detects the reflected light. The sensor's position is precisely controlled by a motion system, and the device captures a series of two-dimensional (2D) cross-sectional images of the surface. The images can then be analyzed to determine various surface texture parameters, such as root mean square (RMS) roughness, peak-to-valley roughness, and skewness.

Laser profilometry has several advantages over contact-based profilometry methods. It can operate at high speeds, making it suitable for large-scale measurements, and it does not damage the surface being measured. Additionally, it can measure surfaces that are difficult to access with contact-based methods, such as curved or angled surfaces.

Miller et al. (2012) discussed the use of laser profiling techniques to improve the characterization of asphalt pavement surface texture and estimate friction characteristics. It suggested that current methods, such as the mean profile depth and mean texture depth, do not capture the range and distribution of surface asperities, which is critical for assessing friction. The study investigated the use of laser profiling systems to measure pavement surface texture and developed models that relate texture parameters to friction, based on analysis of field sections and laboratory samples. The results indicated that laser profiling systems can capture both microtexture and macrotexture spectrum and suggest that a comprehensive friction characterization of asphalt mixtures can be obtained in a laboratory setting, which would improve the tools available to asphalt mixture designers for estimating pavement surface texture and frictional properties. Moreover, Bitelli et al. (2012) experimented on using laser scanner techniques to characterize the texture of various

types of asphalt for road pavement. The use of high-precision laser scanners, such as triangulation types, was proposed to expand the analysis of road pavement from a two-dimensional method to a three-dimensional one, to extend the range of important parameters for these types of applications. The laser scanners could be used innovatively to obtain information on the surface layer through a single measurement, with data homogeneity and representativeness. The described experience highlighted the use of laser scanners for both laboratory experiments and in-situ tests, with attention paid to factors that could potentially affect the survey.

2.6 Surface Parameters and ISO 25178-2

It is possible to calculate roughness parameters in two-dimensional (2D) or three-dimensional (3D) forms. For more than 50 years, 2D profile analysis has been extensively used in research and engineering (Abou El-Atta, 1991; Pancewicz & Mruk, 1996; Rosen, 1993). In recent years, three-dimensional (3D) surface analysis has become increasingly necessary. Recently, the significance of 3D surface topography in research and engineering applications has been highlighted.

Any surface topography can be represented as a superposition of many scale-dependent geometrical forms (from large to very small scales). While the surface's fine structure, and roughness, has a small scale, form, or form deviation, has a wide scale. Figure 2.9 depicts a typical surface with these various size elements. The goal of filtration is to divide surface measurement data into large- and small-scale components. Because each scale component is a byproduct of the manufacturing process and each component affects the functionality of the surface, filtration is crucial for further analysis of the data.

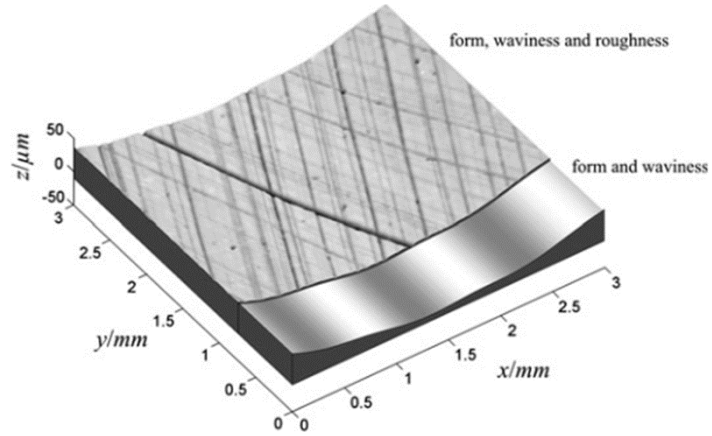

Figure 2.9 Topography of a honed surface with form, waviness, and roughness (Seewig, 2013)

The two surfaces are described in the international standard ISO 25178 Part 2 (2012): The S-F surface and the S-L surface. The letter "S" denotes that a low-pass filter is used to remove the short-wave surface irregularities. The letter "F" denotes that the so-called F-operation was used to exclude the nominal form from the surface dataset. An F-operation is defined such that by default fits the a priori nominal form using total least-squares. In specific situations, such as with freeform surfaces or unidentified nominal forms, a form filter, such as a second-order regression filter following ISO 16610 Part 71 (2011), can be used to eliminate the nominal form. The symbol "L" denotes the high-pass surface filtering. This implies that long-wave surface deviations, such as form deviations or waviness components, can be eliminated. Figure 2.10 shows the signal chain described in ISO 25178-2.

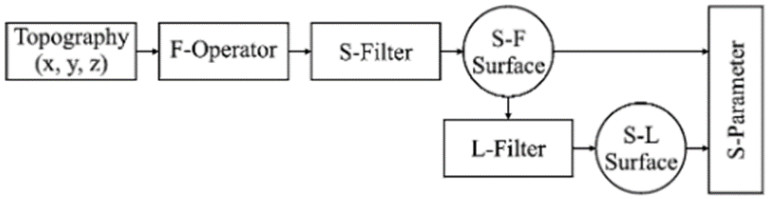

Figure 2.10 Definition of the S-F surface and the S-L surface (ISO 25178-2, 2012)

The application of a filter operation requires two phases. To separate the measurement data into large- and small-scale components of interest, the first step is to select a filter method that is appropriate for the problem at hand, and the second step is to select the right filter parameter. Care should be taken during both processes because the wrong choice of either the filter method or filter parameter can produce inaccurate results. The default values for areal surfaces specified in ISO 25178 Part 3 (2012) should always be used by users with no prior filtration experience.

As it is stated in ISO 25178-2 standard, after the collection of the related data, a "primary surface" is obtained. In ISO 25178-2, the primary surface is defined as a "surface portion obtained when a surface portion is represented as a specified primary mathematical model with specified nesting index." After the extraction of the portion to be investigated, surface filters are applied.

The S-filter, L-filter, and F-operation components of the surface filters are specified in ISO 25178-2. A surface filter called an S-filter removes the small-scale lateral components of the primary surface. An L-filter is a surface filter that filters the primary surface or the S-F surface by removing large-scale lateral components. Finally, the F-operation eliminates the form from the primary surface.

After the application of filters, scale-limited surfaces are obtained. There are two types of scale-limited surfaces which are the S-F surface and the S-L surface mentioned in ISO 25178-2. The surface obtained from the primary surface by eliminating the form with an F-operation is known as the S-F surface. In contrast, the S-L surface is created by employing an L filter to remove large-scale components from the S-F surface. In Figure 2.11, the relationships between S-filter, L-filter, F-operation, and S-F and S-L surfaces are shown.

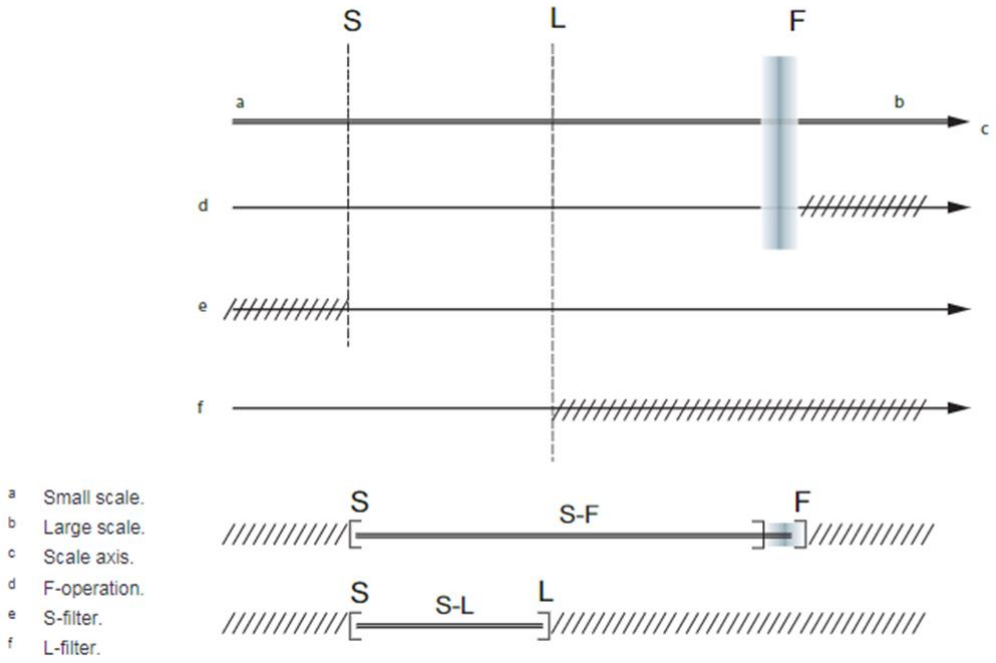

Figure 2.11 Relationship between S-Filter, L-filter, F-operation, and S-F and S-L surfaces (ISO 25178-2, 2012)

F-Operator

The base form that makes up the surface is removed using the F-Operator. An F-Operator for spherical form is used to make a spherical surface appear "flat," as shown in the Figure 2.12a-b. Several F-operators are available, including Tilt, Curvature (also known as a parabolic fit), spherical (also known as a true spherical fit), cylinder, and different combinations. Users can use user-defined parameters for the radius of curvature or configure the F-operator to produce the best-fitting shape using a least-squares fit.

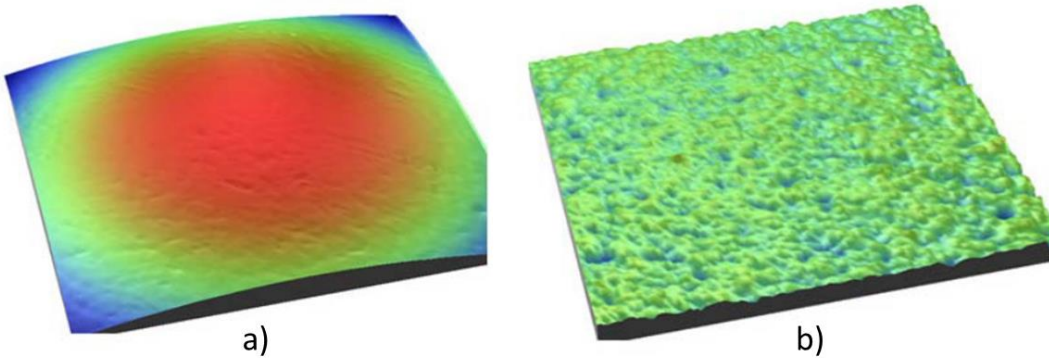

Figure 2.12 F-Operator application to spherical surface a) before b) after (Michmet, n.d.)

Long Wavelength Pass Filter

The S-filter is used to reduce the presence of any short spatial wavelength structures that might have been introduced into the measurement by electronic noise or other measurement abnormalities. Additionally, certain surfaces might have short spatial-wavelength structures that are unrelated to the application being paid to but may have an impact on subsequent assessments. The S-filter used to remove the shorter spatial wavelength components of the texture is shown in Figure 2.13a-b. Long Wavelength Pass is the name of the filtering technique when only an S-filter is employed.

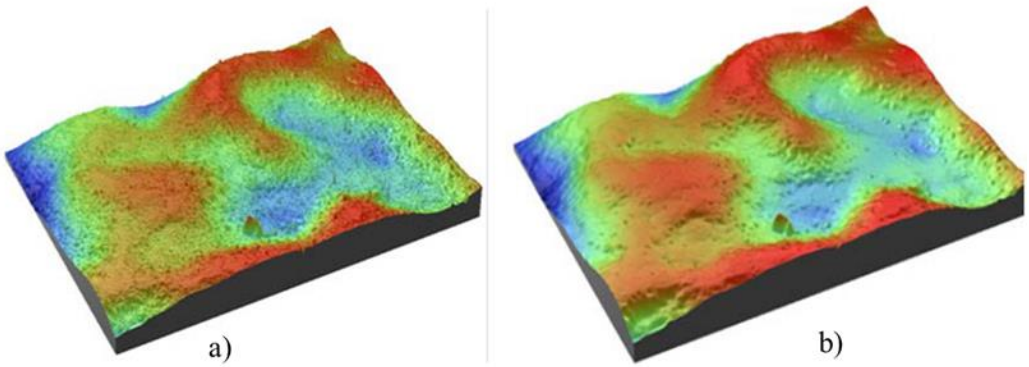

Figure 2.13 Application of S-filter to a measured surface a) before b) after (Michmet, n.d.)

Short Wavelength Filter

The longer spatial wavelength structures that could be present on the measured surface but are unrelated to the application being attended to are attenuated using the L-filter. The Figure 2.14 below shows how to apply an L-filter to reveal the fine-grained texture and peaks by removing the longer-spaced spatial structure. A short-wavelength pass is the name of the filtering technique used when only an L-filter is employed.

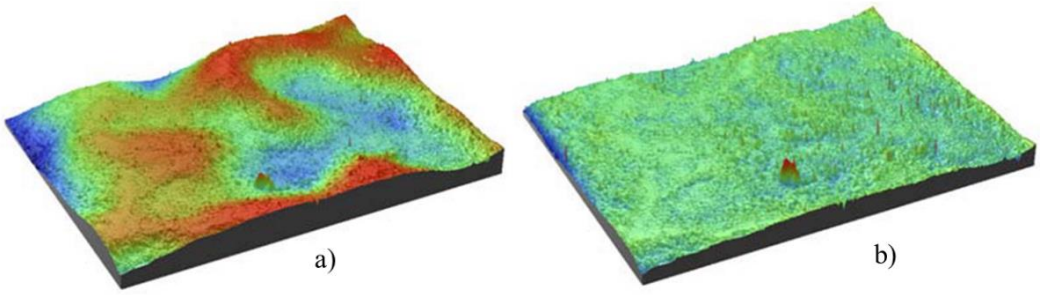

Figure 2.14 Application of L-filter to a measured surface a) before b) after (Michmet, n.d.)

Band Pass Filter

A bandwidth of spatial wavelengths that are used for analysis may be created using the combination of an S-filter and an L-filter. The filter is known as a band-pass filter when the spatial wavelength of the structure to be examined is contained within the S-filter cutoff and L-filter cutoff.

2.6.1 Surface Roughness Parameters

Quantitative values calculated statistically from the profiles are known as roughness parameters. Both 2D profiles and 3D surfaces obtained using different profilometers have been defined by a few international standards (ISO25178-2, 2012; ISO25178-3, 2009; ISO1302, 2002; ANSI/ASME B46.1, 2002; ISO 4287, 1997; ISO 13565-2, 1996). The non-contact profilometer ISO 25178-2 international standard for

Specification and Measurement of 3D Surface Texture provides a thorough illustration of the 3D characteristics in 6 separate categories:

- Height parameters
- Spatial parameters
- Hybrid parameters
- Functional parameters
- Functional volume parameters
- Feature parameters

2.6.1.1 Height Parameters

Height parameters are frequently used to conduct quantitative surface analyses, which permit an approximate description of surface irregularities (Leach, 2013). Seven major parameters comprise height variants which are Sp (maximum peak height), Sv (maximum valley depth), Sz (maximum height), Sa (arithmetical mean height), Sq (root mean square height), Ssk (skewness), and Sku (kurtosis). These variables evaluate the divergence of the surface height from the mean plane.

Maximum peak height (Sp) represents the highest value of the peak. In other words, the distance between the mean plane and the tallest peak inside the specified area. Due to the use of a single peak height value, it should be highlighted that this parameter is highly influenced by misleading irregularity, contamination, and measurement noise.

Maximum valley depth (Sv) represents the deepest possible value of the valley. In other words, the distance between the mean plane and the deepest valley within a specified area. Because of the use of a single pit depth value, this metric, such as the maximum height, is greatly influenced by spurious irregularity, contamination, and measurement noise.

Maximum height (Sz) is equal to the sum of the maximum peak height (Sp) and maximum valley depth (Sv), which is the vertical distance between the highest and lowest points (Eq.2-2).

$$S_z = S_p + |S_v| = S_p + S_v \qquad \text{Eq. 2-2}$$

It should be noted that prior standards describe Rz in a variety of ways, such as the average of the 10 highest and 10 lowest points. The ISO community decided that Sz should be solely the peak-to-valley height over an area measurement in the updated ISO 25178-2.c

Sp, Sv, and Sz tend to produce inconsistent measurements because they can only be obtained from a single point. To produce a statistically meaningful result when employing these three factors, spatial filtering bandwidths must be appropriately configured to remove false peaks and valleys and to average several measurements at random positions along the sample.

Arithmetical mean height (Sa) reflects the arithmetic mean of the absolute ordinate Z (x, y) within the evaluation area (Eq. 2-3). The mean of the typical height difference for a typical plane is one of the most frequently utilized quantities.

$$S_a = \frac{1}{A}\iint_A |z(x,y)|\, dxdy \qquad \text{Eq. 2-3}$$

Root mean square height (Sq) is the ordinate root mean square values within the defined area (Eq. 2-4).

$$S_q = \sqrt{\frac{1}{A}\iint_A z^2\,(x,y)dxdy} \qquad \text{Eq. 2-4}$$

The Sa and Sq parameters serve as general indicators of the overall texture of the surface. In terms of distinguishing peaks, valleys, and spacing of various texture elements, Sa and Sq are insensitive. Sa or Sq may therefore be deceptive because numerous surfaces with drastically different spatial and height symmetry features (such as those that have been milled versus honed) may have the same Sa or Sq yet perform in very different ways. The two extremely dissimilar surfaces in the

preceding figure have identical Sa and Sq values, demonstrating the insensitivity of the Sa and Sq parameters. However, the Sa and Sq parameters can be utilized to highlight major variations in texture properties once the surface type has been determined.

Skewness (Ssk) represents surface skewness, which quantifies the asymmetry of the surface deviation from the mean plane (Eq. 2-5).

$$S_{sk} = \frac{1}{{S_q}^3}\left[\frac{1}{A}\iint_A z^3\,(x,y)dxdy\right] \qquad \text{Eq. 2-5}$$

Kurtosis (Sku) is the sharpness of the surface height distribution. The spread of the height distribution is described by this parameter (Eq. 2-6)

$$S_{ku} = \frac{1}{{S_q}^4}\left[\frac{1}{A}\iint_A z^4\,(x,y)dxdy\right] \qquad \text{Eq. 2-6}$$

As mentioned previously, Ssk denotes the symmetry of the surface height concerning the mean plane. The sign of Ssk denotes whether the surface is dominated by peaks (Ssk>0) or valleys (Ssk<0). Sku identifies whether the texture has excessively high peaks or deep valleys (Sku>3.00) or not (Sku<3.00). Ssk and Sku are 0.00 and 3.00, respectively, if the surface heights are normally distributed (i.e., bell-shaped). Surfaces with Sku (= 3.00) tend to be described as smoothly varying and free of severe peaks or valley features. Ssk is helpful for defining honed surfaces and tracking various wear states. Sku helps detect defects that can appear as peaks or valleys on a surface. To obtain statistically significant results for Ssk and Sku, which require higher-order powers of the surface heights, one must take sufficient measurements and/or choose the right filtering bandwidths to remove false peaks or valleys. In Figure 2.15, the physical definition of the parameters Ssk and Sku are shown.

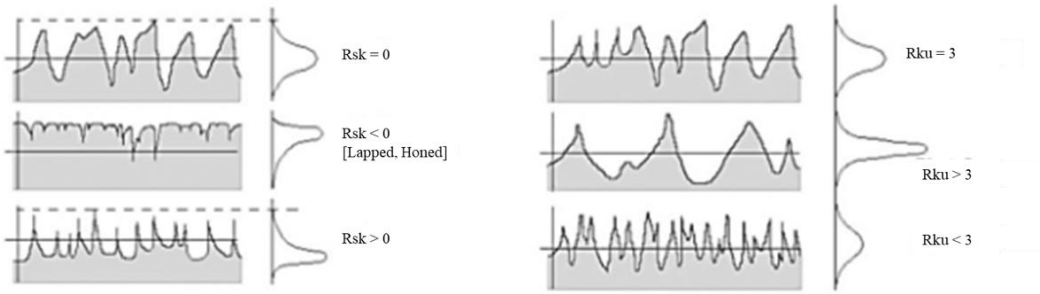

Figure 2.15 Ssk and Sku expressed in 2d profiles as Rsk and Rku (Bitelli et al., 2012)

2.6.1.2 Spatial Parameters

To determine whether a surface is isotropic or anisotropic, a set of spatial parameters describing the surface orientation is available (Leach, 2013). Two parameters are used to describe the spatial attributes. These variables are the texture aspect ratio (Str) and autocorrelation length (Sal). Instead of using height parameters, they are utilized to assess the horizontal size and complexity of the parallel grooves and grains. The mathematical method of the autocorrelation function (ACF) is utilized in the development of spatial parameters.

A duplicate surface (Z (x-Dx, y-Dy)) of the measured surface (Z (x, y)) and the relative lateral displacement (Dx,Dy) between the two surfaces are mathematically multiplied to obtain the ACF (Eq. 2-7). A measure of the amount of overlap between the two functions is produced by multiplying the resulting functions, integrating them, and then normalizing them to Sq. The ACF is 1.00 if the shifted version of the surface is the same as the original surface. The ACF will be close to -1.00 if the shifted surface is designed such that all peaks line with the corresponding valleys.

$$f_{ACF}(t_x, t_y) = \frac{\iint_A z(x,y)z(x-t_x, y-t_y)dxdy}{\iint_A z(x,y)z(x,y)dxdy} \qquad \text{Eq. 2-7}$$

The ACF is a method of determining how similar a texture is at a particular distance from its initial location. For a certain degree of shift, if the ACF remains close to 1.00, the texture is comparable in that direction. The surface is different, and therefore "uncorrelated" with the original measurement location if the ACF rapidly decreases to zero along a particular direction.

For a better understanding of ACF, an example surface is provided below (Figure 2.16a). As the peaks of the shifted surface line up with the mean plane for the turned surface above, the ACF in the X-direction quickly decreases to zero (Figure 2.16b). As the peaks of the surface line up with the valleys of the shifted surface, the ACF along X becomes negative (Figure 2.16b). The surface is almost the same as the original when shifting along the Y-axis, causing the ACF in the Y-direction to stay close to 1.00 (Figure 2.16c).

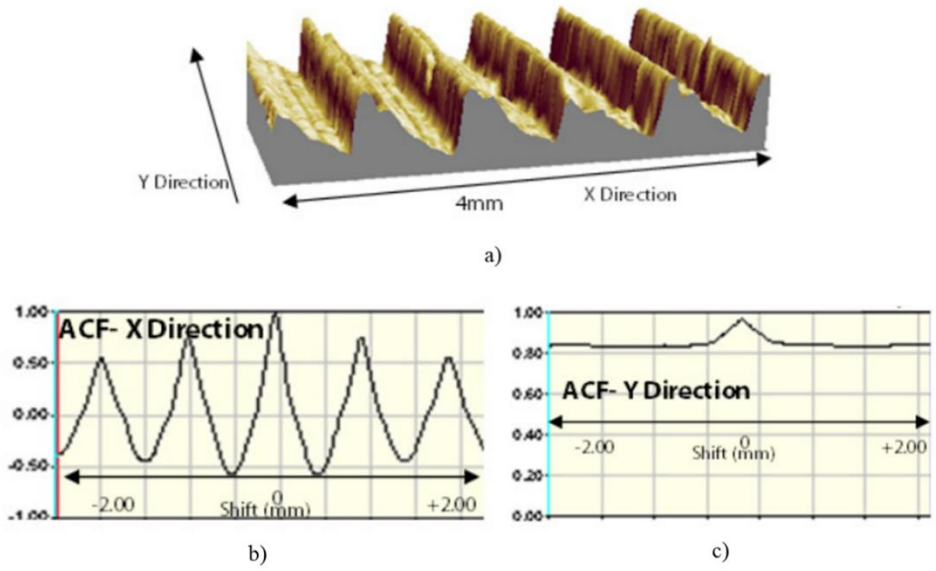

Figure 2.16 Example ACF illustration (Michmet, n.d.)

Autocorrelation length (Sal) is defined as the horizontal distance of the autocorrelation function with the fastest decay to a given value s ($0 \leq s < 1$). In the

computations (Eq. 2-8), s was taken as 0.2 which is a suggested value in ISO 25178-2.

$$S_{al} = \min_{t_x, t_y \in R} \sqrt{{t_x}^2 + {t_y}^2} \; where \; R = \{(t_x, t_y) : f_{ACF}(t_x, t_y) \leq s\} \qquad \text{Eq. 2-8}$$

Sal is a numerical indicator of the length of a surface along which a texture is found that is statistically different from its original location.

Texture aspect ratio (Str) is the ratio of the horizontal distance of the autocorrelation function that decays the fastest to a given value, s, to the horizontal distance of the autocorrelation function that decays the slowest to s ($0 \leq s < 1$) (Eq. 2-9). This demonstrates the effectiveness of isotropic or anisotropic surfaces. Str value ranges from 0 to 1, with Str> 0.5 typically denoting strong isotropy and Str 0.3 denoting strong anisotropy.

$$S_{tr} = \frac{\min_{t_x, t_y \in R} \sqrt{{t_x}^2 + {t_y}^2}}{\max_{t_x, t_y \in Q} \sqrt{{t_x}^2 + {t_y}^2}} \; where \; \frac{R = \{(t_x, t_y) : f_{ACF}(t_x, t_y) \leq s\}}{Q = \{(t_x, t_y) : f_{ACF}(t_x, t_y) \geq s \; and^{**}\}} \qquad \text{Eq. 2-9}$$

Str can be used to determine whether lay is present in any direction. Str can be used to find underlying surface alterations in situations when a surface is created by a number of different processes. A graphical representation of the procedure to calculate Sal and Str is given in Figure 2.17a-d.

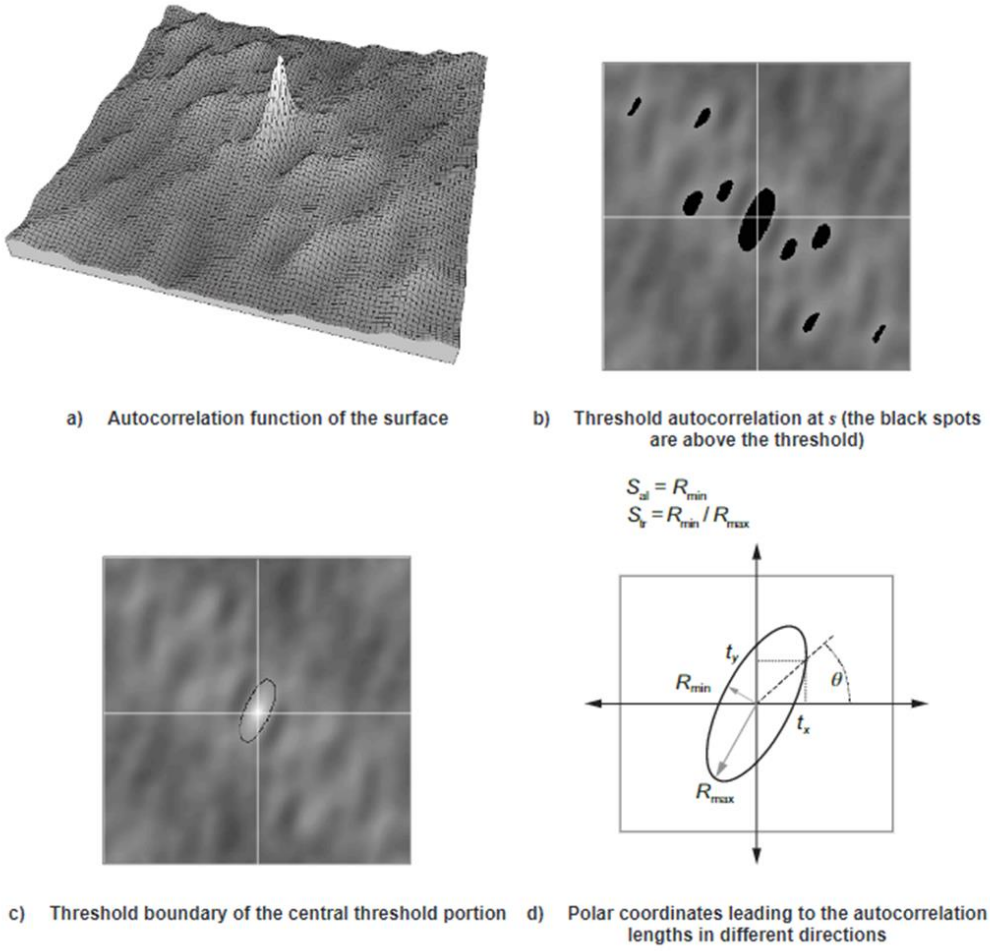

Figure 2.17 Procedure to calculate Sal and Str (ISO 25178-2, 2012)

2.6.1.3 Hybrid Parameters

The hybrid parameters are a set of two parameters that concentrate on the height and direction of the plane. The root mean square gradient (Sdq) and developed interfacial area ratio (Sdr) are the parameters.

Root mean square gradient (Sdq) is the Root Mean Square (RMS) Surface Slope measured in all directions (Eq. 2-10).

$$S_{dq} = \sqrt{\frac{1}{A}\iint_A \left[\left(\frac{\partial z(x,y)}{\partial x}\right)^2 + \left(\frac{\partial z(x,y)}{\partial y}\right)\right] dxdy} \qquad \text{Eq. 2-10}$$

To distinguish surfaces with identical average roughness, Sa, Sdq is a general measurement of the slopes that form the surface. Sdq may be used to determine the extent to which surfaces are soaked in different liquids. Both the texture amplitude and spacing affect Sdq. Accordingly, for a given Sa, a texture with a wider spacing may suggest a lower Sdq value than a surface with the same Sa but finer spacing.

Developed interfacial area ratio (Sdr) is calculated as the proportion of the additional surface area that the texture contributes to as compared to an ideal plane that is the same size as the measurement region (Eq. 2-11).

$$S_{dr} = \frac{1}{A}\left[\iint_A \left(\sqrt{\left[1 + \left(\frac{\partial z(x,y)}{\partial x}\right)^2 + \left(\frac{\partial z(x,y)}{\partial y}\right)\right]} - 1\right) dxdy\right] \qquad \text{Eq. 2-11}$$

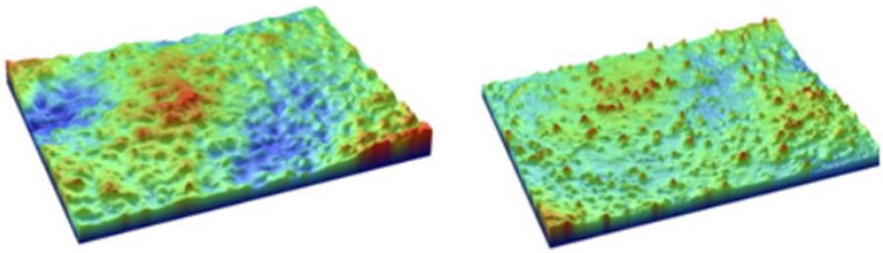

Sa= 0.52 µm, Sdr=0.0023%. Sa= 0.33 µm, Sdr=0.0623%.

a) b)

Figure 2.18 Comparison of Sdr values with different Sa values (Michmet, n.d.)

Sdr can further distinguish between surfaces with identical amplitudes and average roughness values. Whether or not Sa changes, Sdr often increases as the texture's spatial intricacy. Both the texture amplitude and spacing affect Sdr. Therefore, a texture with a higher Sa and wider spacing may have a lower Sdr (Figure 2.18a) value than a texture with a lower Sa but finer spacing (Figure 2.18b).

2.6.1.4 Functional Parameters

Functional parameters describe the functional behavior of the surface, such as wear, lubrication, and contact, and are related to the distribution of heights and their cumulative curve (known as the Abbott-Firestone curve). They can be considered statistical parameters because they are global (field parameters). The areal material ratio (Smr), inverse areal material ratio (Smc), and areal section height difference, also called the material ratio height difference (Sdc), are three parameters that will be discussed later in this study.

The parameters Smr, Smc, and Sdc for the 3D (Areal) surface texture are all obtained from the Areal Material Ratio curve based on the ISO 13565-2:1996 standard.

Areal material ratio (Smr(c)) is the proportion of the cross-sectional area of the surface at a height (c) to the cross-sectional area used for evaluation. The height (c) can be calculated as the depth from the areal material ratio curve's (Figure 2.19,) maximum point or as the height from the least-squares mean plane that best fits the data.

The height (c) is taken as 0.001 mm below the highest peak and applied to all the surfaces that had been studied. This value was chosen considering all the surfaces to have a general understanding.

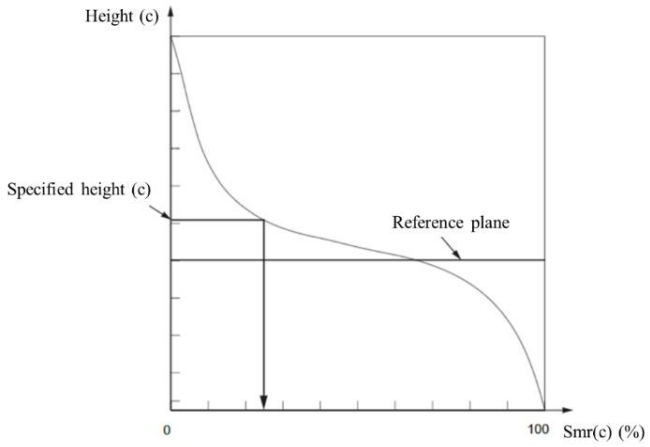

Figure 2.19 Areal material ratio (ISO 25178-2, 2012)

Inverse areal material ratio (Smc(mr)) is the height [c] that gives the areal material ratio p% (Figure 2.20).

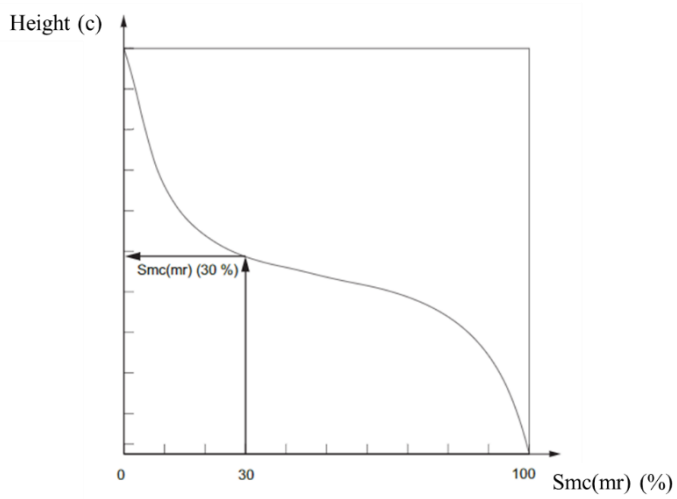

Figure 2.20 Inverse areal material ratio (ISO 25178-2, 2012)

2.6.1.5 Miscellaneous parameters

"Texture direction" (Std), which denotes the direction angle of the texture, is the single parameter in this category (parallel groove orientation, etc.). It is obtained from the angle of two-dimensional Fourier transformation images that maximizes the spectrum angle. The directional chart can also be used to establish the second- and third-strongest angles, but the standard indicates the angle for the strongest orientation.

In other words, Std is the major direction of lay derived from f_{APS} (s-Θ) by setting s equal to Std. Std is defined relative to the Y axis (Figure 2.21a). Thus, a surface with a lay along the Y axis will return a Std of 0 deg.

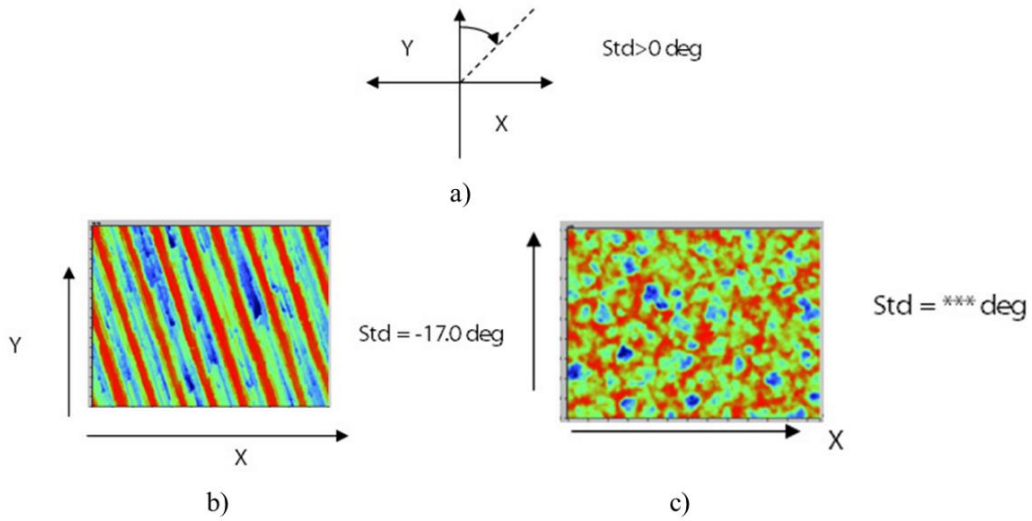

Figure 2.21 Application of Std and example surface (Michmet, n.d.)

In Figure 2.21b, the Std value is -17.0 degrees considering the lay angle with the Y axis. However, in Figure 2.21c, the Std value is indeterminate because there is no lay (spatially isotropic).

By placing the part in the instrument in a known orientation, the Std can be used to determine the lay direction of a surface in relation to a datum. A slight shift in the direction of the surface texture may have negative effects in particular applications such as sealing. Std may also be used to identify the presence of an earlier surface modification technique.

2.6.1.6 Functional Volume Parameters

Using the Abbott-Firestone curve, functional parameters can be effectively used to evaluate the tribological characteristics of contact-exposed machine components such as roller bearings (Leach, 2013). Functional volume parameters include Void volume (Vv(mr)), Dale void volume (or Pit void volume) (Vvv(p)), Core void volume (Vvc (p, q)), Material volume (Vm(mr)), Peak material volume (Vmp(p)) and Core material volume (Vmc (p, q)).

Void volume (Vv(mr)) is the area of space bounded by the surface texture between the lowest valley and a plane at a height determined by the "mr" value. Any value between 0% and 100% can be entered for "mr.". (Eq.2-12)

$$V_v(mr) = k\int_{mr}^{100\%}[Smc(mr) - Smc(q)]dq \qquad \text{Eq. 2-12}$$

Dale void volume (or Pit void volume) (Vvv(p)) is the area of space bounded by the surface texture from a plane at a height equal to level "p" of the material ratio (mr) to the lowest valley. "p" value is 80% by default, although it can be modified as necessary (Eq.2-13).

$$Vvv = Vv(mr2) \qquad \text{Eq. 2-13}$$

Core void volume (Vvc(p,q)) is the volume of space bounded by the texture at heights corresponding to the values of "p" and "q" in the material ratio. "p" and "q" have default values of 10% and 80%, respectively. (Eq. 2-14)

$$Vvc = Vv(mr1) - Vv(mr2) \qquad \text{Eq. 2-14}$$

As determined by the selected material ratio(s), Vv(mr), Vvv(p), and Vvc(p, q) all provide measurements of the void volume offered by the surface between different heights. Thus, these three void volume parameters represent the amount of fluid that fills the surface between the selected material ratio (mr) values (normalized to the measurement area). For instance, a Vv (25%) = 0.5 $\mu m^3/\mu m^2$ in that a 0.5 µm thick film placed over the measuring area would supply the amount of fluid required to cover the measured surface from a height equal to mr=25% to the lowest valley.

When considering fluid flow, coating applications, and debris entrapment, the void volume characteristics are helpful. Vv (0%), which represents the complete initial void volume provided by the texture, can be used to specify a new surface. Once a surface has been run-in, resulting in a decrease in the peak heights, it may be beneficial to determine how much core space is available using the core void volume, or Vvc. After a surface has undergone severe wear, the Dale Void Volume, Vvv(p), may help determine the probable residual volume.

Material volume (Vm(mr)) is the volume of material that makes up the surface from a height that corresponds to mr to the surface's highest point. Any value between 0% and 100% can be entered for "mr." (Eq. 2-15).

$$Vm(mr) = k \int_{0\%}^{mr} [Smc(q) - Smc(mr)]\, dq \qquad \text{Eq. 2-15}$$

Peak material volume (Vmp(p)) is the volume of the material that makes up the surface from the height corresponding to a material ratio level, "p," to the highest peak. 10% is the default value for "p," although it can be altered as necessary (Eq. 2-16).

$$Vmp = Vm(mr1) \qquad \text{Eq. 2-16}$$

Core material volume (Vmc(p,q)) is the volume of material that makes up the texture between heights corresponding to the material ratio values of "p" and "q". Both "p" and "q" have default values of 10% and 80%, respectively; however, these values can be modified as necessary (Eq. 2-17).

$$Vmc = Vm(mr2) - Vm(mr1) \qquad \text{Eq. 2-17}$$

Vm(mr), Vmp(p), and Vmc(p,q) represent the measurements of the material constituting the surface at various heights between or below the highest peak of the surface, as described by Vmc (p,q). For instance, Vm(10%) =0.35 $\mu m^3/\mu m^2$ would mean that all the material from the highest peak to the 10% point on the bearing area curve would be contained in a layer 0.35 µm thick across the measured cross section.

Different material volume parameters can be used to determine the amount of material available for load support after the top layers of a surface are worn away (i.e., Vmc(p,q)) and the amount of material that may be worn away at a certain depth of the bearing curve (i.e., Vmp(p)). Vvc(p,q) may then provide details regarding the ensuing void volume for fluid entrapment or leakage for sealing applications, whereas Vmp(p) may provide insight into the quantity of material available for seal engagement.

In Figure 2.22, the relationship between void volume and material volume parameters is given as the “Areal material ratio (%) vs Height” graph.

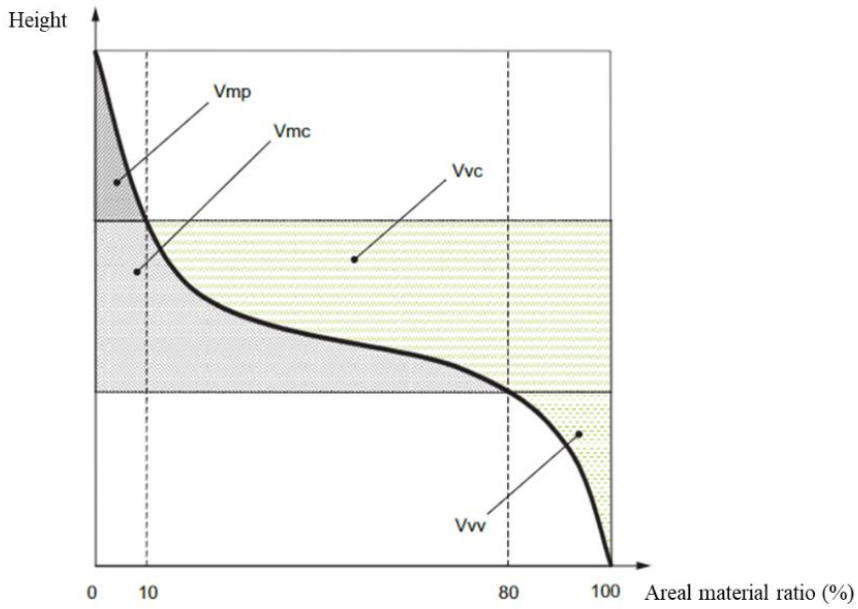

Figure 2.22 Void volume and material volume parameters (ISO 25178-2, 2012)

2.6.1.7 Feature Parameters

Areal feature parameters are a collection of parameters used to identify and characterize individual peaks and valleys on a surface. Additionally, these parameters can be used to assess the frequency of occurrence. Field parameters, which consist of height, functional, functional volume, hybrid, and spatial parameters, calculate every surface point, unlike the feature parameters.

Feature parameters only account for identified surface features. The significance of these characteristics lies in their role in specific functions. For instance, in mechanical engineering applications, large peaks and hills serve as contact zones, whereas points in the valleys do not. Surface segmentation allows the identification of these essential features.

The selection of these characteristics relies on a discrimination technique, known as pruning. Subsequently, the parameters were calculated to quantify the attributes of the selected features. By emphasizing the selected features, the areal feature parameters offer a targeted method for comprehending the functional properties of the surface (Leach, 2013).

Peak Density (Spd) is determined by dividing the total number of peaks by the unit area. It is expressed in units of [1/mm^2] or [peaks/mm^2] (Figure 2.23). The Spd parameter can be utilized in applications where contact is necessary, typically in conjunction with other factors, such as the minimum or maximum height parameters. A higher Spd value indicates a larger number of contact points with other objects.

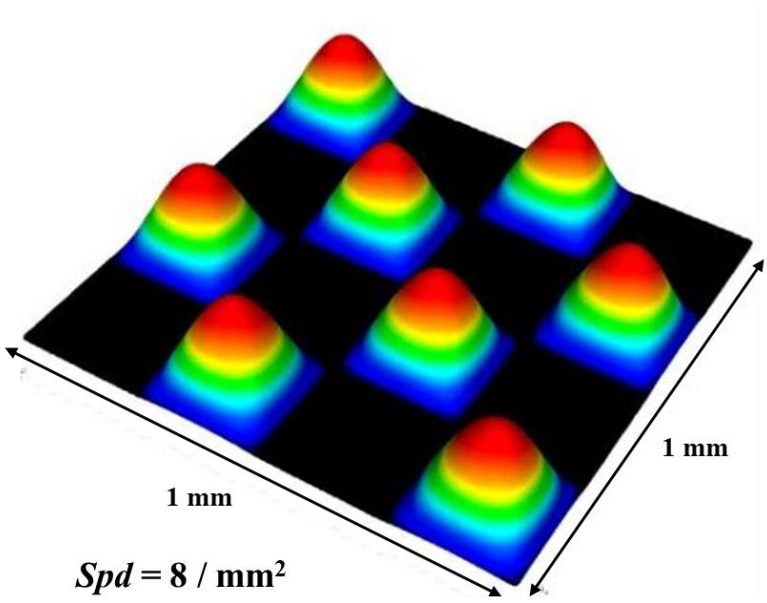

Figure 2.23 Illustration of Peak Density, Spd (Keyence, n.d.)

Arithmetic mean peak curvature (Spc) is the arithmetic mean of the principal curvature of the surface peaks (Figure 2.24).

A lower value indicates that the contact points with other objects have circular shapes, whereas a higher value indicates that the contact points have pointed shapes. As the curvature is inversely proportional to the radius of curvature, a high value of

Spc corresponds to a short radius of curvature. In such situations, the peaks are pointed at and susceptible to plastic deformation or wear during static or sliding contact.

A low Spc value, on the other hand, results in a large radius of curvature and more rounded contact points. If the peaks are broad, then the contact characteristics are enhanced. These rounded peaks may be susceptible to elastic deformation rather than to plastic deformation in situations involving static contact. By comprehending the relationship between Spc and the radius of curvature, it is possible to predict the behavior and durability of a surface during different forms of contact more accurately.

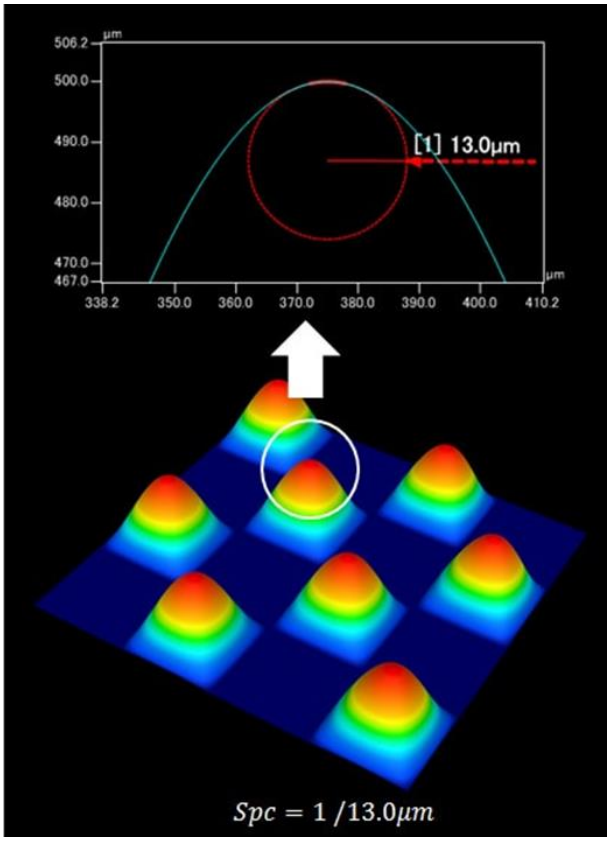

Figure 2.24 Illustration of arithmetic mean peak curvature, Spc (Keyence, n.d.)

Ten-point height (S10z) is defined as the average of the heights of the five peaks with the highest global peak height multiplied by the average of the heights of the five pits with the highest global pit height, within the definition area.

Five-point peak height (S5p) is defined as the average value of the heights of the five peaks with the largest global peak height, within the definition area.

Five-point pit height (S5v) is defined as the average value of the heights of the five pits with the largest global pit height, within the definition area

Mean dale area (Sda) is the average area of dales connected to the edge at a designated height.

Mean hill area (Sha) is the average area of hills connected to the edge at a designated height.

Mean dale volume (Sdv) is the average volume of dales connected to the edge at a designated height.

Mean hill volume (Shv) is the average volume of hills connected to the edge at a designated height.

ISO 25178 - 2 outlines nine surface analysis feature parameters. Spd is frequently associated with extreme height parameters such as S5p or S5v. The arithmetic mean peak curvature, Spc, only considers significant peaks and dales, where a larger value indicates a peak with a steeper slope and a smaller value indicates a peak with a less steep slope. The formula for calculating the ten-point height parameter, S10z, is S10z = S5p + S5v. The parameters for the five-point peak height, S5p, and five-point pit height, S5v, are both positive and only considered the greatest peaks or pits. The mean dale area, Sda(c), and mean hill area, Sha(c), refer to the horizontally projected areas. It is possible to calculate the mean dale volume, Sdv(c), mean hill volume, and Shv(c), Sda(c), and Sha(c) parameters based on whether they are open or closed at height c. Some applications of this series of parameters are listed in Table 2.2.

Table 2.2 Some applications for areal feature parameters (He et al., 2021)

Application \ Symbol	S_{pd}	S_{pc}	S_{10z}	S_{5p}	S_{5v}	$S_{da}(c)$	$S_{ha}(c)$	$S_{dv}(c)$	$S_{hv}(c)$	References
Flat lapping		√	√	√	√	√	√			(Pawlus et al.,2013)
Grinding	√	√	√	√					√	
Vertical milling		√			√		√			
Anisotropic stone surface		√	√	√	√	√				
Laser surface treatment		√								
Vapor blasting	√	√	√	√	√					
Turned surface with burnishing		√				√	√	√	√	
Cartilage wear		√		√			√			(Tian et al., 2011)
Biomedical titanium surface texture		√	√	√						(Wang et al., 2011)

2.7 Image-Based Analysis (Photogrammetry)

Photogrammetry is the science of making measurements from photographs. It involves the use of photographs, typically taken from an aircraft or satellite, to extract information about the earth's surface and its features. Photogrammetry can be used for a wide range of applications, including mapping, surveying, land use planning, resource management, and disaster response (Mikhail et al, 2001).

The basic principle of photogrammetry is that by measuring the position and orientation of a camera in space at the time of exposure, and the position of features in the image, it is possible to calculate the position of those features in space. This is done by using geometric principles and computer algorithms to analyze the photographs and extract the information needed.

There are two main types of photogrammetry: aerial photogrammetry and close-range photogrammetry. Aerial photogrammetry is used to generate maps and measure large areas, while close-range photogrammetry is used to make measurements of smaller, more detailed objects and structures (Schenk, 2005). In recent years, photogrammetry has also been used in computer vision and robotics to create 3D models of objects and environments and to assist with navigation and localization. With the advent of affordable and accessible 3D scanning devices,

photogrammetry and 3D scanning are becoming more and more integrated in many fields (Lachambre et al., 2017). Overall, photogrammetry is a powerful tool that can be used to obtain accurate and precise measurements of the earth's surface and features and has many applications in various fields such as geomatics, civil engineering, architectural, archaeology, cultural heritage, and many more (Lachambre et al., 2017).

According to the aforementioned superiority, photogrammetry is a technique that can be used for the analysis of surface texture. The general methodology for conducting a photogrammetry analysis of surface texture includes the following steps:

- **Preparation:** The surface to be analyzed must be prepared for measurement. This may include cleaning the surface with a solvent, polishing it with a fine abrasive, or using a mechanical stylus to remove any surface contaminants.
- **Photography:** The surface is photographed using a high-resolution camera. The camera should be mounted on a stable tripod and multiple images should be taken from different angles and positions to cover the entire surface.
- **Data collection:** The images are then processed using photogrammetry software. This software uses the overlapping areas in the images to create a 3D point cloud, which can be used to extract information about the surface's height, slope, and roughness.
- **Analysis:** The data is analyzed to determine the surface's roughness, texture, and other characteristics. This may include calculating parameters such as root mean square roughness (Rq), average roughness (Ra), and peak-to-valley height (PV).
- **Interpretation:** The results are interpreted to determine the quality of the surface and whether it meets specific standards. This may include comparing the results to established standards, such as ISO or ASME standards, or evaluating the effectiveness of a surface treatment process.

- **Reporting:** The results of the analysis are reported in a report that includes all the measurements, data, analysis, and conclusions.

These stages can also be used for other purposes such as topography, volume calculation, mapping, and many more. Overall, photogrammetry can be used to analyze large and complex surfaces and can also be used to analyze surfaces that are difficult to access using other techniques. Additionally, it has the advantage of being a non-contact method, which means it does not cause any damage to the surface being measured. In the Materials and Method section of this thesis, the detail of the utilized photogrammetry method is discussed in detail.

2.8 Summary of the Chapter

This literature review provides a comprehensive overview of the relevant concepts and methodologies associated with roller-compacted concrete (RCC) pavements, surface properties, and surface characterization techniques. It begins with an overview of rigid pavements and highlights the significance of surface characteristics for the durability and safety of these pavements. The review then delves into RCC's particulars, examining studies and issues related to RCC pavement.

The discussion of surface characteristics is an important part of the review, with subsections devoted to microtexture, macrotexture, unevenness, megatexture, road-tire friction, and skid resistance. This review provides a thorough analysis of these characteristics and how they affect safety, comfort, and fuel efficiency while driving.

The literature review also discusses various surface characterization methods and laboratory tests, including the British Pendulum Tester (BPT), sand patch test, dynamic friction test, and outflow test. This review also covers surface parameters, ISO 25178-2, contact and non-contact profilometers, and other related topics.

The final section of the literature review examines image-based analysis (photogrammetry), which serves as the foundation for the innovative 3D

photogrammetry technique developed and used in this study. The chapter summary highlights the crucial ideas raised and how they relate to research.

This study contributes to the literature by investigating the effects of RCC mixture proportions on macro- and microtexture characterization, which has been less explored in previous research. The application of a novel 3D photogrammetry technique for surface characterization provides a new viewpoint in the field. The results of this study will be useful for enhancing RCC pavement mix design, comfort while driving, and road safety.

CHAPTER 3

MATERIALS AND METHODS

This chapter initially discusses materials and mixture proportioning which originated from the Ph.D. thesis titled “Effects of Mixture Design Parameters and Compaction Methods on the Properties of Roller Compacted Concrete Pavements", since the samples prepared within that thesis are analyzed (Sengun, 2019). Then, laboratory experiments that are conducted on the samples and the details of the proposed photogrammetry process and setup are described in detail.

3.1 Materials and Mixture Design

In the preparation of all RCC mixtures, CEM I 42.5 R type standard Portland cement produced according to TS EN 197-1 standard and crushed limestone aggregate were used by Sengun (2019). In that study, two different cement dosages, 200 and 400 kg/m^3, were chosen. While mixtures with a dosage of 200 kg/m^3 represented low-dosage RCC mixtures with normal strength, mixtures with a dosage of 400 kg/m^3 were preferred to obtain high-performance RCC mixtures. The grain size distribution of the aggregate batches for three different aggregate sizes (fine aggregate 0-5 mm, coarse aggregate 5-12 mm, and coarse aggregate 12-19 mm) used is given in Figure 3.1.

The physical properties of the aggregates were presented according to ASTM standards and presented in Table 3.1.

Table 3.1 Physical properties of fine and coarse aggregates (Sengun, 2019)

Physical Properties	Fine Aggregate FA (0-5 mm)	Coarse Aggregate CA (5-12 mm)	Coarse Aggregate CA (12-19 mm)
Maximum aggregate size (mm)	5	12	19
Specific gravity (SSD)	2.67	2.69	2.71
Specific gravity (OD)	2.64	2.68	2.7
Bulk density in compacted condition (kg/m^3)	1791	1540	1488
Bulk density in loose condition (kg/m^3)	1668	1466	1395
Absorption (%)	1.24	0.29	0.18
Fineness modulus	3.2	-	-

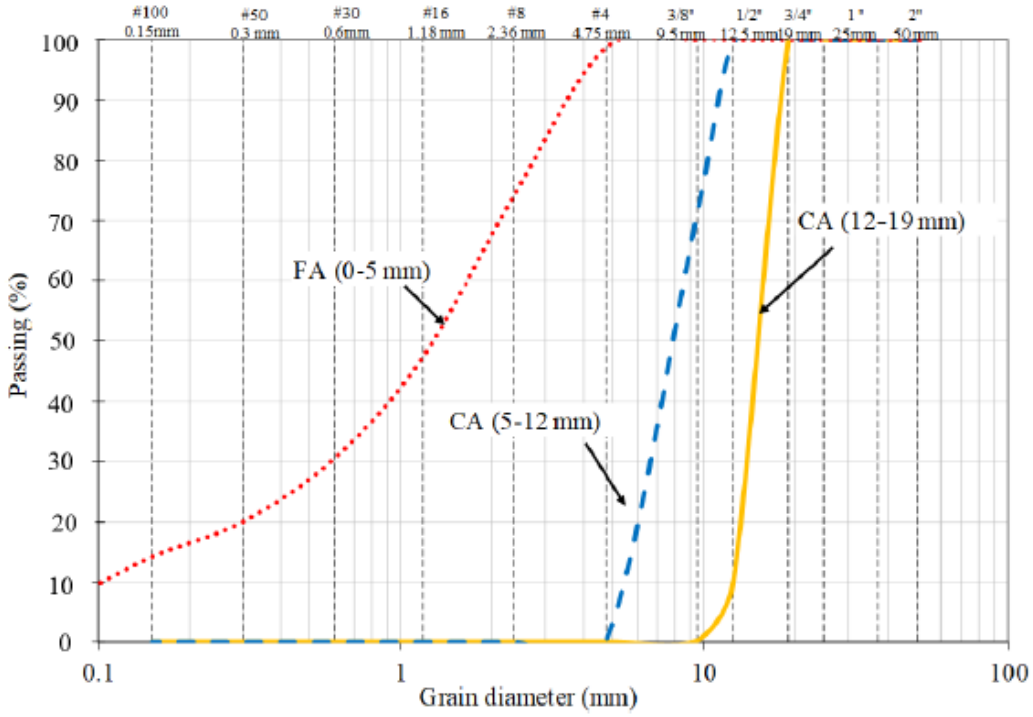

Figure 3.1 Grain size distribution of fine and coarse aggregates (Sengun, 2019)

The intended gradation of the aggregate combination was established by considering the hot mix asphalt (HMA) gradation limits from the Turkish General Directorate of Highways (GDH) (KGM, 2013) and RCC gradation limits from the American Concrete Pavement Association (ACPA, 2014) as given in Table 3.2.

Table 3.2 Lower and upper limits used to determine aggregate gradation in RCC mixture designs (ACPA, 2014; KGM, 2013)

Aggregate Gradation Limits for HMA (KGM, 2013)				
Sieve Size (mm)	Lower Limit (D_{max} 19 mm)	Upper Limit (D_{max} 19 mm)	Lower Limit (D_{max} 12 mm)	Upper Limit (D_{max} 12 mm)
19	100	100	100	100
12.5	88	100	100	100
9.5	72	90	80	100
4.75	45	52	55	72
2	25	35	36	53
0.425	10	20	16	28
0.18	7	14	8	16
0.075	3	8	4	8
Aggregate Gradation Limits for RCC (ACPA, 2014)				
19	95	100	100	100
12.5	70	95	81	100
9.5	60	85	71	91
4.75	40	60	49	70
2.36	30	50	33	54
1.18	20	40	24	40
0.6	15	30	15	30
0.3	10	25	10	25
0.15	2	16	2	16
0.075	0	8	0	8

As seen in Figure 3.2, both gradation limits were similar, which is mostly because both asphalt and RCC pavements were laid and compacted using the same equipment and methods. For the mixes with a maximum aggregate size of 12 mm, the aggregate combination was determined to be 65% (0-5 mm) – 35% (5-12 mm) – 0% (12-19 mm), and for the mixes with a maximum aggregate size of 19 mm, it was decided to be 50% (0-5 mm) – 40% (5-12 mm) – 10% (12-19 mm).

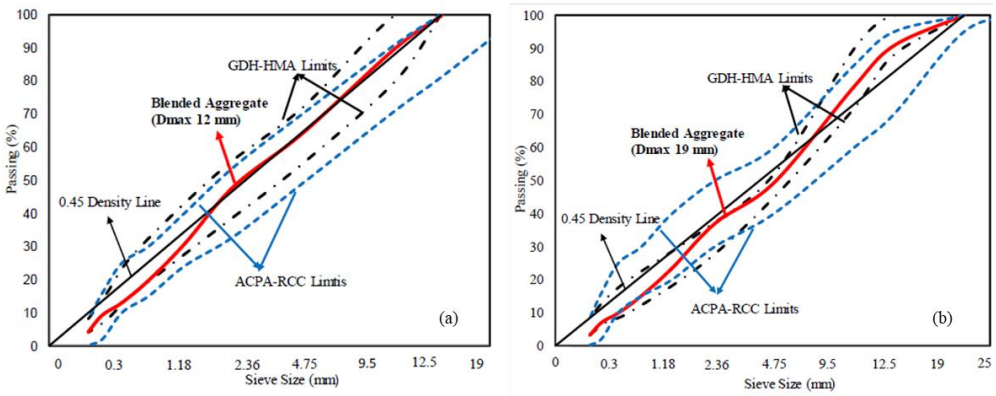

Figure 3.2 The combined aggregate gradations (a) Dmax 12 mm (b) Dmax 19 mm (Sengun, 2019)

Within this study, a total of twelve RCC mixture designs were developed utilizing two different cement dosages (200 and 400 kg/m^3), two different aggregate gradations (Dmax 12 mm and 19 mm), and three different water ratios, 4-5-6%. While designing these mixtures, the proportioning of the concrete mixtures was carried out with the classical weight/volume calculation with the assumption of 2% air volume, in accordance with the RCC road pavements guide prepared by the USA Concrete Road Technology Center. The design of the mixtures is given in Table 3.3.

Table 3.3 RCC mixture proportions for a cubic meter (Sengun, 2019)

No	Mix ID	C (kg)	D_{max} (mm)	W (%)	Water Content (kg)	FA (0-5 mm) (kg)	CA (5-12 mm) (kg)	CA (12-19 mm) (kg)	w/c	C (%)	S/A
1	C200-D12-W4	200	12	4	96	1424	770	-	0.48	8.35	0.65
2	C200-D12-W5	200	12	5	117	1388	750	-	0.59	8.55	0.65
3	C200-D12-W6	200	12	6	137	1353	731	-	0.69	8.76	0.65
4	C200-D19-W4	200	19	4	96	1095	880	222	0.48	9.20	0.50
5	C200-D19-W5	200	19	5	117	1067	857	216	0.59	9.42	0.50
6	C200-D19-W6	200	19	6	137	1040	835	211	0.69	9.64	0.50
7	C400-D12-W4	400	12	4	97	1312	709	-	0.24	16.52	0.65
8	C400-D12-W5	400	12	5	118	1275	689	-	0.30	16.92	0.65
9	C400-D12-W6	400	12	6	139	1240	670	-	0.35	17.32	0.65
10	C400-D19-W4	400	19	4	97	1009	810	205	0.24	18.03	0.50
11	C400-D19-W5	400	19	5	118	981	788	199	0.30	18.44	0.50
12	C400-D19-W6	400	19	6	139	953	766	194	0.35	18.88	0.50

Notes. C; the cement dosage, Dmax; the maximum aggregate size, W; the water content percentage, FA; fine aggregate, CA; coarse aggregate.

The water percentage indicated in the above table is the percent of water to the overall cement and aggregate. w/c is the ratio of water to cement. C is defined as the ratio of cement to the overall cement and aggregate, and S/A is the ratio of the fine aggregate to the total aggregate.

3.1.1 Production of Samples

In the study of Sengun (2019), Superpave Gyratory Compactor (SGC) was used to mimic the field compaction of RCC in laboratory conditions. Since SGC more accurately simulates the compaction conditions in the field, it has been preferred as a standard method for designing asphalt mixes. In other words, unlike other laboratory methods (impact-based compaction methods), it represents the field conditions in the laboratory environment as it applies compression by kneading around its longitudinal axis. Another critical benefit of SGC is that it allows setting variable gyration numbers and heights to achieve desired densities and compaction levels. Although new studies continue on the production of RCCs with SGC, 50-60 gyration numbers are currently recommended for RCCs to reach the desired density in ASTM C1800.

In this study, three different gyration numbers (50, 60, and 75) were chosen to analyze the effect of compaction on the mechanical and physical characteristics of RCC samples. For each mix design, 9 specimens were prepared, three specimens per each gyration number. Due to the sample size limitations of SGC, the dimensions of the final sample were ϕ15×15cm (Figure 3.3). For further testing, the samples were cured for up to 28 days using wet cloths. The mechanical and physical characteristics of RCC samples were broadly discussed by Sengun (2019). This thesis only focuses on the surface properties of laboratory-manufactured samples.

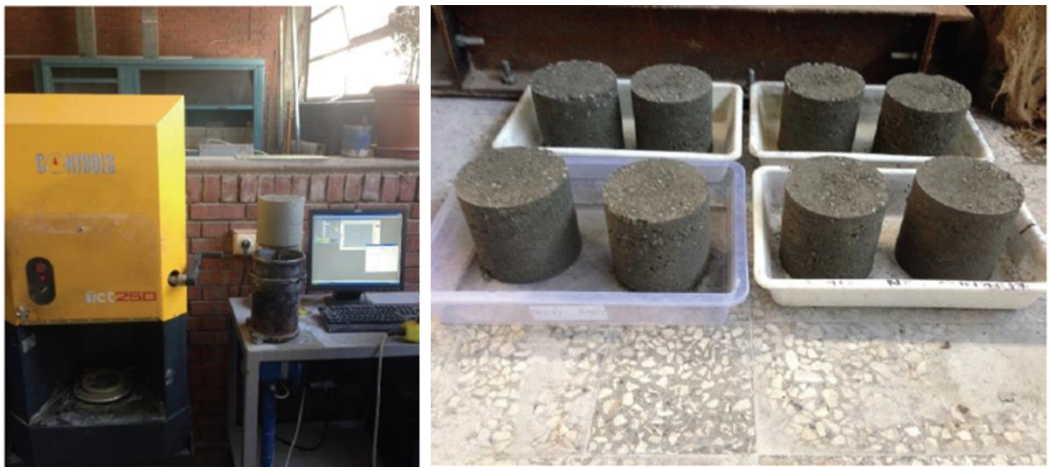

Figure 3.3 Compaction of RCC mixtures by SGC method

3.2 Determination of Surface Properties

In this study, the sand patch test for macrotexture and the British pendulum test for microtexture was used to determine the surface properties of RCCs. Although both methods are often preferred in the literature as well as in practice, they only help in measuring road safety at low speeds.

3.2.1 Sand Patch Test

In this study, the sand patch test, which is one of the most commonly used methods in the world (Jalalkamali et al., 2021; see also Sarsam and Ali, 2015; Yaacob et al., 2014; Sengoz et al., 2012; Elunai et al., 2010; Chamberlin and Amsler, 1982; Doty, 1975), was preferred for determining the depth of pavement surface macrotexture, especially because it is easy to apply.

The sand patch test is a method of measuring the roughness of pavement surfaces. In this test, a known volume of sand is applied to the pavement surface and the depth of the depression created by the sand is measured. The depth of the depression is then used to calculate the mean texture depth (MTD), which is a measure of the surface roughness.

The average texture depth (MTD) of the pavement surface was determined in experiments conducted in accordance with the ASTM E965 procedure by measuring the total area covered by uniformly distributed 90% round glass balls of known volume on clean and dry pavement surfaces. This procedure (Figure 3.4). was performed using a round disc. For this purpose, a known volume of glass balls and a number of standard-size glass balls that at least 90% pass through the No. 60 sieve opening and have a gradation above No. 80 are spread out in a circle to fill the coating recesses on the surface. The average diameter of the circle and the volume of the glass balls were then used to determine MTD.

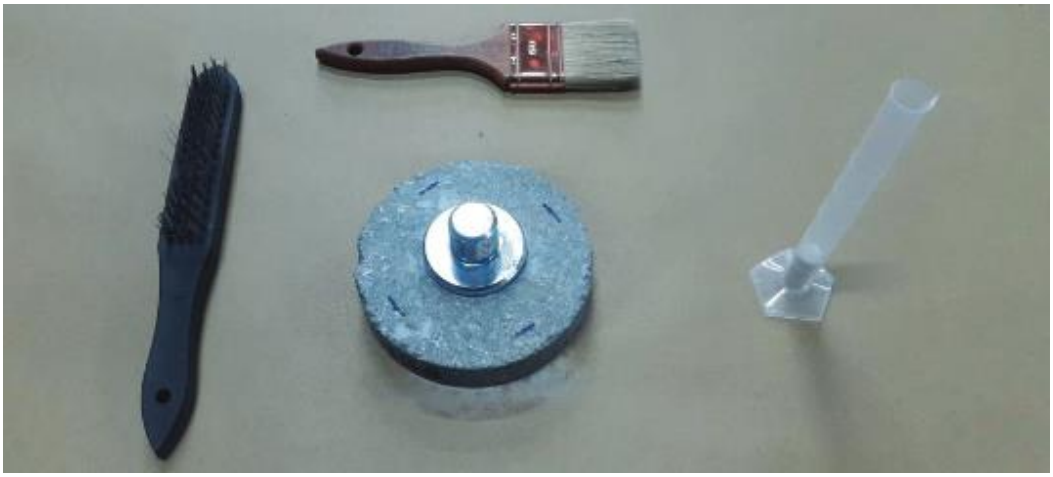

Figure 3.4 Sand patch test on RCC samples

3.2.2 British Pendulum Tester

One tool for evaluating the skid resistance of road surfaces is the British Pendulum Tester (BPT), Figure 3.5. It consists of a pendulum arm with a weight at one end and a rubber slider at the other. The pendulum is released from a fixed height while the slide is on the pavement. The deflection of the pendulum arm is used to quantify the force required to cause the slider to skid, and the results are reported as a Skid Resistance Value (SRV).

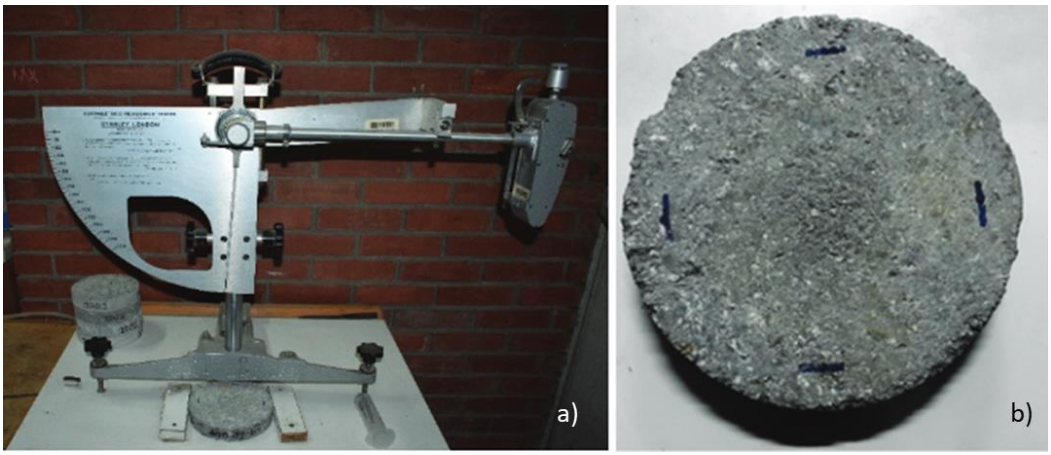

Figure 3.5 a) Measurement of RCC samples with the British pendulum test, b) marked sample

Because of its ease of use and low cost, BPT is frequently used to evaluate the skid resistance of pavement surfaces. Because it can simulate the conditions that can cause sliding, it is particularly useful for testing wet or slippery surfaces. The SRV can be used to assess whether a surface meets safety requirements or to compare the skid resistance of different pavements.

The sand patch test is frequently used in conjunction with the BPT to provide a more thorough evaluation of the pavement surface. It is important to note that a number of variables, such as the type of pavement, ambient humidity and temperature, and the age and condition of the slider, can affect the results of BPT.

Sample surfaces must be cleaned and BPT test equipment must be adjusted prior to each sample according to the ASTM E303 procedure. As SGC was used to prepare the specimens for this study, BPT was applied to 150 mm diameter round specimens in both dry and wet conditions. This was done to observe how the frictional properties of RCCs change in wet conditions.

For each specimen, four points were selected at 90° angles within 1.5 cm of the specimen edge, and four measurements were taken from each point to obtain average BPN values (Figure 3.5b). Although ASTM E303 specifies that the surface should

be adequately wetted, it does not elaborate on experiments on wet surfaces. No details of the procedure were given in the studies published in the literature. A preliminary investigation was conducted to estimate the amount of water required to thoroughly wet the 150 mm diameter specimens. 20 ml and 50 ml of water were applied to the surface for wet condition measurements. Obtained BPN results indicated that 50 ml of water was sufficient for all samples and that a film layer initially formed on the surface of the sample. Prior to each measurement, the top surface of the specimen was wetted as required by the standard.

Table 3.4 Classification of skid potential (Yıldız, 2018)

Class	***BPN Number***	***Cof (μ)***	***Skid Probability***	***Skid Potential***
Z	<24	<0.25	1/20	Very High
Y	25-34	0.25-0.34	1/200	High
X	35-44	0.36-0.46	1/10,000	Moderate
W	45-54	0.47-0.59	1/100,000	Low
V	>54	>0.59	1/million	Very Low

3.3 Imaging Procedures and 3D Photogrammetry

The fundamentals of photogrammetry, the science of taking measurements from photographs, serve as the basis for the theory of 3D photogrammetry. 3D photogrammetry extends the idea of photogrammetry to create a digital model of a surface in three dimensions using images to extract information.

To use 3D photogrammetry to analyze the surface texture analysis, the user typically takes a series of photographs of the surface using a camera or other imaging device. The photos are then processed using specialized software, mentioned later in this chapter, that extracts features from the images and creates a digital model of the surface. 3D photogrammetry can be used to extract a variety of surface texture parameters from a pavement surface, including roughness, texture depth, and other

features. The flow of the Imaging Procedure is given in Figure 3.6, starting from the photography process.

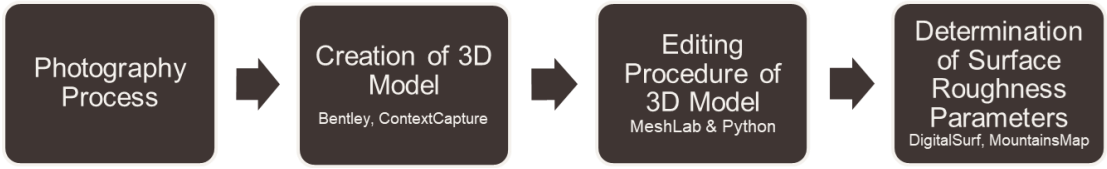

Figure 3.6. The flow of Imaging Procedure

3.3.1 Sample Preparation

In Figure 3.7a, the setup for 3D photogrammetry is shown. Before capturing the images, the sample (Figure 3.7b) was placed in the setup. To ascertain the actual sizes of the samples, circular papers (Figure 3.7c) with approximately 5.80 mm diameter adhered to the surface of the samples as reference measurements. It should be noted that the size and form of the reference paper are not important for the technique, and users can connect a reference of a variety of sizes or shapes to apply this methodology. To avoid covering irregularities on the surface of the sample, the reference paper should be as small as possible.

Figure 3.7 3D photogrammetry setup (a) setup (b) sample (c) reference circle

3.3.2 Setup

Pictures were taken in this work utilizing a handheld DSR camera and a Nikon D3400 digital camera with an 18-5 mm lens, using the suggested photogrammetry method. Each image was approximately 12 MG and 6000 × 4000 pixels.

It is crucial to correctly illuminate the sample during the shooting session to obtain high-resolution 3D models. Three continuous lights (800 W) with reflectors at the height of the sample were used to illuminate it. They were spaced approximately 1200 apart from one another. Newspapers were placed on top of white reflectors to portray the sample accurately. Because the background is used as a reference by 3D modeling software during rendering (when an image lacks positional information), an uneven background will aid in accurate rendering by photogrammetry programs. Adding two more continuous lights (800W each) with soft boxes that reflected light from a higher elevation also helped reduce shadows. The lights were randomly placed in these spots in accordance with the illumination requirements (Figure 3.8)

Figure 3.8 3D photogrammetry setup for shooting

3.3.3 Photography Process

During the photo shoot, zoom and flash were not used. The camera was raised using a tripod at three different heights to capture pictures of the samples (Figure 3.9a). The sample was placed. While snapping the photos, the camera should be located 20-30 cm away from the sample. The side and top camera positions are shown in Figure 3.9b and Figure 3.9c, respectively. Starting from the Elevation (0) - outer ring, a tripod was used to position the camera at a 50° to 150° angle to the sample surface. By moving in a circular motion, as depicted in Figure 3.9d, approximately 70 photos that were 50 mm away from one another were captured. Approximately 30 photos, spaced 100 apart, were taken in Elevation (1) – middle ring after raising the camera's elevation by approximately 500 to 600 compared to the surface of the sample. Finally, the camera was positioned approximately 750 - 800 away from the surface of the sample for the Elevation (2) - inner ring. To prevent the camera from casting

shadows on the sample surface, these elevations should not be 90°. At the highest elevations, ten more pictures were captured. The entire imaging process lasted between 60 min and 90 min for each sample. However, this process can be significantly shortened by utilizing a motorized turning setup.

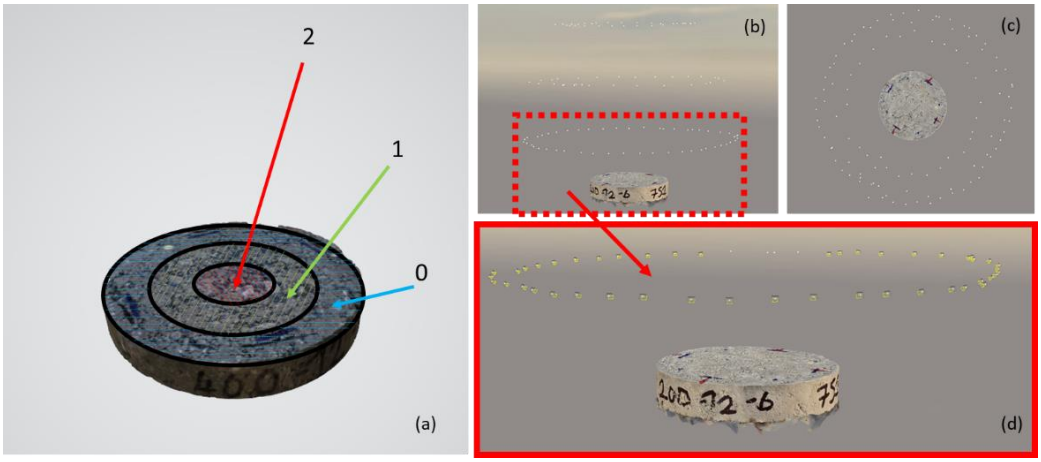

Figure 3.9 Camera positions (a)elevations (b)side view (c)top view (d)closer side view

3.3.4 Creation of 3D Model

Both commercial and free programs can help obtain a 3D point cloud or 3D mesh of any object, such as Autodesk ReCap, Elcovision 10, and ContextCapture. In this study, 3D models were created from 2D images using ContextCapture's educational license. Any compact digital, smartphone, DSLR, or fisheye camera can be used with ContextCapture software to analyze the captured images. The quality and scope of the final product are dependent on the camera resolution, even though the software has no minimum pixel requirements. In other words, a high-resolution camera can capture more data than a low-resolution one. As a result, more photos are needed to fully depict the object in 3D when using a low-resolution camera, which will lengthen the rendering time and vice versa. In this study, each image was approximately 12 MG and 6000 × 4000 pixels.

Additionally, the software accepts inputs in several digital image formats, including JPEG, TIFF, and PNG. ContextCapture can generate 3D models from photographs without location information by exploiting arbitrary position, rotation, and scale of the image. The software is compatible with 64-bit Windows XP/Vista/7/8/10 operating systems, 1 GB of AMD or NVIDIA graphics, and a minimum of 8 GB of RAM.

Two main nodules constitute the ContextCapture software, and both are necessary (Bentley Systems, 2019):

- ContextCapture Master: Data input, process setting editing, rendering process monitoring, and result visualization are all done using this module.
- ContextCapture Engine: Without user input, this module operates in the background environment. The function of the module is to perform aerotriangulation or 3D reconstruction.

The characteristics of the computer used for rendering and analysis in this study are as follows.

- 64-bit Windows 10 education operating system.
- Processor: Intel(R) Core (TM) i7-9750H CPU @ 2.60GHz, 6 Core(s), 12 Logical Processor(s).
- 32.0 GB RAM.
- Intel(R) UHD Graphics 630 and NVIDIA GeForce GTX 1650 graphic cards.

In this study, photographs were fed to ContextCapture using a DSLR camera (Nikon D3400) and the method described in the previous section. To pinpoint the locations of each photo, the photographs were subjected to aerotriangulation. The ContextCapture Engine was used to process the aerotriangulation. As shown in Figure 3.9b, the aerotriangulation procedure establishes the camera location for each image. To create a 3D Mesh in "obj" format, the sample's 3D Model had to be rebuilt. Depending on the number of pictures, a 3D mesh was created between 60 and 90 minutes for each sample. The configuration of the computer significantly affects the

duration of the operation and can be shortened by enhancing the computer configuration. After this stage, the Model was further edited to analyze the sample surface.

3.3.5 Editing 3D Model

The output model needs further work. Since the focus of this study was on the surface of the specimens, the sides and unnecessary parts of the objects had to be cut off. In Figure 3.10, an approximate cut is shown with a yellow dotted square, the region of interest for further analysis. In addition, measuring the actual dimensions of the specimens was a problem. Scaling was performed using the actual diameter of the reference paper. To obtain the actual dimensions of the specimens, the dimensions of the reference paper were measured in units in the editing program.

Software for altering the 3D mesh is widely available for free and/or commercially (MeshLab, Meshmixer, etc.). The open-source software used in this study for processing and manipulating 3D triangular meshes is MeshLab (Cignoni et al., 2008). It offers a selection of tools for texturing, converting, rendering, cleaning, and repairing meshes. It provides functionality for handling unprocessed data generated by 3D digitization equipment and devices, as well as for obtaining models ready for 3D printing. In addition, the interface is user-friendly. Consequently, it was employed in this study to edit 3D sample models and measure the dimensions.

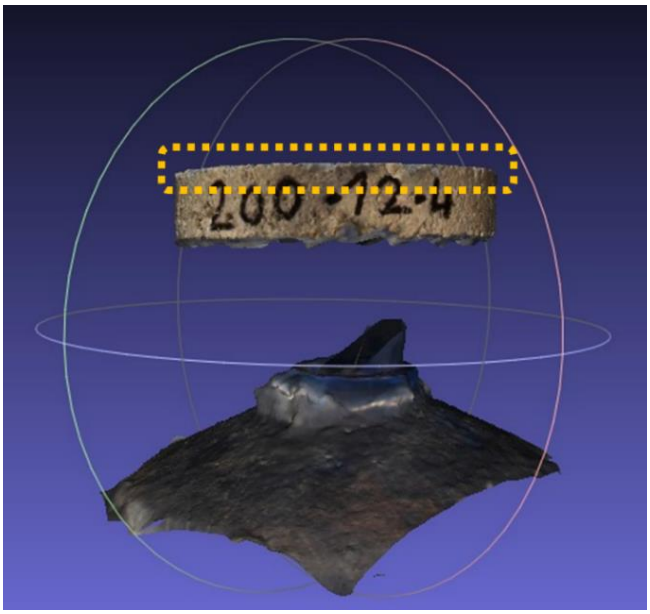

Figure 3.10 One of the samples needs editing

To prepare the sample model for further analysis, the "obj" file that was extracted from ContextCapture was imported into MeshLab (Figure 3.11a). Since the surface had the highest importance in this study, the surface of the sample was extracted simply using the cutting options of the MeshLab, as shown in Figure 3.11b-3.11e.

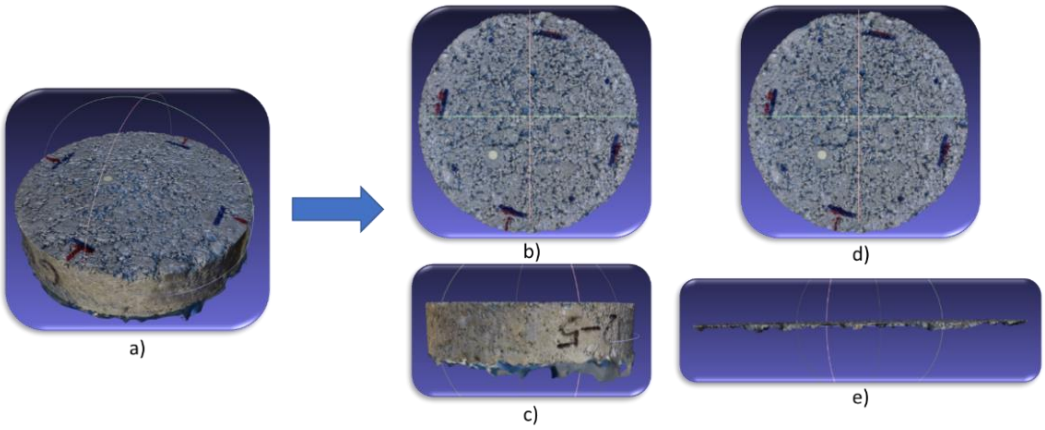

Figure 3.11 Editing 3D Model of sample a)3D sample model in MeshLab obtained from ContextCapture b) top view of the sample before editing c)side view of the sample before editing d)top view of the sample after editing e)side view of the sample after editing

The true sizes of the samples were determined using the pixel vise dimensions of the reference circle sticker. Using MeshLab's measuring tool, the lengths of several approximative diameters of the reference, as shown in Figure 3.12 (lines going through the approximative center), were measured.

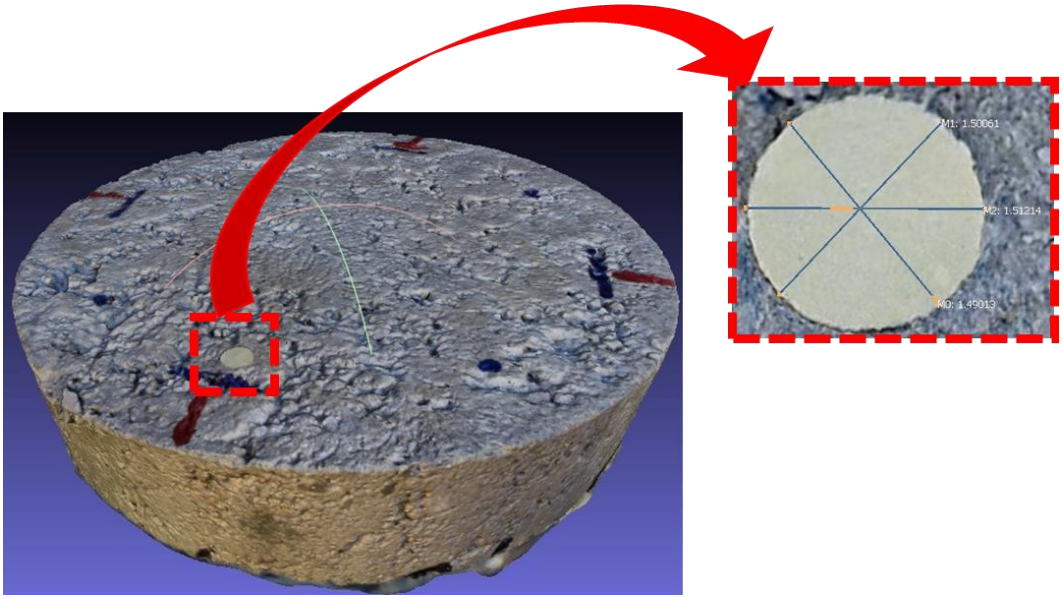

Figure 3.12 Reference circle and approximate diameters

To determine the actual dimensions of the sample in the future, the average length (dr: diameter of reference) was noted. Using the reference paper, conversion factors were obtained for each sample individually. All of the dr values were stored in a "txt" file to be used after the editing procedure conducted with Python Programming Language.

The PLY (Polygon File Format) file was extracted for each sample's standard triangulated 3D mesh. Subsequently, additional analyses were performed utilizing the Python programming language and DigitalSurf program.

3.4 Analysis with Python

PLY file of the model and PNG file of the texture for that specific model were extracted from MeshLab for further analysis with Python Programming Language. PLY files are a type of file used to store 3D geometric information, such as the form and appearance of objects in three dimensions. Applications for computer graphics and 3D modeling frequently employ the PLY file format created by the Stanford University. PLY can keep track of the details of the vertices, faces, edges, and other characteristics of 3D objects. Software tools can easily read and write data in this format because they support both binary and ASCII encoding. For further processing, PLY files are exported without Binary Encoding. When the sample model 1st plotted, a slightly tilted model and some unwanted points which are not coplanar were observed (Figure 3.13). Points not coplanar were due to missed points that were supposed to be deleted. The overall application conducted with Python is presented in Figure 3.14.

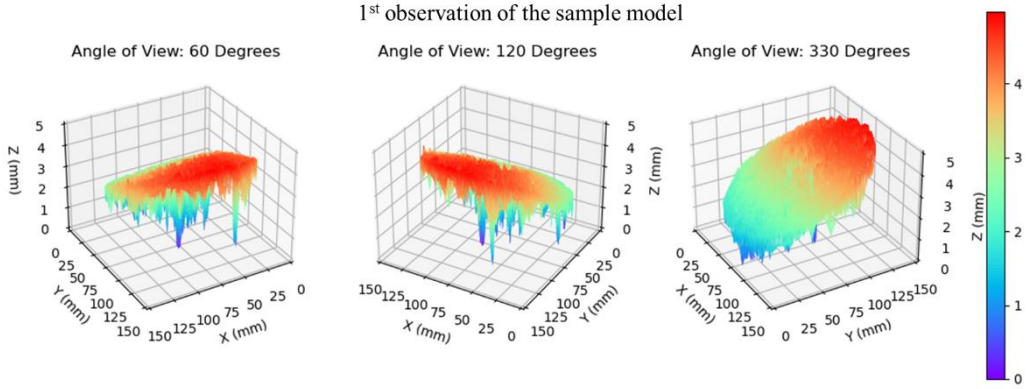

Figure 3.13 1st observation of sample model from three different angles

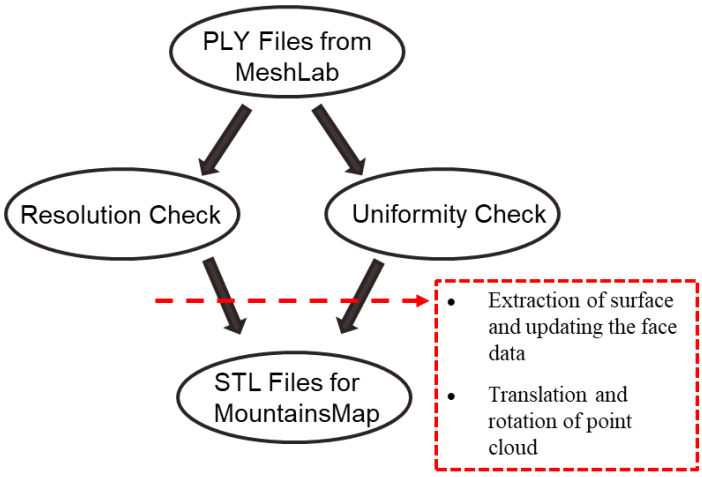

Figure 3.14. Flow chart of Python Application

3.4.1 Uniformity

To ensure the uniformity of the point clouds, further study with Python was conducted. This code is intended to analyze a collection of PLY-formatted point cloud files to determine if they are nonuniform. It calculates three distinct measurements for each file: mean minimum distance (Illian, Penttinen, Stoyan, & Stoyan, 2008), local density (Diggle, 2013), and Ripley's K-function (Ripley, 1976; Baddeley, Rubak, & Turner, 2015). Based on these measurements, non-uniform files were identified and removed from the list of PLY files that will later be processed. The three approaches are explained in detailed as follows.

The uniformity of the 3D point cloud was assessed using the mean minimum distance, as the first approach. The average distance between each cloud point and its closest neighboring point was calculated with the use of a KD tree. Since the 3D KD-tree is complex to explain the working principle, the 2D KD-tree is used for further explanation. 10 example points are chosen for illustration (See Figure 3.15).

The process of building a KD-Tree begins at a depth of 0, which serves as the root of the tree. During the preliminary phase, all the existing data points were considered. The aforementioned points are arranged in ascending order based on their X-

coordinates; subsequently, the median point is designated as the root. The root node was established at coordinates (6,7) based on the provided data. As a result, data points with an X-coordinate value lower than six are designated to the left subtree, whereas those with an X-coordinate value exceeding six are designated to the right subtree.

Upon descending to a depth of 1, attention is directed towards the left subtree owing to the presence of points (1,3) in that region. The points contained in this subtree are arranged in ascending or descending order according to their Y-coordinates. The median point (1,3) is identified as the root of this subtree based on the given arrangement. Within this particular context, any point that possesses a Y-coordinate value that is lower than three is designated to the left subtree of the node in question. Conversely, any point that possesses a Y-coordinate value greater than three is designated to the right subtree of the same node.

Advancing to a depth of 2 leads to the traversal of the right subtree originating from the node located at coordinates (1,3), owing to the presence of points (4,4) in that direction. The points in this subtree are arranged in ascending order based on their X-coordinate values. The root node of this subtree is determined by the median point located at coordinates (4,4) within the given collection. Following the established pattern, points possessing an X-coordinate value less than 4 are assigned to the left subtree of the given node, while those with an X-coordinate value greater than 4 are assigned to the corresponding right subtree.

At a depth of 3, the exploration proceeds towards the left subtree originating from the node located at (4,4), as point (2,5) is positioned within that subtree. The residual points within this subtree were arranged in a manner that adhered to a sorting criterion based on their Y-coordinate values. The median point, specifically (2,5), was designated as the root node of this subtree. At present, all available points are allocated and subdivided, resulting in the absence of any offspring for this particular node.

In a KD-tree, the approach to locating the nearest point is both systematic and iterative, starting at the root of the tree and delving deeper recursively, similar to a binary search. Each level of the tree is inspected, and based on the point's relative location to the current node (considering the X or Y coordinates), the algorithm explores either the left or right subtree. Upon reaching a leaf node, this point is temporarily regarded as the "closest." However, the actual nearest neighbor may not be this point because the search could have overlooked a subtree with potentially closer points. To verify the closest point, the algorithm retraces its steps and scrutinizes the unexplored half of the split at each level to determine if there is a closer point. This was determined by comparing the distance between the search point and the decision boundary with the distance between the search point and the current closest point. If the former is lower, there is a possibility that the other half contains a closer point, prompting a check. The procedure persists until the algorithm returns to the root, ensuring that all the subtrees that may hold a closer point have been examined. The point with the shortest distance to the search point among all inspected points was deemed the nearest neighbor (Figure 3.15a – the dashed line between (4,4) and (5,2).

The coded function that accomplishes the minimum distance search initiates from the root and moves recursively to the leaf nodes, continuously updating the minimum distance and the associated points throughout its journey. After examining all the feasible nodes and subtrees (Figure 3.15b), it outputs the smallest distance and associated points.

In the written code for the 3D KD-tree, the working principle was the same. After dividing the point cloud into batches for memory efficiency, each batch is used for the construction of the KD tree. The method employs the query function of KDTree for every element within the group, with a specified k value of 2 to determine the two nearest points, including the query point. The minimum distance between the query point and the nearest point was appended to a list named batch_min_distances. The query point was not considered in this calculation. The list stores the smallest distance for each point within the group. Upon completion of the processing of all

the groups, the aforementioned function calculates and subsequently yields the mean value of the minimum distances. The resulting value functions as a metric for evaluating the homogeneity of the point cloud. A uniform allocation of points is likely to result in reduced minimum distances, which are more consistent across the dataset.

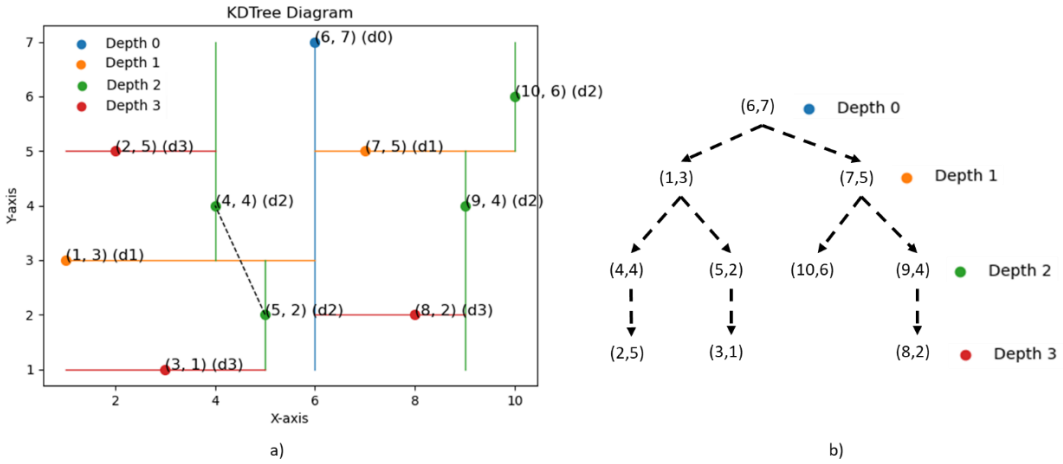

Figure 3.15. 2D KD-tree illustration a) Coordinate plots b) KD-tree branches

The 2nd approach used for the detection of uniformity was local density. A separate function was used to calculate the local density. The iterative process used in this function is the core component. It uses the query_ball_point method of KDTree to find all the points within a given radius for each point in the batch. The function then determines the local density for each point after identifying them. To do this, the volume of the sphere is divided, which is defined by the number of points that fall within it.

The local densities are kept in the list of initialized densities after the calculation is completed for each point in the batch. As each batch was processed, this process was repeated until all points were handled.

The function then calculates and returns the mean of these local densities after all batches are processed, and all local densities are calculated and stored. A general

metric for the uniformity of the point cloud is provided by the mean value. If the local densities are generally consistent throughout the cloud, a uniform distribution is suggested. However, a non-uniform distribution or clustering of points may be indicated by a significant variation in local densities.

In Figure 3.16a, the selected branch for the illustration of local density is shown with red arrows. In Figure 3.16b, the local density of the root point (Depth 0) is detected as 2 (including the query point shown in red). Local density is given as the number of points within the dashed green circle. In Figure 3.16c, d, and e, each local density is shown for each point.

For the 3D point cloud, this approach was also applied using the radius specific to the case. At the end of the analysis of local density, all of the files were found to be uniform.

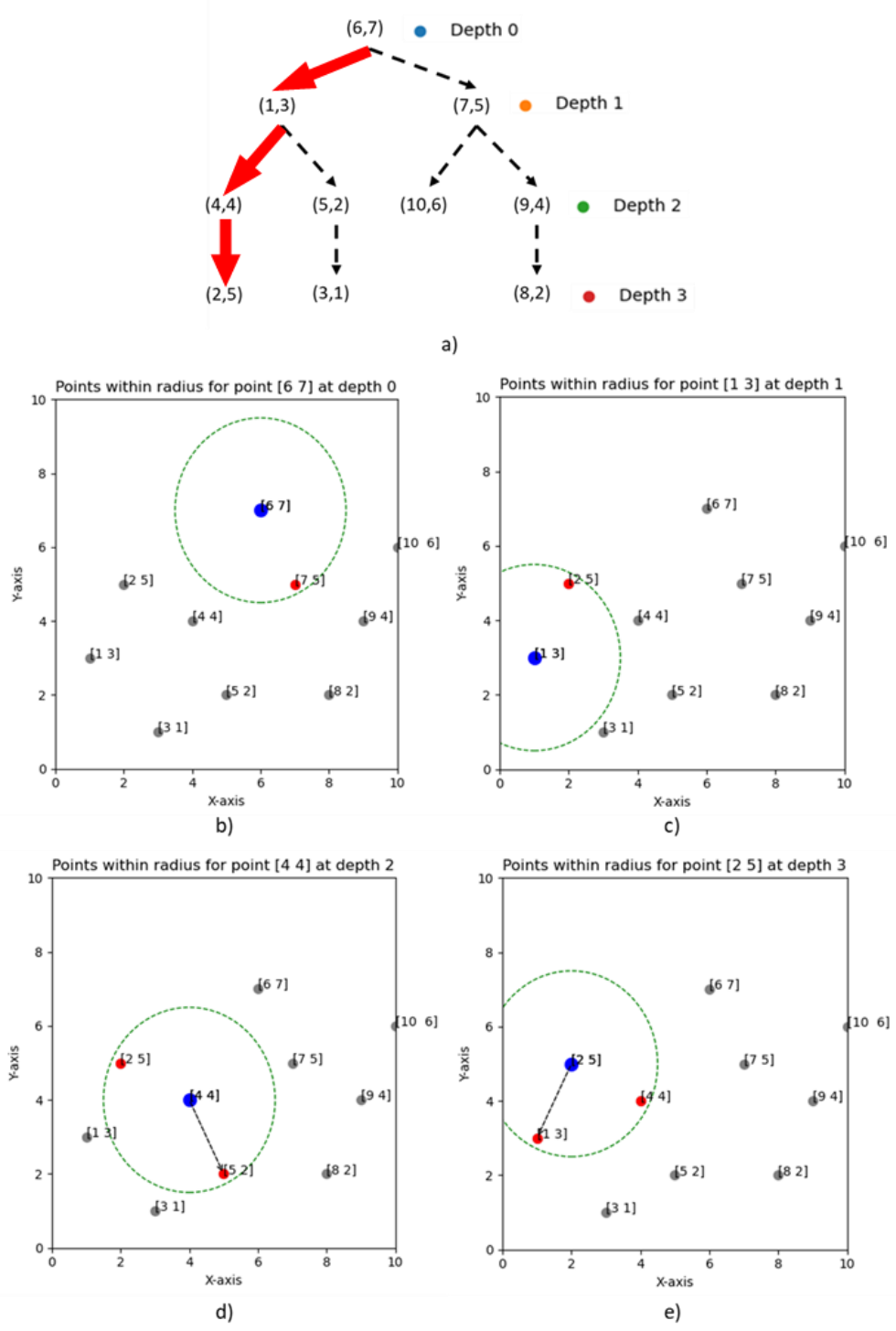

Figure 3.16. Local density using KD-tree a) Branches b) Depth 0 c) Depth 1 d) Depth 2 e) Depth 3

The 3rd approach used for the detection of uniformity was Ripley's K-function. The calculate_ripley_k function is an analytical tool that offers crucial insights when working with 3D point cloud data. This function calculates Ripley's K-function, a spatial statistic that enables the examination of the spatial arrangement of data points in a given set. By implementing this function, it becomes possible to ascertain if the points in the dataset are distributed uniformly, gathered in clusters, or scattered across the study area.

In executing the calculate_ripley_k function, three input parameters are required. These include the 'points', represented as a NumPy array holding the 3D point cloud data, 'radius', defining the sphere within which the K-function will be computed, and 'batch_size', which allows for the processing of points in batches, and defaults to 1000 if not specified.

Initially, the function determines the total count of batches needed to process all the points. This is achieved by dividing the total number of points by the batch size and rounding up the result. A blank list, known as k_values, is then created to hold the calculated K-function values for every batch.

The function proceeds by processing each batch. It identifies the start and end indices for the current batch, then retrieves the 3D coordinates of points within this batch. A structure is then created with these points, enabling quick spatial queries. The function then queries this structure for each point within the batch to identify all points lying within the specified radius. The K-function for the batch is computed using these counts by averaging the number of points inside the radius and dividing this by the volume of the sphere defined by the radius. The resulting K-function value for the batch is then stored in the k_values list.

Finally, the function calculates the overall Ripley's K-function by taking the mean of all K-function values computed for each batch, and this value is returned. In summary, the calculate_ripley_k function provides a mechanism to understand the spatial distribution of points within a 3D point cloud. This understanding becomes instrumental in shaping subsequent data processing and analytical strategies. In

particular, it allows for the assessment of point cloud uniformity, a critical aspect when making decisions concerning data segmentation, filtering, and other processing tasks.

3.4.2 Resolution

Because the point cloud is generated using photogrammetry and the sampled surfaces are primarily uniform owing to the use of SGC, it is reasonable to estimate the resolution using the mean of the minimum distances.

Python was used to calculate the x, y, and z coordinates of each vertex in a 3D model using the PLY file. Using tools such as NumPy and Pandas, these coordinates, which indicate the location of each vertex in the 3D space, were examined further. Using a conversion factor (dr) and dictionary references, the coordinates were converted to millimeters. The generated arrays were then centered around the origin by subtracting the minimum value of each position. The centroid of the model was determined using the **findCenter** function. Each sample was edited to eliminate unnecessary data (from the sides of the sample). After determining the approximate middle coordinates of the sample using the **findCenter** function, which was anticipated to be approximately (x= 75 and y = 75 mm) given that each sample was anticipated to have a diameter of 150 mm, the distances of each point to the approximate center were calculated and stored. To remove side points, points farther than 70.0 mm from the center were eliminated from the dataset. The modified x, y, and z coordinate lists were used to generate NumPy arrays, and the face editing procedure was used to modify the faces in the PLY file for the removed points. This procedure returned a new face list with the faces from the original face list that contained any of the modified data points removed as well as the indices of those data points.

When point cloud data is analyzed and transformed into a 3D model, the coordinates of each point represent pixels that collectively create an image of the surveyed area,

such as a cityscape, countryside, building, or transportation network. The accuracy and clarity of a 3D model depend on the density of the point cloud, similar to how the resolution of an image improves with more pixels per unit area. Therefore, a higher point density results in a more precise and detailed 3D digital model. In Figure 3.17, 3D edited sample (a), meshed 3D edited sample (b), and a closer look at the meshed sample (c) are given in MeshLab.

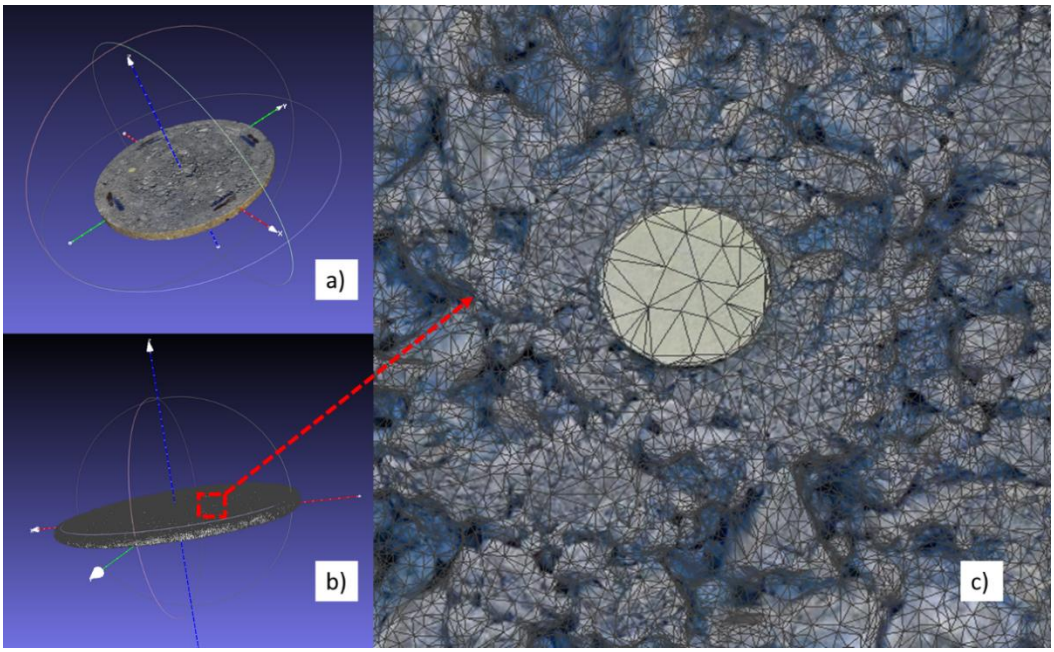

Figure 3.17 3D sample a) edited b) meshed c) closer look

To gain more insight into the resolution of the samples, further analyses were conducted. Another script was designed to analyze and process a collection of PLY-formatted 3D point-cloud files. Its primary function was to compute the minimum distance between points within each point cloud and perform various statistical analyses on the resulting data. The code also identifies outlier files, filters them, and further analyzes the filtered dataset. NumPy, pandas, SciPy, Open3D, and Matplotlib were utilized for calculations and visualizations. The workflow of the code includes the import of libraries, loading of data from a specified directory and a separate text file, and extraction and scaling of coordinates from point cloud data before

preprocessing. It then calculates the minimum distances for each point cloud using KDTree, identifies minimum distances, and computes summary statistics for the minimum distances.

As mentioned before, 108 samples were produced. While evaluating the roughness parameters, which is discussed later in this chapter, to have more consistence data some of the results are eliminated and in the end 91 of the samples were used. The resolution of these samples is also calculated considering the mean minimum distance of those samples (Figure 3.18a and b). The median distance of 0.0027 mm in this sample set was close to the mean, with a mean minimum distance of 0.0029 mm. A tightly packed distribution of the data is also indicated by a lower standard deviation of 0.0014. The minimum and maximum values in this dataset were 0 and 0.0061 mm, respectively. The Q1, Q3, and IQR values of the filtered dataset were 0.0018 mm, 0.0038 mm, and 0.0020 mm, respectively, showing a reduced spread of the middle 50% of the data. The distribution of the filtered dataset was less skewed than that of the original dataset, with positive skewness of 0.3134. As a result, the resolution was obtained to be 0.003 mm.

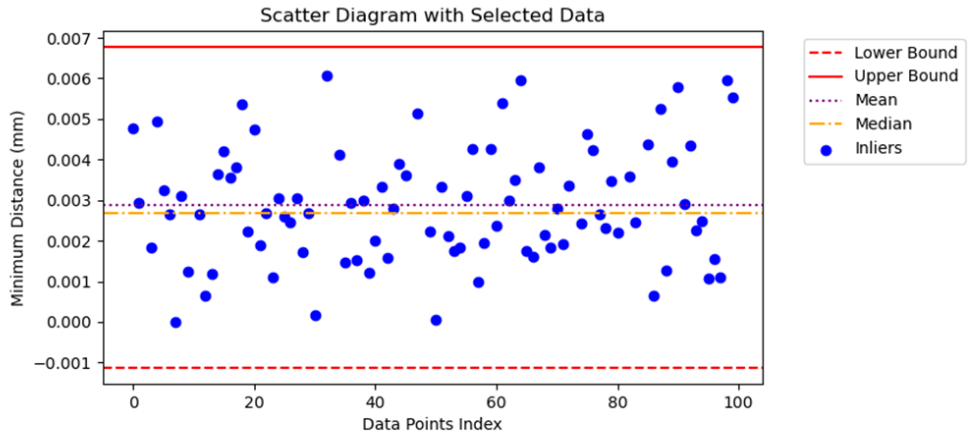

a)

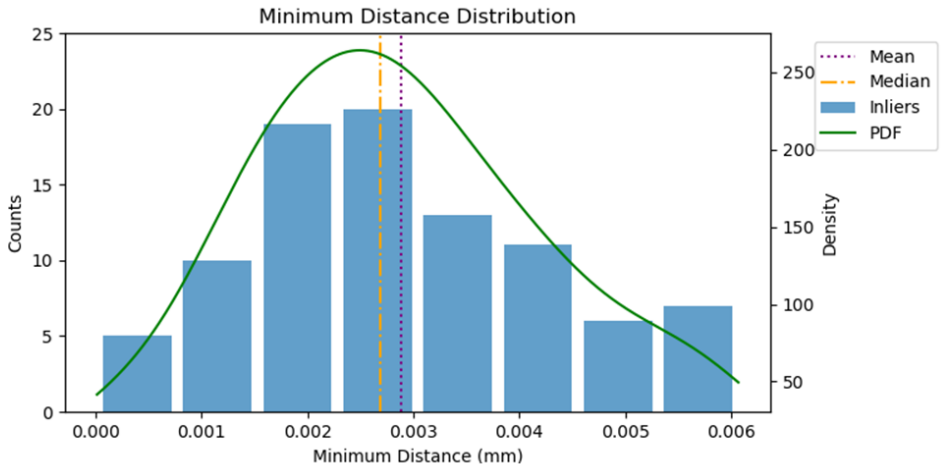

b)

Figure 3.18 Plots of selected samples a) Scatter b) Histogram

3.4.3 STL file production

The code also addresses the common issue of aligning two sets of corresponding 3D point data by using least-squares errors. This issue has emerged in various fields, including mechanical technology and PC vision. To achieve this alignment, the code uses either a Rigid or Euclidean transform, executing a succession of interpretations and turning point information. First, translation is performed by adding a translation

vector to the x-, y-, and z-coordinates of the point data. Next, a rotation matrix was applied to the translated point data for each point to perform the transformation Figure 3.19a-b.

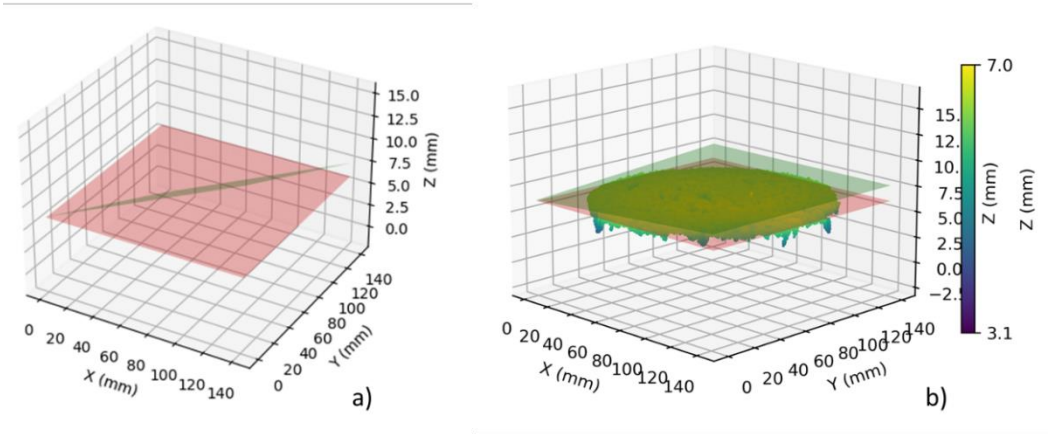

Figure 3.19 a) Reference plane (red) and mean plane of the sample (green) b) Best-fit planes with point cloud data

In Figure 3.20a and b, before and after plots and in Figure 3.20c height distribution of the output point cloud is given.

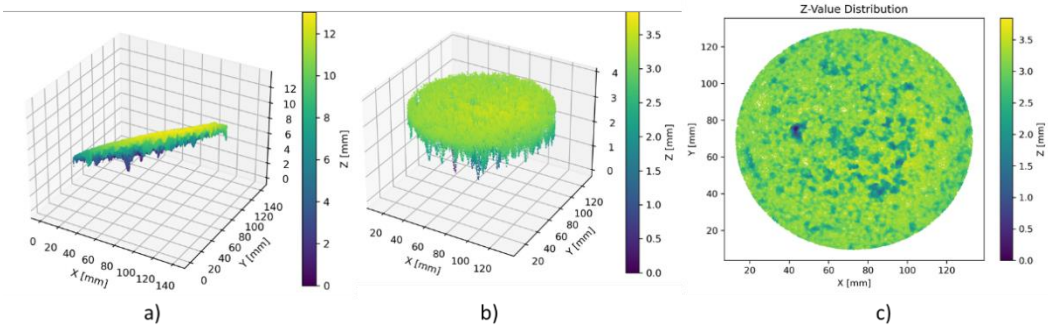

Figure 3.20 a) Original point cloud b) Side points removed and rotated point cloud c) Height distribution of point cloud at the end of all the processes

3.5 Analysis with MountainsMap

MountainsMap Premium is a software launched by DigitalSurf, a French company. Mountains® software has been recognized as the standard for surface and image analysis by engineers, scientists, and researchers worldwide. It comprises five product families with specific solutions for spectroscopy, scanning probe microscopy, electron microscopy, profilometry, and multi-instrument data confluence. MountainsMap Premium 9.3.10200 was used in this thesis.

The steps of the analysis done with MountainsMap are shown below with a flow chart (Figure 3.21) and each step is discussed in detail later in this chapter.

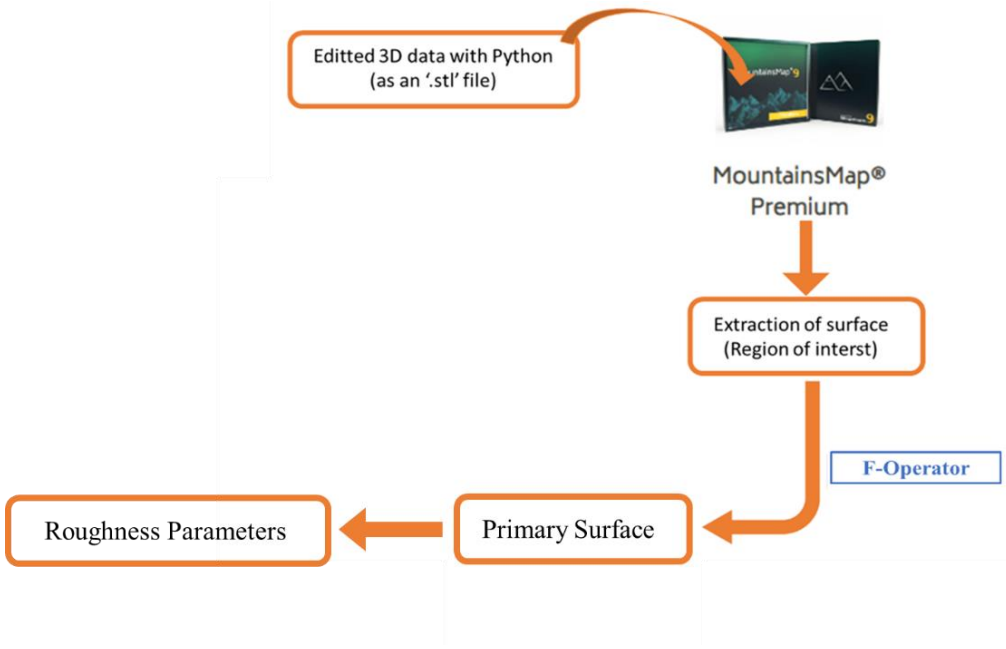

Figure 3.21 Flow chart of the analysis

The Python analysis output STL (Figure 3.22a) files were imported into MountainsMap Premium 9.3.10200 software for further evaluation of the surface parameters. To conduct this analysis, surface subtraction was performed, as suggested by ISO 25178-2, which suggests the use of square surfaces for such evaluations (Figure 3.22b).

Following the extraction of the appropriate surface areas, an F-operator, specifically the least-squares plane (LSPL) method, was implemented. This procedure resulted in the formation of a primary surface that was used for a more thorough examination of surface parameters, which were discussed in Chapter 2 in detail.

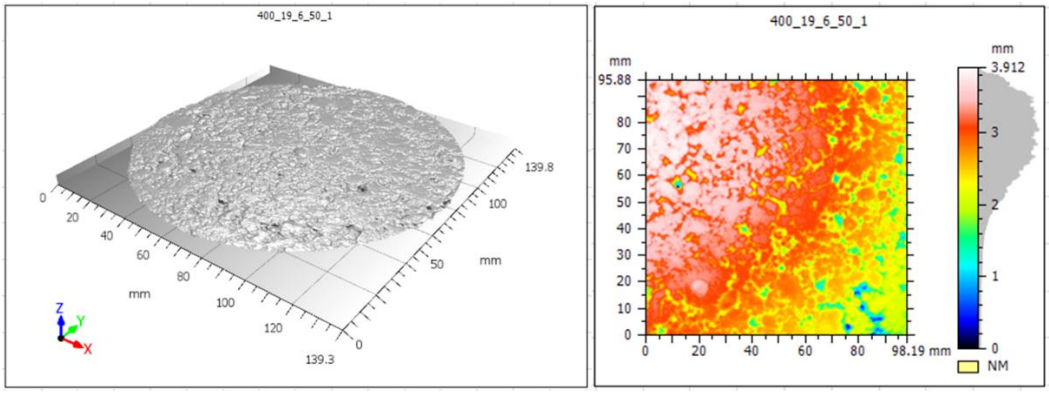

a) b)

Figure 3.22 a) STL file b) Extracted surface

CHAPTER 4

RESULTS AND DISCUSSION

This chapter presents a thorough experimental design aimed at evaluating different RCC mix designs. In addition, laboratory experiments were conducted to examine the impact of RCC mixing parameters on the macrotexture and microtexture properties, and the results are reported herein. This study employed various image-based analysis techniques, including 3D photogrammetry, Python-based methods, and MountainsMap software, to investigate the impact of RCC mix design parameters on surface texture.

4.1 Laboratory Experiments

As discussed in the previous chapter, British Pendulum and sand patch tests were implemented. MTD and wet and dry BPN values for RCC combinations were given in Table 4.1. The results are the average values of three samples in each case. In addition, Vebe consistency times from a previous study by Sengun et al. (2019) are also shown in the corresponding table to analyze their relationship with surface properties.

As shown in Table 4.1, the surface depth for 200-dose mixtures averages 0.46 mm, while for 400-dose mixtures it varies as a function of aggregate size, being 0.32 mm for Dmax-12 mm and 0.25 mm for Dmax-19 mm. The MTD value of the 400-dose mixes was measured very low given these results, even though the MTD value of the 200-dose mixes was following the values of the Highways Technical Specification for Concrete Road. In Figure 4.1a, b, and c, MTD values of RCC samples are presented.

Table 4.1 Macro and microtexture surface properties of RCC values (Shabani et al., 2021)

Cement Dosage (kg/m^3)	Dmax (mm)	Water Content (%)	Vebe Time	Gyration No	Compaction Ratio(%)	Average Texture depth(mm)	Skid Resistance Number(BPN)*	Skid Resistance Number(BPN)**
200	12	4	55	50	94.4	0.50	73	64
				60	94.1	0.49	71	65
				75	94.9	0.47	71	71
		5	32	50	96.2	0.51	71	66
				60	95.4	0.52	71	67
				75	95.8	0.51	70	67
		6	21	50	97.0	0.42	69	64
				60	99.0	0.39	68	65
				75	99.1	0.37	70	64
	Avg.					**0.46**	**70**	**66**
	19	4	60	50	95.2	0.49	69	62
				60	94.8	0.42	69	62
				75	94.8	0.43	69	61
		5	28	50	96.2	0.50	72	65
				60	96.9	0.48	70	63
				75	97.5	0.49	69	64
		6	10	50	97.1	0.54	69	62
				60	97.8	0.46	68	62
				75	98.6	0.35	68	61
	Avg.					**0.46**	**69**	**62**
400	12	4	70	50	92.4	0.31	70	62
				60	92.5	0.25	73	62
				75	92.8	0.32	70	60
		5	73	50	94.3	0.41	72	66
				60	93.9	0.37	71	66
				75	95.0	0.35	70	63
		6	70	50	97.8	0.29	70	65
				60	98.1	0.30	67	64
				75	98.9	0.31	65	63
	Avg.					**0.32**	**70**	**63**
	19	4	81	50	92.8	0.24	70	60
				60	92.7	0.20	69	60
				75	92.9	0.20	70	58
		5	51	50	93.8	0.27	70	64
				60	94.3	0.32	69	62
				75	94.5	0.33	70	64
		6	28	50	97.5	0.24	69	61
				60	97.4	0.25	70	63
				75	97.5	0.20	69	56
	Avg.					**0.25**	**69**	**61**

Notes: (*): BPN numbers for dry condition, (**): BPN numbers for wet condition (50 ml)

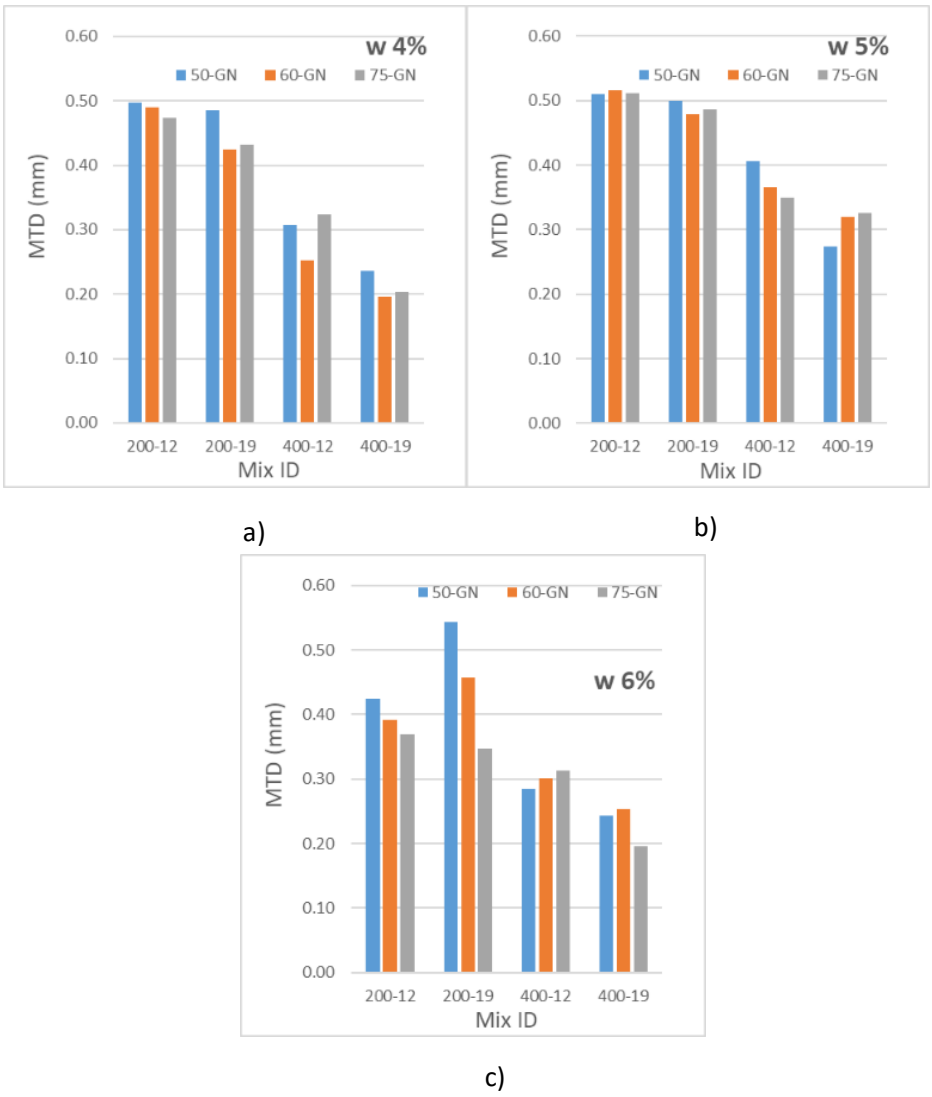

Figure 4.1 The measured MTD values of RCC mixture for water contents of a) 4% b) 5% c) 6% (Shabani et al., 2021)

The wet BPN values (presented in Figure 4.2a, b, and c) were lower than the dry BPN values (presented in Figure 4.3a, b, and c) when examining the surface properties of the microtexture. Looking at the average values for all RCC mixes, the BPN value for the dry surface was 70, for 200 dosages 64, and 400 dosages 62. These BPN values show that RCC pavements belong to the "Class V" and "extremely low slip" classes compared to the slip classification values in Table 3.4.

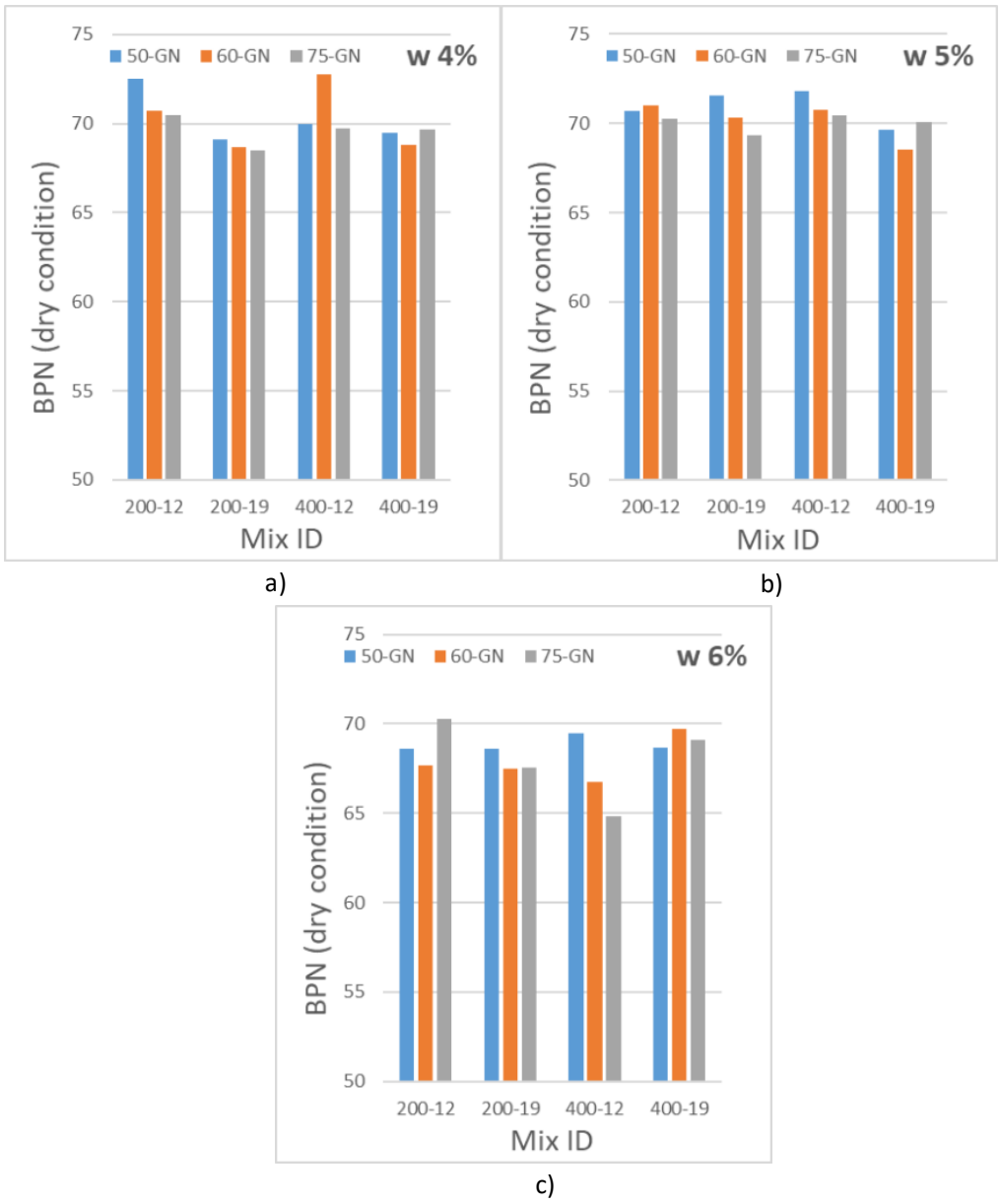

Figure 4.2 The measured BPN values in dry condition of RCC mixture for water contents of a) 4% b) 5% c) 6% (Shabani et al., 2021)

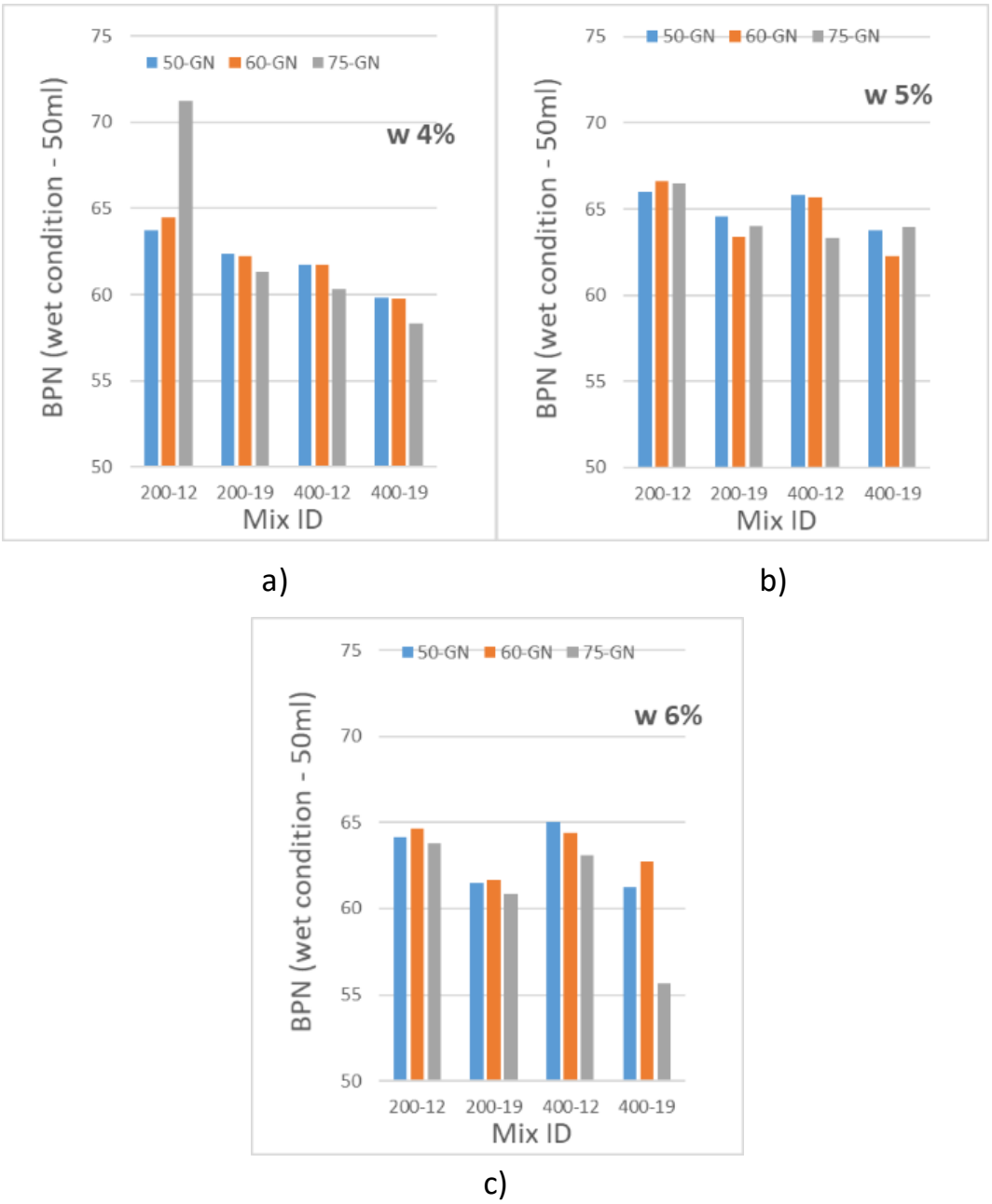

Figure 4.3 The measured BPN values in the wet condition of RCC mixture for water contents of a) 4% b) 5% c) 6% (Shabani et al., 2021)

These results are critical in highlighting the effect of cement dosage and Dmax on improving the surface properties of RCC in the Institution of Civil Engineers Highway Design and Management Guide (ICE). To improve the surface properties of RCC, the guide recommends increasing the cement dosage and decreasing the

maximum aggregate grain size in the mix design. However, the effects of mix settings on the surface properties of macro- and microtexture were not studied separately. In the laboratory experiments of this study, it was found that combinations with a lower Dmax had a more favorable effect on road safety in terms of MDT and BPN values while increasing the cement dosage resulted in a noticeable deterioration, especially of the macro-surface texture. It should also be emphasized that the amount of cement added in this study is well above the mix ratio of RCC commonly used in rural roads.

Statistical analyses were performed on the data in Table 4.1 and examined in Sections 4.1.1 and 4.1.2 to better understand the effects of RCC mixing parameters on micro- and macrotexture properties.

4.1.1 Effect of RCC Mixing Parameters on Macrotexture

One-way (one-factor) analysis of variance (ANOVA) was performed to determine the influence of the RCC mix parameters of cement dosage, water content, Dmax, and gyration number on the RCC macrotexture (Table 4.2) (Shabani et al., 2021). A total of 108 sample results were used in the statistical analysis of ANOVA and parameters with a p-value less than 0.1 ($p < 0.1$) were assumed to have a significant effect on the results. The significance value (p-value) was determined by choosing a confidence interval of 90%. Moreover, the fact that the p-value is less than 0.01 (1%) indicates that the dependent variable in question has a significant influence on the independent variable.

Cement dosage and water content, two RCC mixing parameters, were quite effective ($p < 0.01$) on the MTD, as shown by the p-values calculated independently for each parameter. Therefore, it should be clear that the water content in RCC mixes influences surface texture properties in addition to strength

Table 4.2 Statistical analysis of the effects of RCC mixing parameters on macrotexture (Shabani et al., 2021)

Source of Variation	ANOVA Results					
		SS	df	MS	F	**P-value**
Cement Dosage	Between Groups	0.821	1	0.821	179.820	**0.000**
	Within Groups	0.492	106	0.005		
	Total	1.314	107			
Dmax	Between Groups	0.034	1	0.034	2.822	**0.096**
	Within Groups	1.280	106	0.012		
	Total	1.314	107	0.034		
Gyration No	Between Groups	0.024	2	0.012	0.992	**0.374**
	Within Groups	1.289	105	0.012		
	Total	1.314	107	0.012		
Water Content	Between Groups	0.108	2	0.054	4.726	**0.011**
	Within Groups	1.205	105	0.011		
	Total	1.314	107	0.054		

Note: SS; Sum of squares, MS; Mean Square, df; degree of freedom

For the same samples, ANOVA analysis was repeated and the significance value (p-value) was determined by choosing a confidence interval of 95%. Also, while Shabani et al., (2021) considered one fixed variable, in this study, multiple variable analysis was conducted. In Table 4.3, an ANOVA analysis of MTD values was given. With the performed analysis, the effect of design parameters and a group of parameters on MTD could be observed (The color red is used to highlight p-values less than 0.05).

The statistical analysis demonstrates that with p-values less than 0.05, the variables Cement Dosage, Dmax, W (%), and GN have significant effects on the MTD (Table 4.3). This suggested that when considered separately, each of these factors had a significant effect on the outcome variable.

As the maximum aggregate size (Dmax) increased, the MTD decreased at a constant cement dosage (Figure 4.4a). Larger aggregates occupied more space within the matrix, which created a more uneven surface, potentially reducing the macrotexture and MTD. The performance of a pavement under diverse traffic conditions might be affected by the skid resistance provided by a surface with a reduced macrotexture.

Table 4.3 ANOVA analysis of MTD

ANOVA for MTD (Crossed Design)					
Source	Sum of Squares	Degrees of Freedom	Mean Square	F	p Value
Cement Dosage	0.822	1	0.822	348.661	0.0000
Dmax	0.0340	1	0.0340	14.425	0.0003
W(%)	0.109	2	0.0543	23.058	0.0000
GN	0.0243	2	0.0121	5.152	0.0081
Cement Dosage*Dmax	0.0282	1	0.0282	11.969	0.0009
Cement Dosage*W(%)	0.0219	2	0.0109	4.636	0.0128
Cement Dosage*GN	0.00804	2	0.00402	1.706	0.1889
Dmax*W(%)	0.0184	2	0.00919	3.899	0.0247
Dmax*GN	0.00793	2	0.00397	1.683	0.1930
W(%)*GN	0.0235	4	0.00588	2.496	0.0502
Cement Dosage*Dmax*W(%)	0.00629	2	0.00315	1.335	0.2697
Cement Dosage*Dmax*GN	0.00428	2	0.00214	0.909	0.4077
Cement Dosage*W(%)*GN	0.00797	4	0.00199	0.845	0.5010
Dmax*W(%)*GN	0.0237	4	0.00592	2.511	0.0491
Cement Dosage*Dmax*W(%)*GI	0.00599	4	0.00150	0.636	0.6386
Within	0.170	72	0.00236		
Total	1.314	107			

As the cement dosage increased, the MTD decreased (Figure 4.4b). The denser cementitious matrix observed could be attributed to the utilization of higher cement dosages. Increasing the density of the matrix produced a more uniform surface texture, which led to decreased macrotexture, thereby causing a decrease in the MTD. The decrease in MTD could potentially affect the skid resistance of the pavement. This was because a decrease in texture may lead to a reduction in the capacity of the surface to sustain traction with the vehicle tires.

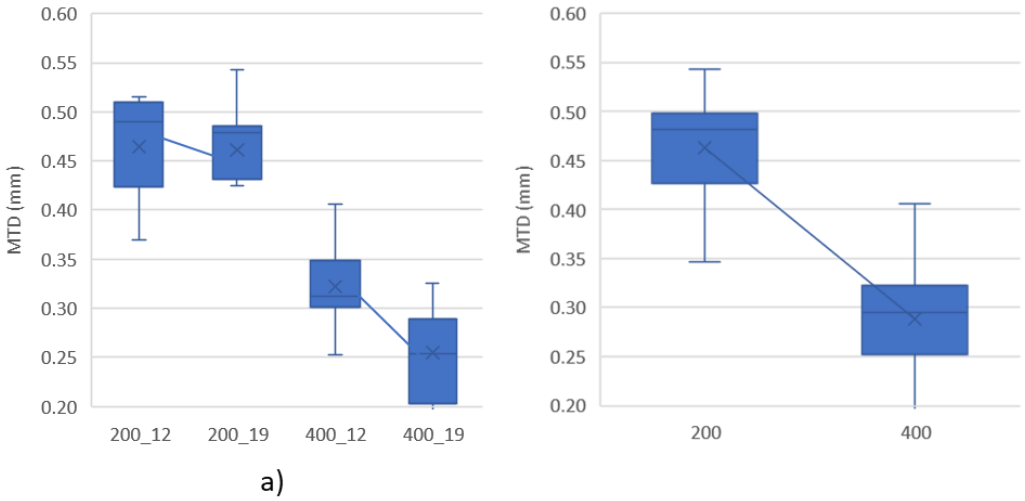

Figure 4.4 The MTD change under the effect of a) Dmax b) Cement Dosage

The role of water content in the MTD is noteworthy, as evidenced by the curve-like pattern observed across three distinct water content levels (4%, 5%, and 6%) as shown in Figure 4.5.

The apex of the MTD was observed to have a water content of 5%. This implies the existence of an optimum water content that maximizes the formation of the macrotexture. Insufficient hydration of the cement may occur because of the lower water content (4%), leading to ineffective packing and potentially larger voids, which may result in a higher MTD. An increased water content of 6% has the potential to induce greater shrinkage and compaction while the material is undergoing the curing process. This can lead to the development of a more compact matrix with a reduced MTD. The attainment of the highest MTD and the consequent improvement in skid resistance is facilitated by the equilibrium achieved through the utilization of an ideal water content of 5%.

Statistical analysis revealed that the p-value associated with the gyration number was 0.0081, suggesting that it exerts a significant impact on MTD. The number of gyrations quantifies the degree of compaction achieved during pavement manufacturing. An increased gyration number indicates greater compaction, leading

to a reduction in MTD and a smoother surface texture. In contrast, a decreased gyration number indicates reduced compaction, potentially resulting in a coarser surface texture and increased MTD.

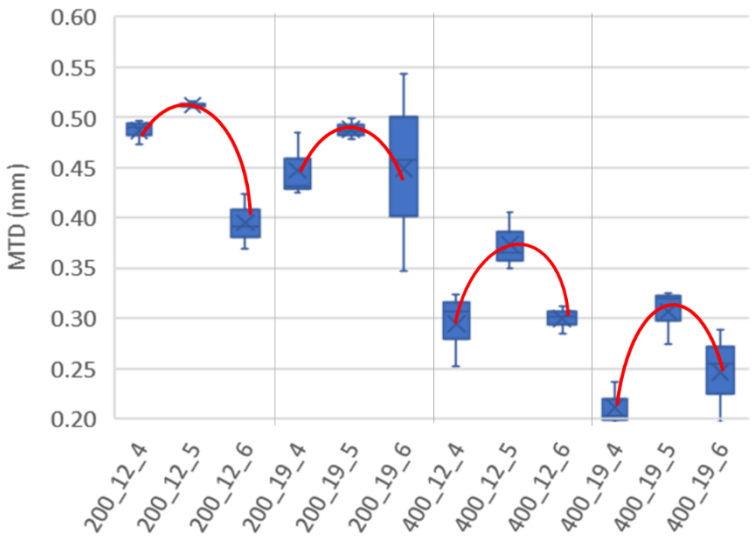

Figure 4.5 Water content effect on MTD

4.1.2 Effect of RCC Mixing Parameters on Microtexture

The BPN values measured both in dry and wet conditions are presented in Figure 4.6, Figure 4.7, Figure 4.8, and Figure 4.9. As expected, when the surface gets wet BPN values get smaller. The ANOVA results obtained for BPN values for both conditions were presented in Table 4.4 for dry conditions and Table 4.5 for wet conditions. The results indicated that gyration number and maximum aggregate size combined with water content, were the common sources, that significantly affected BPN values in both conditions.

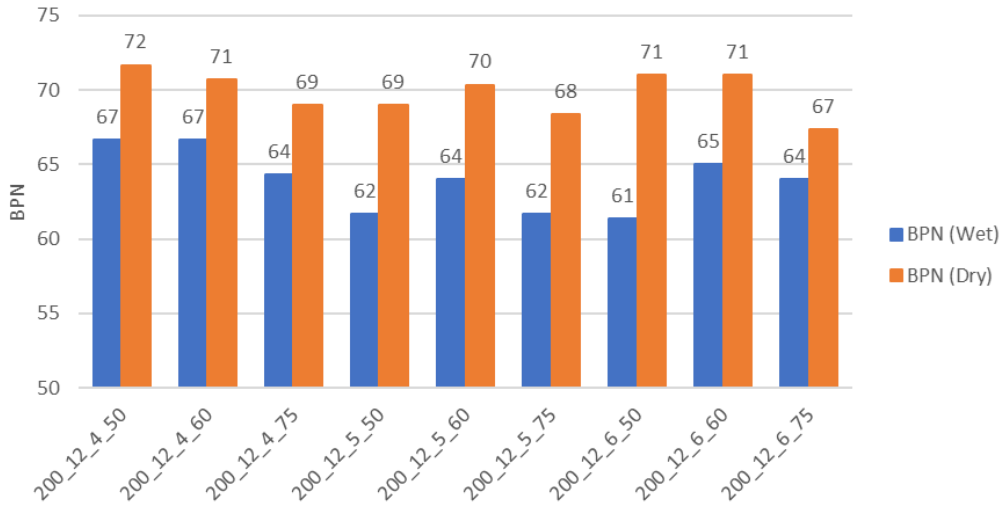

Figure 4.6 BPN results for CD:200 and Dmax:12 comparison for both conditions (dry and wet)

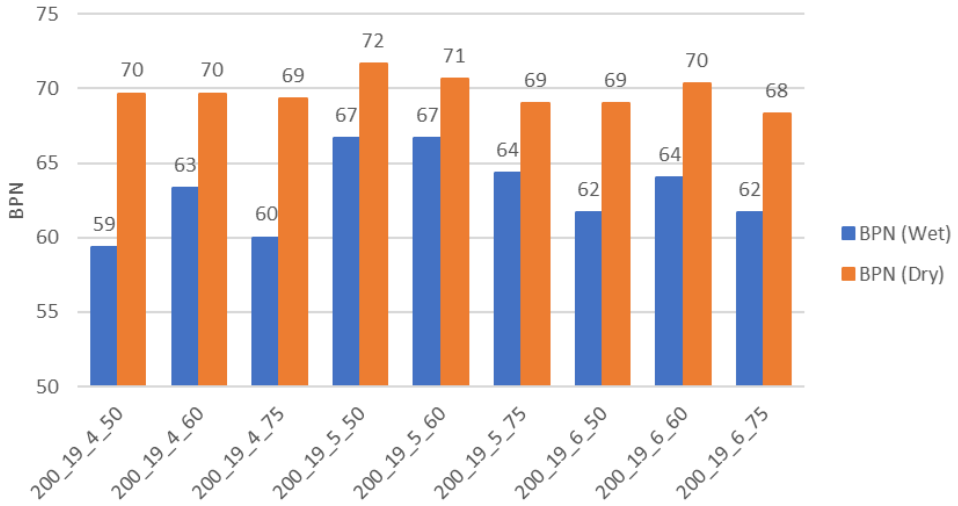

Figure 4.7 BPN results for CD:200 and Dmax:19 comparison for both conditions (dry and wet)

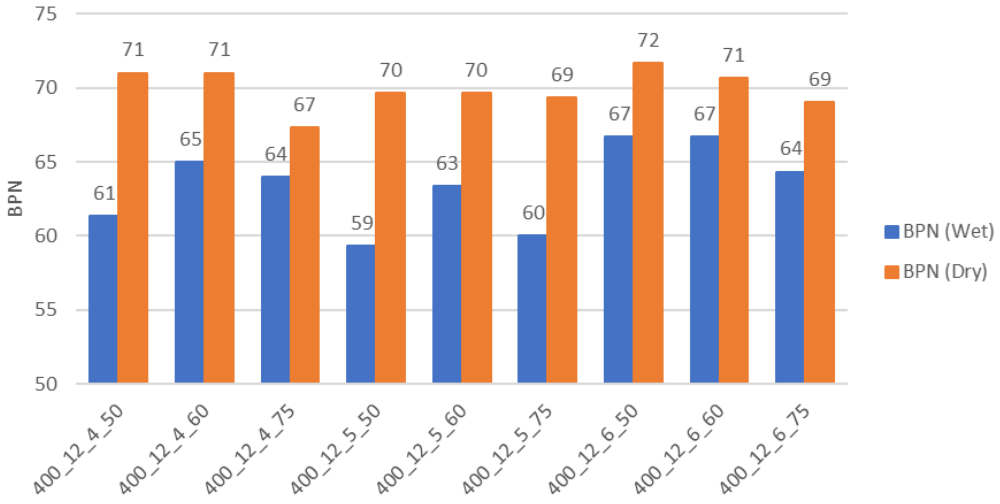

Figure 4.8. BPN results for CD:400 and Dmax:12 comparison for both conditions (dry and wet)

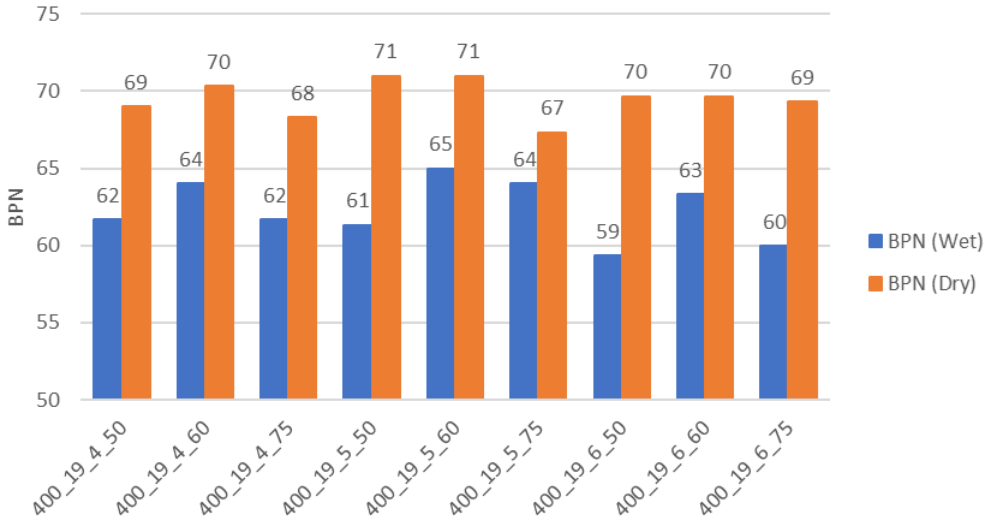

Figure 4.9. BPN results for CD:400 and Dmax:19 comparison for both conditions (dry and wet)

Table 4.4 ANOVA analysis of BPN in dry condition

ANOVA for BPN (dry) (Crossed Design)					
Source	Sum of Squares	Degrees of Freedom	Mean Square	F	p Value
Cement Dosage	0.0833	1	0.0833	0.060	0.8072
Dmax	1.565	1	1.565	1.127	0.2920
W(%)	0.000	2	0.000	*	*
GN	84.50	2	42.25	30.420	0.0000
Cement Dosage*Dmax	0.750	1	0.750	0.540	0.4648
Cement Dosage*W(%)	4.667	2	2.333	1.680	0.1936
Cement Dosage*GN	0.0556	2	0.0278	0.020	0.9802
Dmax*W(%)	12.52	2	6.259	4.507	0.0143
Dmax*GN	3.574	2	1.787	1.287	0.2825
W(%)*GN	0.000	4	0.000	*	*
Cement Dosage*Dmax*W(%)	2.000	2	1.000	0.720	0.4902
Cement Dosage*Dmax*GN	1.722	2	0.861	0.620	0.5408
Cement Dosage*W(%)*GN	10.44	4	2.611	1.880	0.1232
Dmax*W(%)*GN	28.59	4	7.148	5.147	0.0011
Cement Dosage*Dmax*W(%)*G	3.778	4	0.944	0.680	0.6081
Within	100.0	72	1.389		
Total	254.3	107			

Table 4.5 ANOVA analysis of BPN in wet condition

ANOVA for BPN (50 ml) (Crossed Design)					
Source	Sum of Squares	Degrees of Freedom	Mean Square	F	p Value
Cement Dosage	12.00	1	12.00	3.823	0.0544
Dmax	27.00	1	27.00	8.602	0.0045
W(%)	0.000	2	0.000	*	*
GN	136.5	2	68.25	21.743	0.0000
Cement Dosage*Dmax	0.593	1	0.593	0.189	0.6652
Cement Dosage*W(%)	27.56	2	13.78	4.389	0.0159
Cement Dosage*GN	5.056	2	2.528	0.805	0.4509
Dmax*W(%)	216.0	2	108.0	34.407	0.0000
Dmax*GN	1.056	2	0.528	0.168	0.8456
W(%)*GN	0.000	4	0.000	*	*
Cement Dosage*Dmax*W(%)	73.19	2	36.59	11.658	0.0000
Cement Dosage*Dmax*GN	2.352	2	1.176	0.375	0.6889
Cement Dosage*W(%)*GN	24.22	4	6.056	1.929	0.1148
Dmax*W(%)*GN	8.444	4	2.111	0.673	0.6131
Cement Dosage*Dmax*W(%)*G	35.04	4	8.759	2.791	0.0325
Within	226.0	72	3.139		
Total	795.0	107			

The gyration number is indicative of the degree of compaction exhibited by the RCC specimens and is a factor that exerts an impact on the texture of the pavement surface. The ANOVA findings (Table 4.4a and b) revealed that the p-value for the gyration number was zero for both dry and wet conditions, signifying a statistically significant impact on BPN values. The data exhibited an obvious trend wherein the BPN values reached their maximum values (under both dry and wet conditions) at a gyration number of 60 (Figure 4.10, Figure 4.11, Figure 4.12, and Figure 4.13).

This phenomenon could be attributed to the fact that a moderate level of compaction, characterized by a gyration number of 60, achieves an optimal balance between surface roughness and smoothness, thereby leading to an improvement in skid resistance. The implementation of lower or higher compaction levels may result in a surface that is excessively rough or smooth, thereby causing a decrease in the skid resistance.

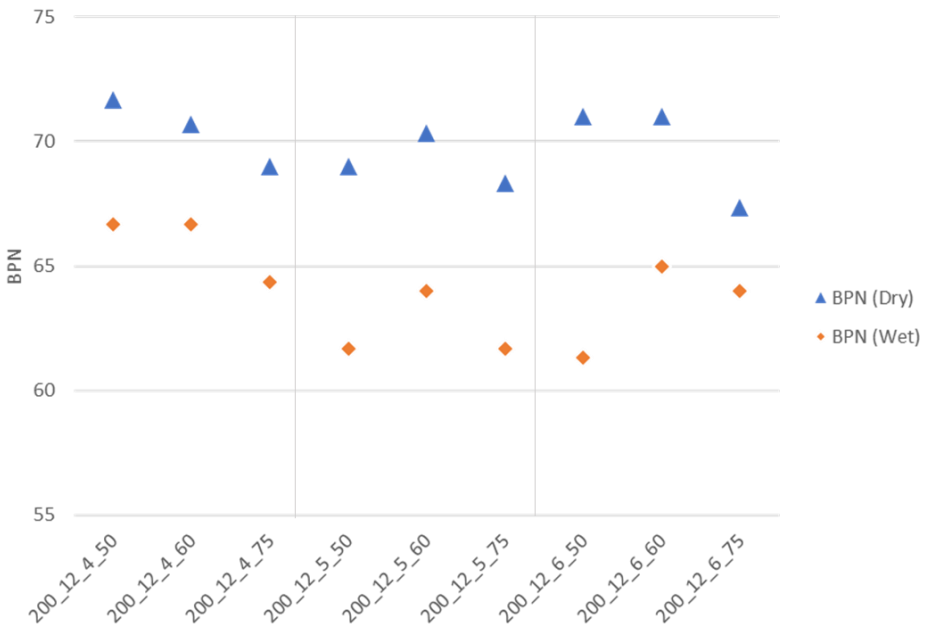

Figure 4.10 Gyration number effect on BPN values for CD:200 and Dmax:12 comparison for both conditions (dry and wet)

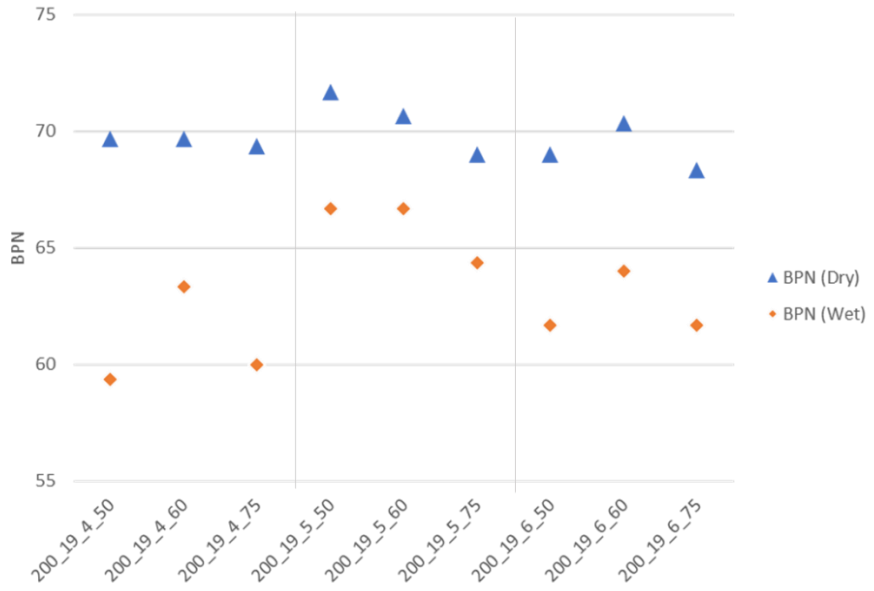

Figure 4.11. Gyration number effect on BPN values for CD:200 and Dmax:19 comparison for both conditions (dry and wet)

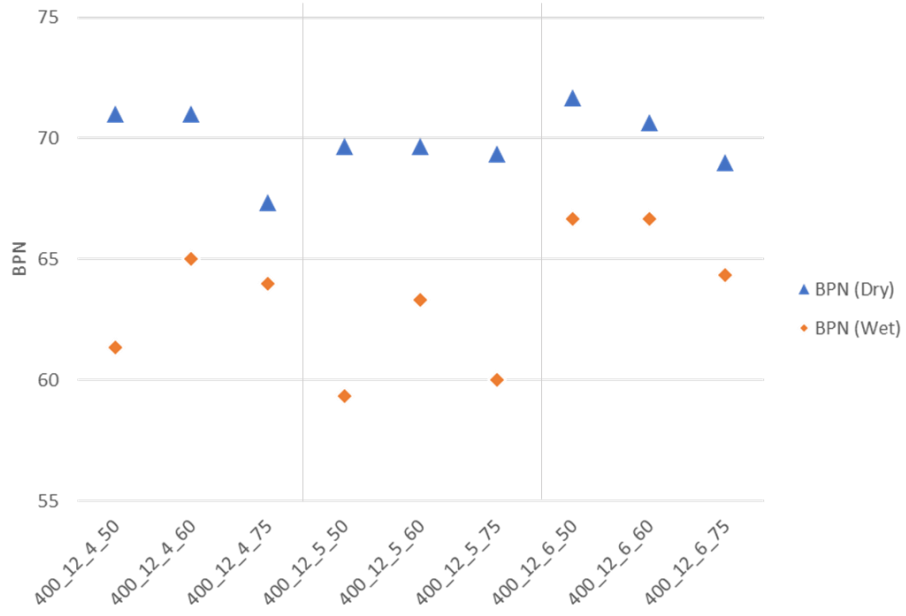

Figure 4.12. Gyration number effect on BPN values for CD:400 and Dmax:12 comparison for both conditions (dry and wet)

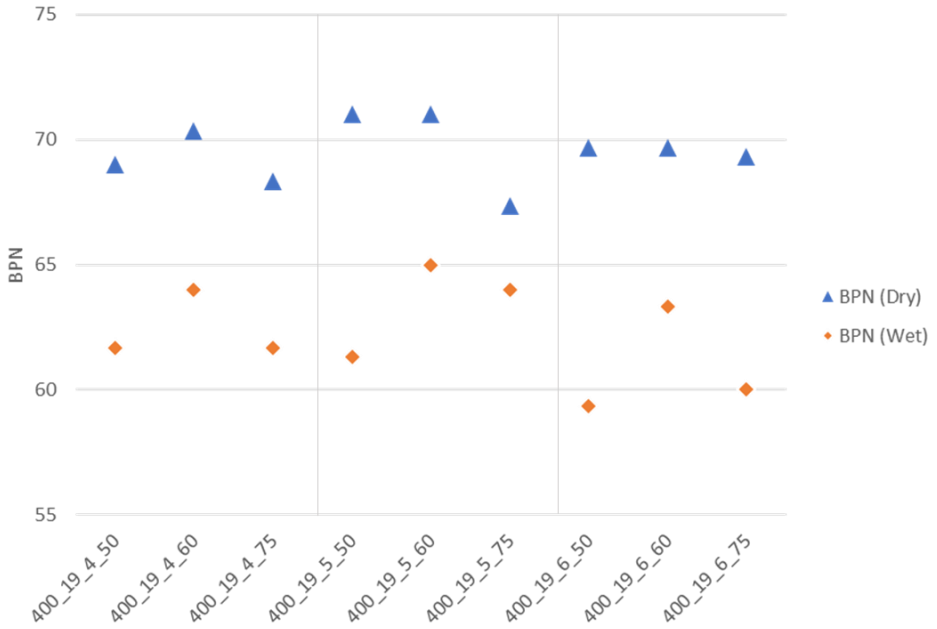

Figure 4.13. Gyration number effect on BPN values for CD:400 and Dmax:19 comparison for both conditions (dry and wet

The statistical analysis reveals that the impact of both maximum aggregate size (Dmax) and water content on BPN values in dry and wet conditions remained significant, as evidenced by the p-values of zero when considering the three distinct water contents of 4%, 5%, and 6% (Table 4.4a and b).

The relationship between BPN values and Dmax and water content exhibited different trends for lower and higher Dmax values and showed different patterns depending on the specific water content.

BPN dry and wet demonstrated a curvilinear pattern for lower Dmax values, whereby the minimum value was observed at a water content of 5%. The aforementioned observation implies that an optimum water content (5%) could potentially result in a more even surface and subsequently decrease skid resistance, particularly for smaller aggregate particles. In contrast, it can be observed that BPN dry and BPN wet exhibited a curve-like trend for higher Dmax values, wherein the maximum value was attained at 5% water content. This suggests that intermediate water content leads

to an increase in surface roughness and skid resistance for larger aggregate sizes (Figure 4.14).

The relationship between pavement surface texture trends, water content, and aggregate size can be explained by examining the respective roles of these factors. Aggregate particles with lower Dmax values may require a reduced amount of water to achieve an optimal balance between surface roughness and smoothness. When the water content reaches 5%, there is a possibility that the surface may become smoother, which could result in a decrease in skid resistance. Nevertheless, when using larger aggregates (higher Dmax values), it is probable that an intermediate water content of 5% is sufficient to ensure appropriate surface roughness and texture, leading to improved skid resistance.

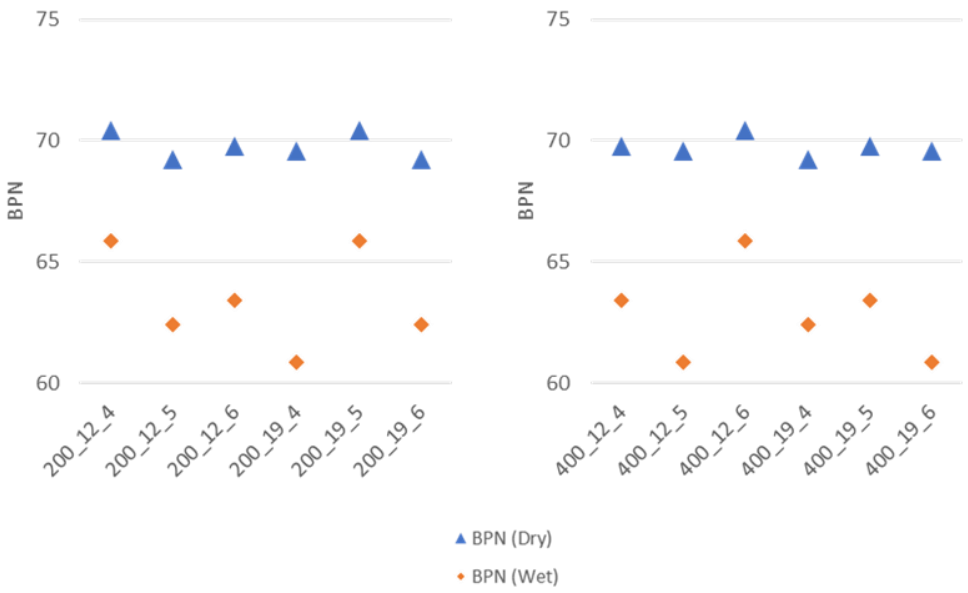

Figure 4.14 Water content and Dmax combined effect on BPN values

It is also worth mentioning that the BPN values under wet conditions are significantly affected by Dmax (Figure 4.15), unlike the BPN values under dry conditions. As the cement dosage varied, an increase in Dmax resulted in a decrease

in the BPN-wet values. One possible explanation for this phenomenon was that the existence of larger aggregates might lead to increased surface roughness, which, in turn, might promote the accumulation of water between aggregates when exposed to water. The accumulation of water on the surface might result in hydroplaning, which could potentially lead to a decrease in skid resistance.

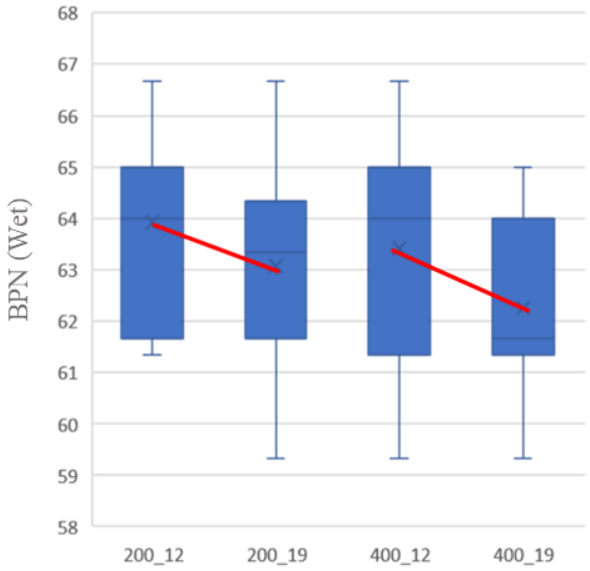

Figure 4.15 Effect of Dmax on BPN in wet condition

4.2 Image Based Analysis

4.2.1 Influence of design parameters on surface texture considering roughness parameters

ANOVA is a statistical technique used to examine the differences between two or more groups. It is frequently employed in crossed designs in which all possible combinations of levels and factors are included. The objective of this study was to identify significant differences between the groups. A confidence interval, typically set at 0.95, indicates the degree of certainty regarding the true difference between

group means. The procedure entailed defining factors, collecting data, conducting an ANOVA, calculating confidence intervals, and interpreting the results. All ANOVA results were obtained using SPC for Excel (BPI Consulting, LLC, 2023), a program that simplifies statistical analysis for businesses worldwide. It provides tools for data visualization, trend detection, problem-solving, and process improvement. It also supports Lean, Six Sigma, and Process Improvement through training programs, consulting services, and an extensive library of materials on statistical process control (SPC).

Height Parameters

Seven height parameters were analyzed on the RCC samples. Three parameters, namely, maximum peak height, maximum valley depth, and maximum height are prone to be affected by isolated high or low points. Therefore, these were excluded from the analysis.

Root mean square height (Sq) and Arithmetical mean height (Sa)

The impact of cement dosage, water content, and maximum aggregate size on the Sa, the arithmetical mean height, and Sq, the root mean square height, values can be explained by their effect on the uniformity of the cement matrix, ease of workability, and distribution of the aggregate. When optimizing the surface texture of concrete, it is crucial to consider these factors. Nonetheless, it is essential to keep in mind that relying only on Sa and Sq might not fully understand the characteristics of a surface, given their inability to differentiate between distinct surface attributes, such as peaks, valleys, and spacing. To comprehensively characterize a surface for its intended application, it is vital to incorporate supplementary surface texture parameters.

As demonstrated by the ANOVA results, variations in cement dosage and water content significantly affected Sq and Sa (p-value=0.0). With increasing cement dosage, both the Sa and Sq values decreased (Figure 4.16 and Figure 4.17). An increase in the cement content yields a denser and more cohesive matrix, thereby producing a surface with reduced irregularities and improved smoothness.

Consequently, the arithmetic mean height (Sa) and root mean square height (Sq) decreased.

The results (Figure 4.16 and Figure 4.17) indicated that there exists an optimal level of water content that produces the most favorable surface texture, as demonstrated by the higher Sa and Sq values observed at 5% water content as compared to those at 4% and 6%. Optimization of the cement particle distribution and improvement of workability could be achieved without causing excessive porosity at a water content of 5%. This phenomenon resulted in an improved surface texture, which consequently yielded higher Sa and Sq values. Inadequate workability and a rough surface texture might arise from a reduced water content of 4%, whereas an increased water content of 6% might lead to increased porosity and a negative effect on the surface texture.

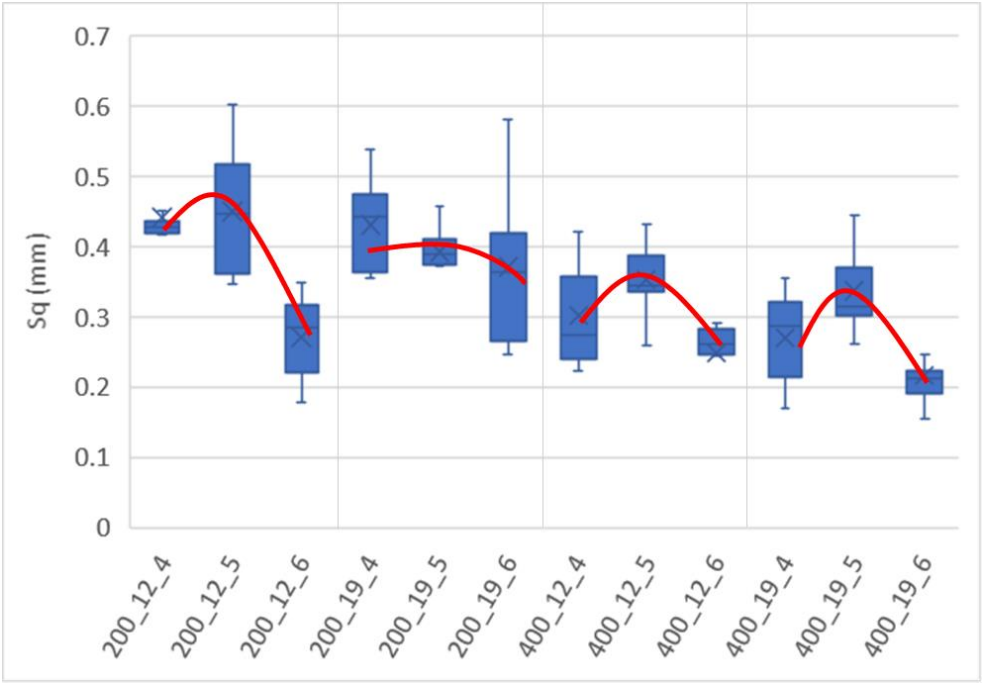

Figure 4.16 W (%) effect on Sq

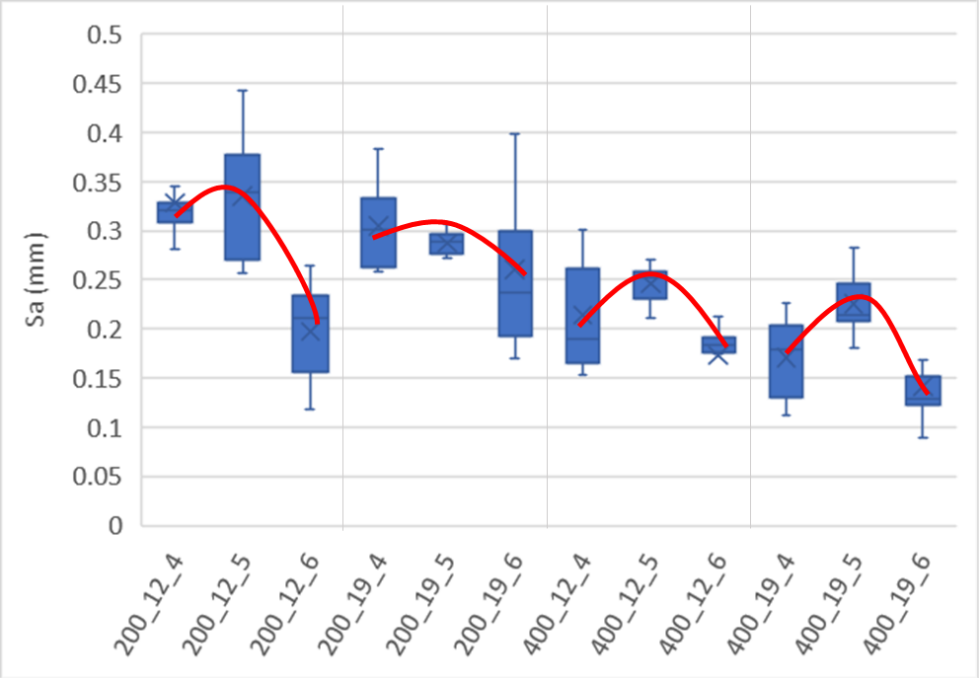

Figure 4.17 W (%) effect on Sa

Sa also is affected by Dmax (p-value = 0.0317). The correlation between Dmax and Sa indicated that an increase in the maximum aggregate size resulted in a decrease in Sa, given a constant cement dosage (Figure 4.18).

This phenomenon might be attributed to the idea that larger aggregates produce a more uniform and well-distributed mixture, leading to a smoother surface texture with reduced irregularities. Consequently, the average height (Sa) was lower.

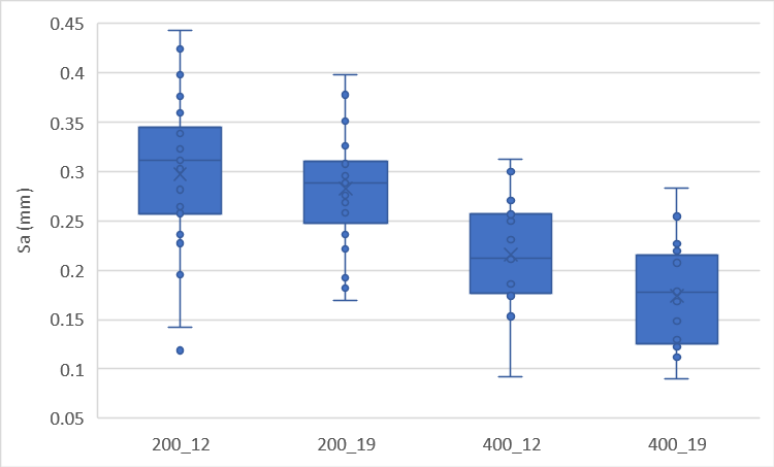

Figure 4.18 Cement dosage and maximum aggregate size effect on Sa

Skewness (Ssk) and Kurtosis (Sku)

As stated previously, skewness is a measure of the asymmetry of the distribution of surface valleys and peaks, indicating whether the distribution is skewed toward higher or lower elevations. A positively skewed distribution consisted of more peaks, whereas a negatively skewed distribution consisted of more valleys. Kurtosis is a measure of the "tailness" of a distribution that describes the extreme surface features and concentration of valleys and peaks. A high kurtosis indicates a landscape with more extreme features and a predominant concentration of peaks, whereas a low kurtosis suggests a more uniform distribution of features and valleys and peaks that are less extreme. To comprehend the shape and characteristics of the surface valley and peak distribution, both skewness and kurtosis are essential.

A decrease in Ssk was observed with an increase in cement dosage (Figure 4.19Figure 4.16. These findings indicate that a higher cement dosage results in an increased amount of uniformity in the surface texture, accompanied by a decrease in the amount of asymmetry in the surface deviations from the mean plane. An increase in the amount of cement used in the mixture led to a denser and more cohesive structure, which could potentially decrease the occurrence of peaks on the surface. Consequently, the distribution of the surface may exhibit a greater number of valleys,

indicating negative skewness. As the maximum aggregate size increased, Ssk decreased at a constant cement dosage. This observation implies that the utilization of larger aggregates leads to the formation of a more consistent and evenly distributed mixture, thereby resulting in a smoother surface texture with a reduced number of peaks. As a result, the surface exhibited a greater degree of negative skewness, primarily characterized by the presence of valleys.

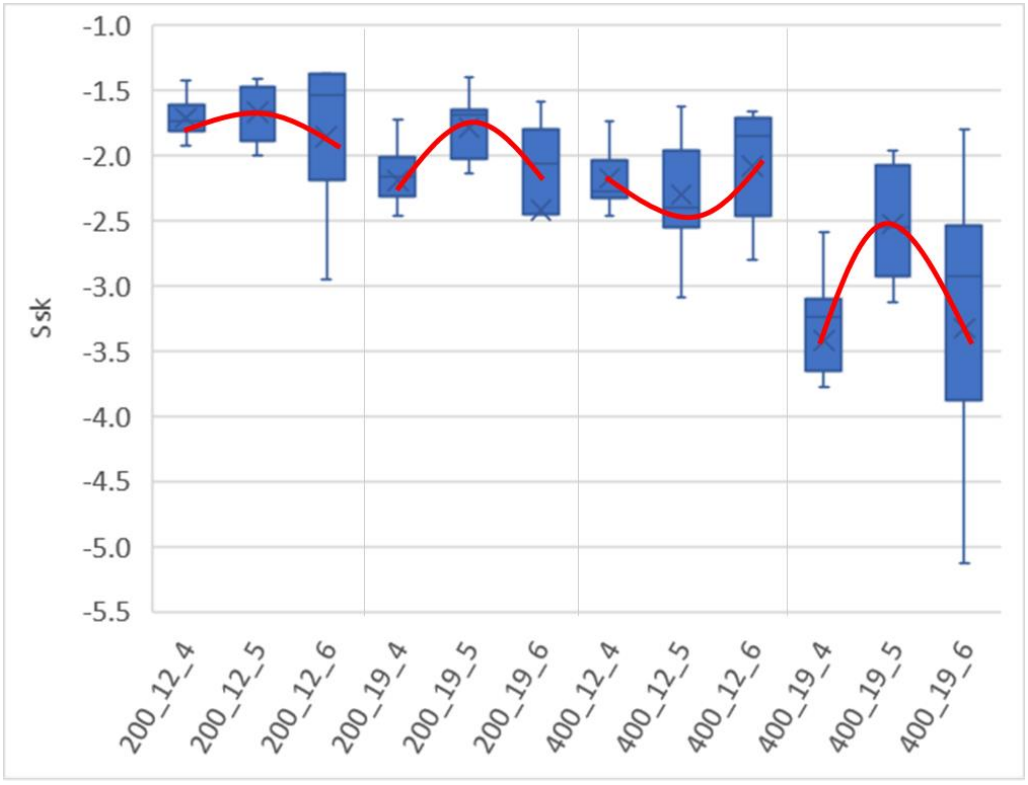

Figure 4.19 Variability chart of Ssk

As the amount of cement used increased, there was a corresponding increase in Sku (Figure 4.20). The aforementioned observations suggest that an increase in cement content leads to an increased susceptibility of the surface to exhibit extreme characteristics, such as elevated peaks or profound valleys. A higher cement content can result in the development of pronounced surface characteristics owing to the

denser and more cohesive matrix that is formed. As the maximum aggregate size increased, the Sku value increased at a constant cement dosage. This suggests that the existence of larger aggregates could potentially result in the emergence of more pronounced surface characteristics such as high peaks or deep valleys. The presence of larger aggregates can result in a less uniform mixture, thereby increasing the concentration of the abnormal features.

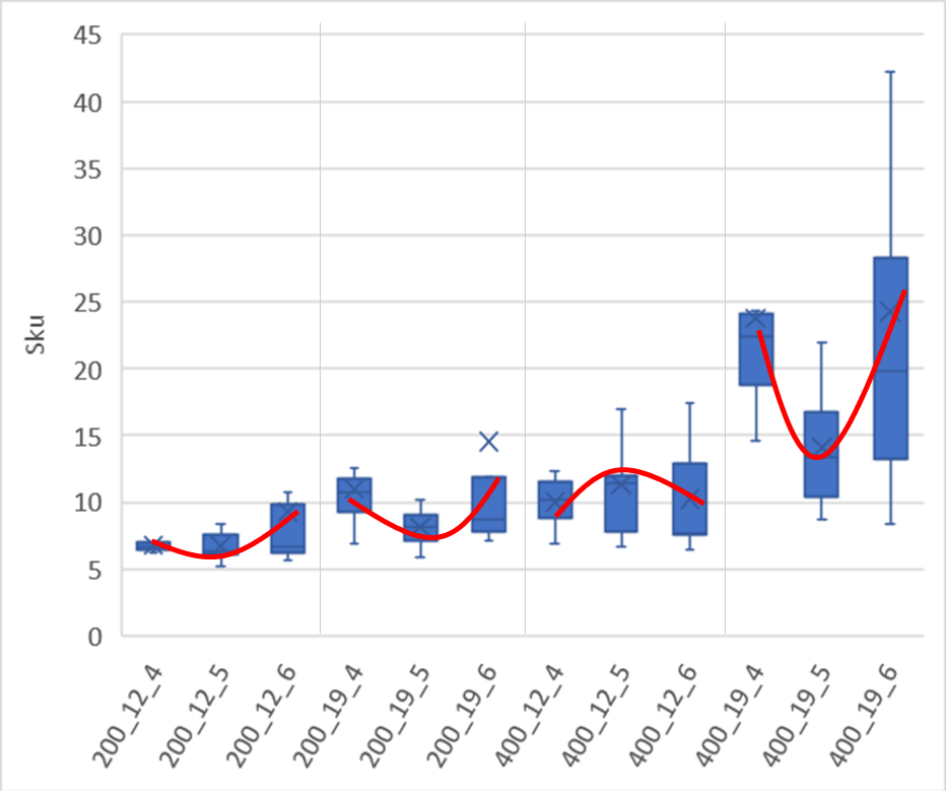

Figure 4.20 Variability chart of Sku

In summary, the surface parameters of skewness (Ssk) and kurtosis (Sku) can be influenced by the cement dosage and maximum aggregate size (Figure 4.21). This was due to the modification of the distribution and concentration of surface features, including peaks and valleys. An increase in cement dosages and maximum aggregate sizes has been observed to lead to a distribution that is more negatively skewed, characterized by valleys, and a greater concentration of extreme features on the surface. Gaining an understanding of these interrelationships and considering the Ssk

and Sku parameters could provide significant insights into surface properties and operational efficacy.

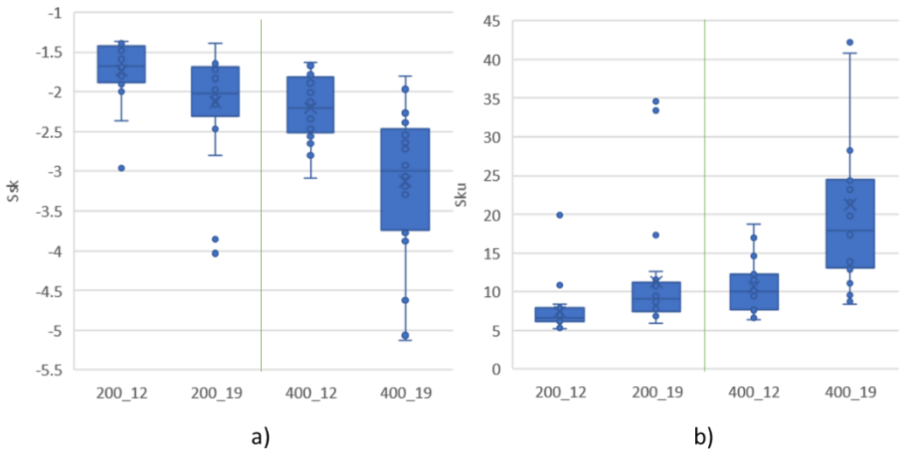

Figure 4.21 Cement dosage and maximum aggregate size effect on a) Ssk b) Sku

Spatial Parameters

The autocorrelation length (Sal) and texture aspect ratio (Str) are essential for the characterization of surface textures and for comprehending their isotropic or anisotropic nature. The Autocorrelation Length, denoted by Sal, is a metric used to evaluate the horizontal distance at which a surface texture pattern begins to exhibit statistical distinctiveness from its initial location. The determination process involves an analysis of the decay of the autocorrelation function to a specific value, which is commonly set to s = 0.2 following the guidelines outlined in ISO 25178-2. Sal offers insights into the repetitive characteristics of a given surface texture.

The Texture Aspect Ratio (Str) is a scale that evaluates the relationship between the horizontal distances of the autocorrelation function with the fastest and slowest decay rates to a common value, s (where s is a value between 0 and 1, inclusive). This parameter has significant utility in evaluating the level of isotropy or anisotropy exhibited by a given surface. The Str values exhibit a range between 0 and 1, with a value exceeding 0.5 indicating a robust state of isotropy, while a value approximately

equal to 0.3 suggests a robust state of anisotropy. The Str parameter can ascertain the existence of a lay, which is a directional pattern, within a surface texture. Furthermore, it can also discern any underlying alterations on the surface that may have been caused by various manufacturing procedures.

The correlation between Sal and Str pertains to their capacity to articulate spatial attributes of a given surface texture. Sal's emphasis is on the statistical distinctness of a texture pattern from its original location, whereas Str places greater emphasis on the uniformity or directionality of a surface texture. Through the analysis of multiple parameters, a thorough comprehension of the textural properties of a surface can be obtained.

According to ANOVA results, they have a common source, cement dosage, affecting them significantly having a p-value equal to zero. A higher cement content produces a more extended and uniform surface texture, with an average Sal of approximately 3.5 for a lower cement dosage and approximately 5 for a higher cement dosage (Figure 4.22). This may be because the cement matrix was more cohesive and denser, which improved the bond between the cement paste and aggregates and produced more uniform surface features over a wider area.

The surface texture becomes more anisotropic (directionally dependent) with higher cement content, with an average Str of around 0.7 for higher cement dosage and around 0.8 for lower cement dosage. The distribution and alignment of surface features are affected by the applied compaction process, cement hydration, changes in the workability of the material, and anisotropy, among other factors.

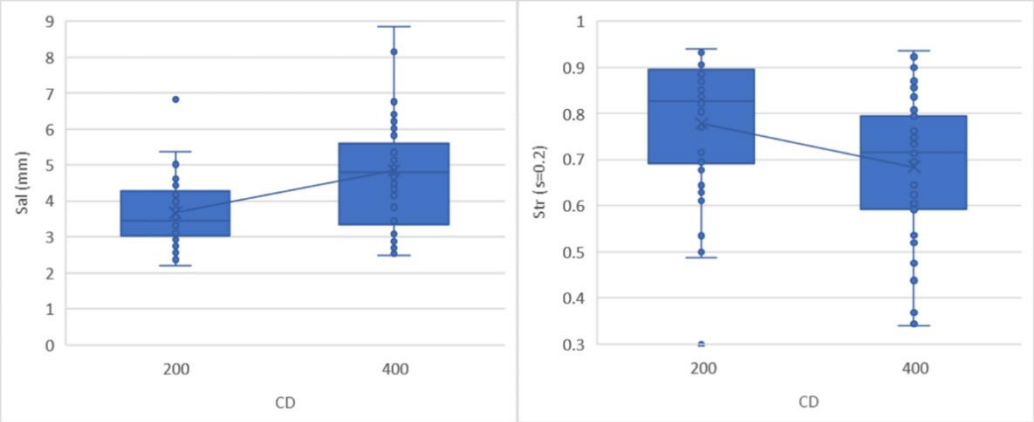

Figure 4.22 The effect of Cement Dosage (CD) on Sal and Str

Additionally, the ANOVA results showed that the water content had a significant impact on Sal (p=0.0454), but not on Str (p=0.8516). This implies that the autocorrelation length may be influenced by water content, which affects the distribution of surface features over specific distances. The consistency of the surface texture might be affected by the ideal water content, but neither the isotropy nor the anisotropy of the surface would be affected (Str).

Gyration number had a non-significant impact on Sal (p=1.1509), but a significant impact on Sal (p=0.0137). This suggests that while the autocorrelation length is unaffected by the gyration number, the texture aspect ratio may be. The isotropy or anisotropy of the surface texture may vary with different gyration numbers, possibly because of modifications to the compaction process, which may affect the Str value.

Hybrid Parameters

The utilization of hybrid parameters, namely, Sdq and Sdr, together with Sa, provides a comprehensive examination of the textural characteristics of a given surface. The parameter Sdq is related to the overall slope steepness, whereas Sdr evaluates the additional surface area introduced by the texture. Both hybrid parameters show a similar trend. An increase in cement dosage and change in water content affects both as shown in Figure 4.23 and Figure 4.24.

The use of Sdq as a metric is useful for distinguishing between surfaces that show identical Sa values by measuring the average steepness of the slopes that form the surface. As a result, it can be inferred that a surface possessing a particular Sa value may exhibit a lower Sdq value if its texture has a wider spacing than a surface with the same Sa value but a narrower spacing.

The use of Sdr enables the differentiation of surfaces with similar amplitudes and average roughness values. The relationship between Sa and Sdr depends on the spatial intricacy of the texture, whereby an increase in the second is often observed, regardless of any changes in the first. Both the amplitude and spacing of the texture affect Sdr. Hence, it can be inferred that a texture exhibiting higher Sa and wider spacing could potentially exhibit a lower Sdr in comparison to a texture with lower Sa but denser spacing.

The measurements indicate that an increase in the cement dosage results in a reduction in the Sdq and Sdr values, which implies a decrease in roughness and steepness. The observed phenomenon may be attributed to the process by which the cement material fills the gaps and discontinuities among the aggregates, resulting in a smoother topography characterized by reduced incidents of pointed peaks and deep valleys. Consequently, there was a decrease in the additional surface area, as indicated by the Sdr values.

The correlation observed between the Sdq and Sdr parameters and water content, as evidenced by the plotted curve for three distinct water content levels (4%, 5%, and 6%), implies the possibility of an optimal water content that can be attained to achieve the desired surface characteristics. Insufficient water can cause the surface to become dry and rough, whereas excessive water can result in a more liquid consistency that distributes unevenly, potentially impacting the surface's overall slope and additional surface area. The nonlinear correlation suggests the existence of an optimal range of water content that yields the most favorable combination of surface characteristics.

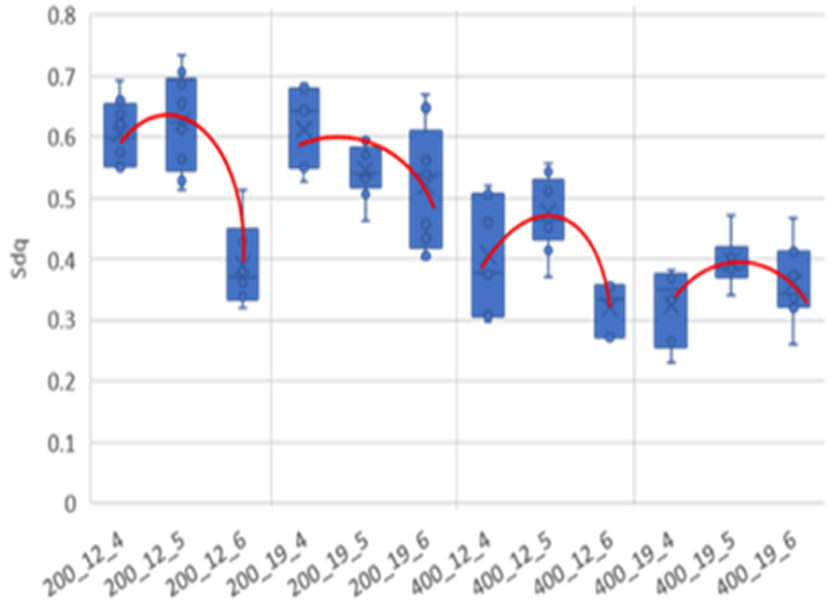

Figure 4.23 Box and Whiskers Plot of Sdq

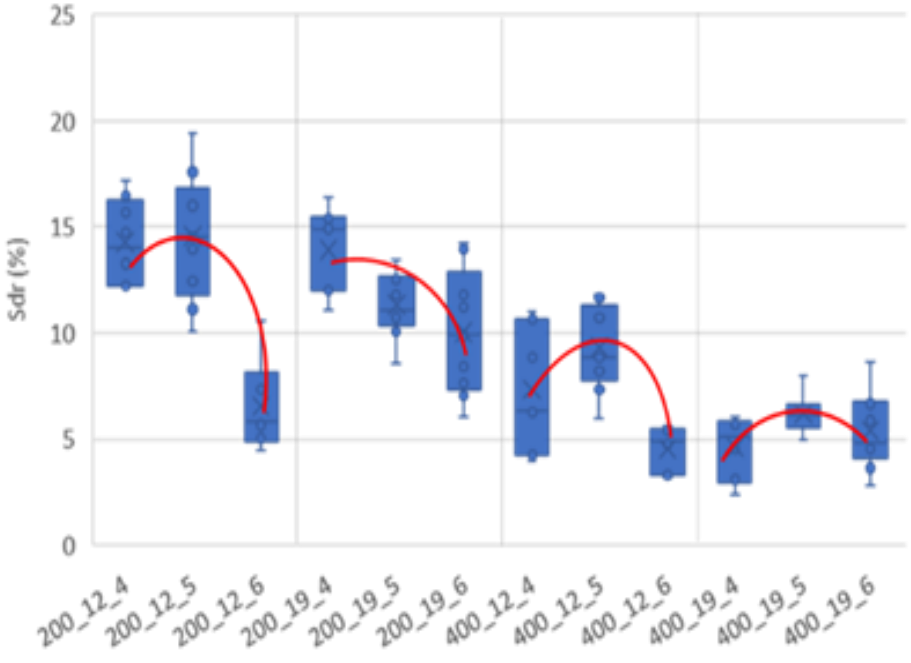

Figure 4.24. Box and Whiskers Plot of Sdr

Functional Volume Parameters

Void volume (Vv(mr)), Dale void volume (Vvv(p)) and Core void volume (Vvc(p,q))

The parameters related to void volume, namely Vv, Vvv, and Vvc, are influenced by cement dosage and water content, as well as their interaction. These factors are of significant importance in a range of applications that involve surface textures. Elevated levels of cement yield compact cementitious structures, thereby causing a decline in void spaces and subsequently reducing the values of Vv, Vvv, and Vvc (Figure 4.25).

An increase in cement dosage is associated with a decrease in mean Vv from 0.38 mm^3/mm^2 to 0.25 mm^3/mm^2, mean Vvv from 80 ml/m^2 to 60 ml/m^2, and mean Vvc from 290 ml/m^2 to 200 ml/m^2. The aforementioned observations suggest that increased amounts of cement result in the formation of a more compact matrix, thereby decreasing the number of unoccupied spaces present within the surface textures.

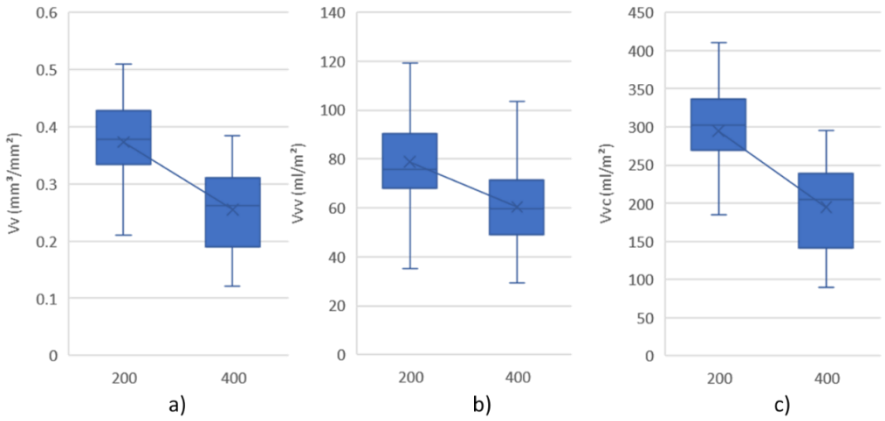

Figure 4.25 Cement dosage effect on a) Vv b) Vvv c) Vvc

The void volume parameters were affected by the water content, whereby the largest void spaces were achieved at an optimal water content of 5%. Insufficient hydration for proper cement packing may result from a lower water content (4%), whereas increased shrinkage and compaction during curing may be observed at a higher water content (6%) (Figure 4.26, Figure 4.27, and Figure 4.28). Achieving an ideal water

content involves achieving balance, whereby the void volume parameters are maximized.

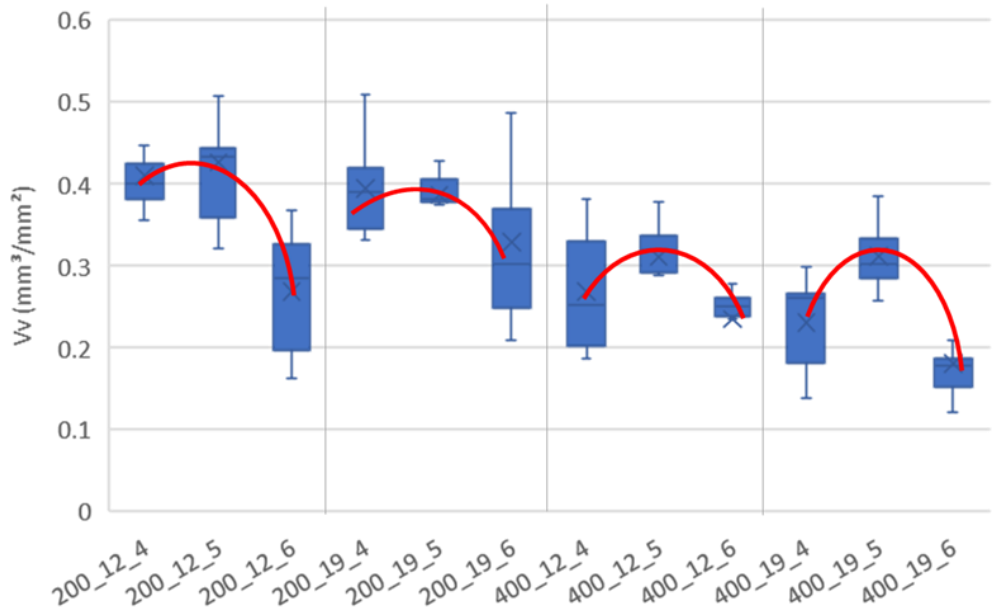

Figure 4.26 Water content effect on Vv

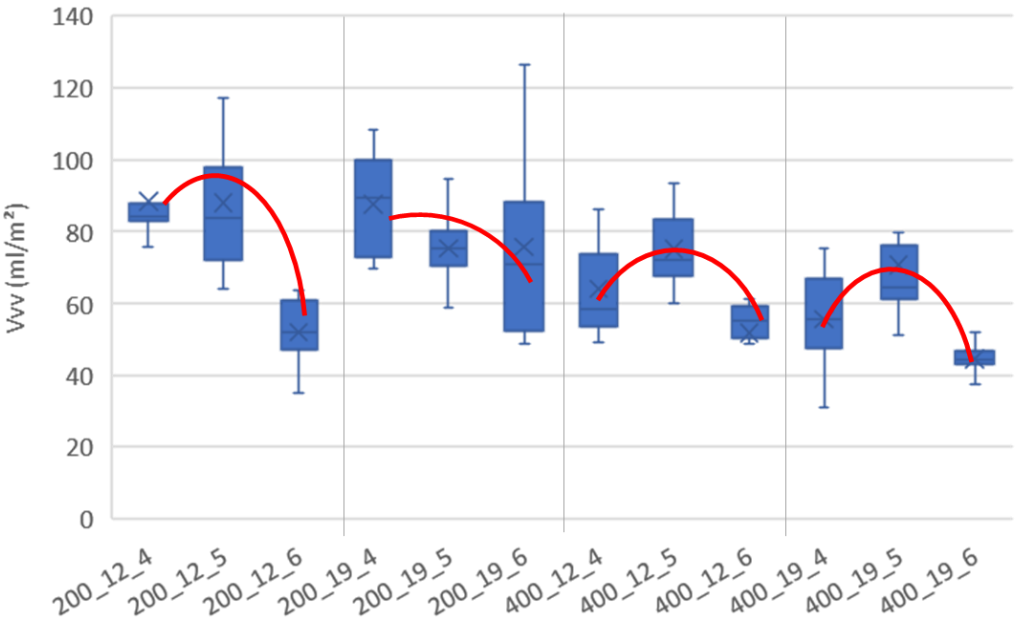

Figure 4.27 Water content effect on Vvv

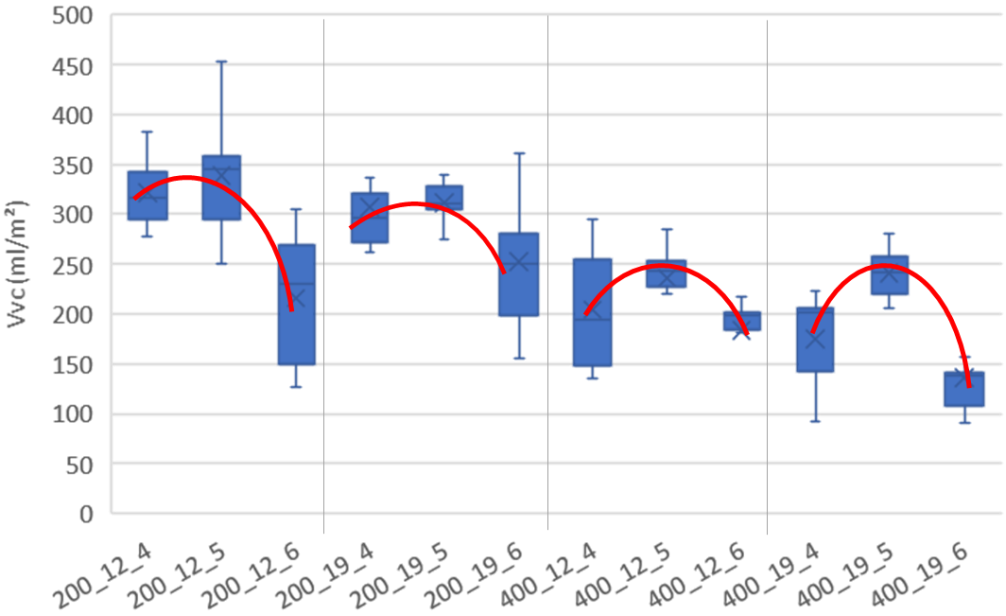

Figure 4.28 Water content effect on Vvc

The relationship between the amount of cement used and the quantity of water present displays complex impacts on parameters related to the volume of voids. The combination of these factors may yield different void volume results based on the amount of cement used. An example of this phenomenon is that an increased amount of cement, in combination with an ideal amount of water, may lead to effective compaction and hydration. Conversely, a decreased amount of cement, combined with an inadequate amount of water, may produce a less compact matrix with larger void spaces. Therefore, it is essential to consider this interaction to comprehend its impact on void volume parameters.

Understanding the correlations between cement dosage, water content, and void volume parameters is crucial for enhancing mix designs and forecasting surface texture performance in various situations, including fluid flow, coating applications, and debris entrapment. By comprehending these interrelationships, engineers can design customized mixes that regulate fluid flow properties, augment coating efficacy and adhesion, and enhance debris entrapment efficiency. This, in turn,

results in better performance, longer service life, and decreased maintenance expenses for these applications.

In brief, understanding the influence of cement dosage, water content, and their interplay on void volume parameters is crucial for enhancing mix design and anticipating surface texture behavior in diverse applications. The acquisition of this knowledge empowers engineers to devise materials and systems that are more proficient, productive, and customized to meet specific application prerequisites.

Material volume (Vm(mr)), Peak material volume (Vmp(p)) and Core material volume (Vmc(p,q))

Parameters Vm(mr), Vmp(p), and Vmc(p,q) offer valuable information regarding the material volume present on a surface at different heights. These parameters may help evaluate the load support, wear resistance, and sealing efficacy. The statistical analysis of variance (ANOVA) revealed that the parameters under consideration were significantly influenced by cement dosage, water content, and maximum aggregate size.

The increase in cement dosage resulted in a decrease in Vm, Vmp, and Vmc, indicating a more compact cementitious structure with a reduced material volume at different elevations (Figure 4.29a, b, and c).

This phenomenon can be explained by the correlation between the increased cement dosage and the formation of a denser matrix, which results in a decrease in the total amount of material present in the surface texture. The reduction in the material volume parameters could potentially lead to diminished load support and wear resistance at specific depths.

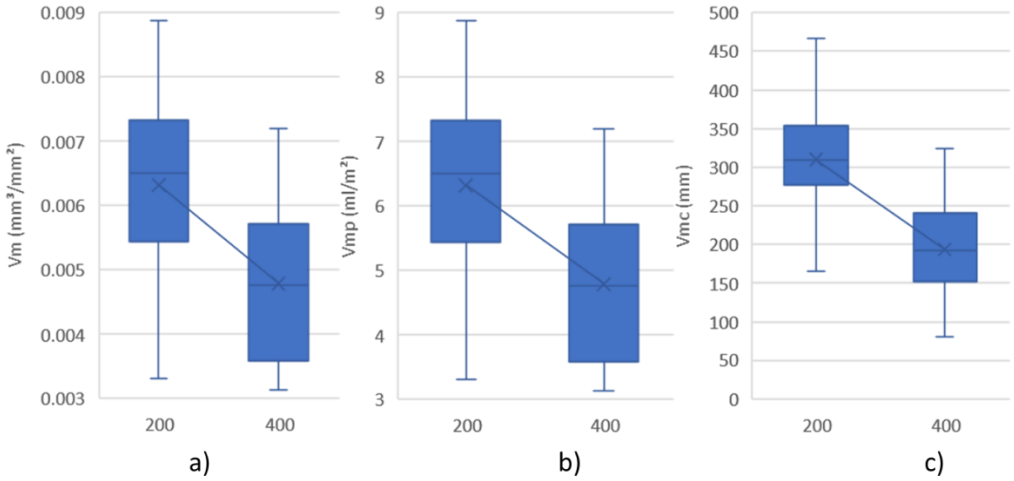

Figure 4.29 Cement dosage effect on Vm, Vmp, and Vmc

The role of water content in Vmc is noteworthy, as evidenced by the non-linear trend observed across three distinct water content levels (4%, 5%, and 6%). The peak of this trend was observed at a water content of 5%, which yielded the highest Vmc value (Figure 4.30).

This implies the existence of an optimum water content that maximizes the volume of the material produced in the surface texture. Insufficient hydration of the cement may occur because of the lower water content (4%), resulting in less effective packing and potentially larger voids, ultimately reducing the overall material volume. An increased water content of 6% can lead to greater shrinkage and compaction while the curing process is underway, ultimately yielding a denser matrix with a reduced material volume. The water content yielding the highest material volume parameters was achieved at an optimal level of 5%.

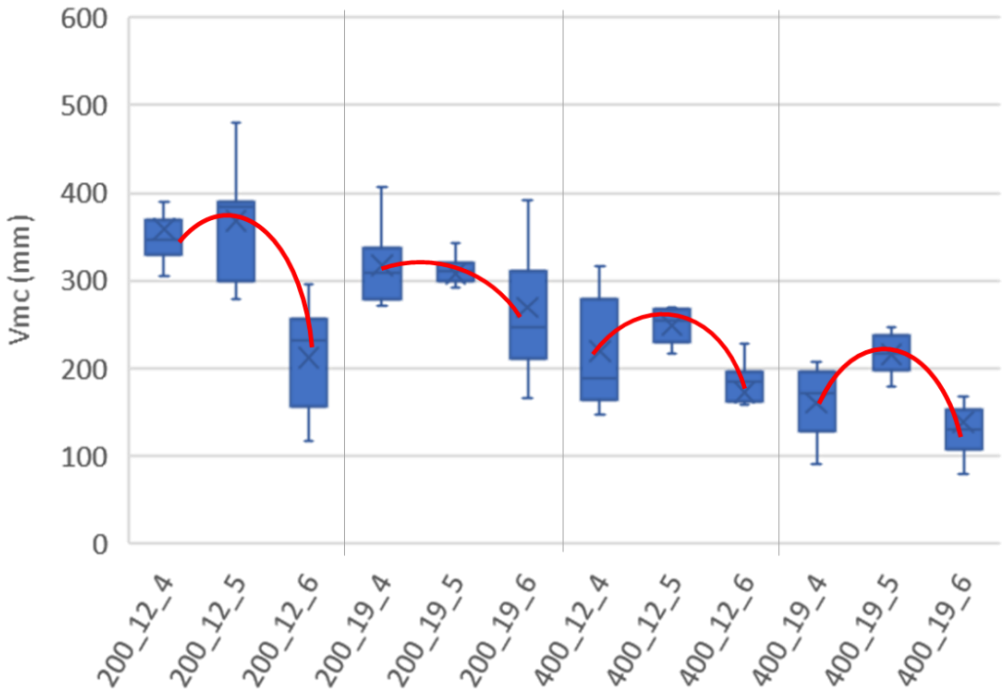

Figure 4.30 Water content effect on Vmc

The maximum aggregate size has a notable impact on Vmc. A decrease in the Vmc values was observed with an increase in the maximum aggregate size (Figure 4.31).

This phenomenon can be explained by the notion that larger aggregates tend to take up more room in the matrix, thereby diminishing the total amount of cementitious material at the disposal. Consequently, the density of the matrix decreased, and its material volume for load support and wear resistance decreased.

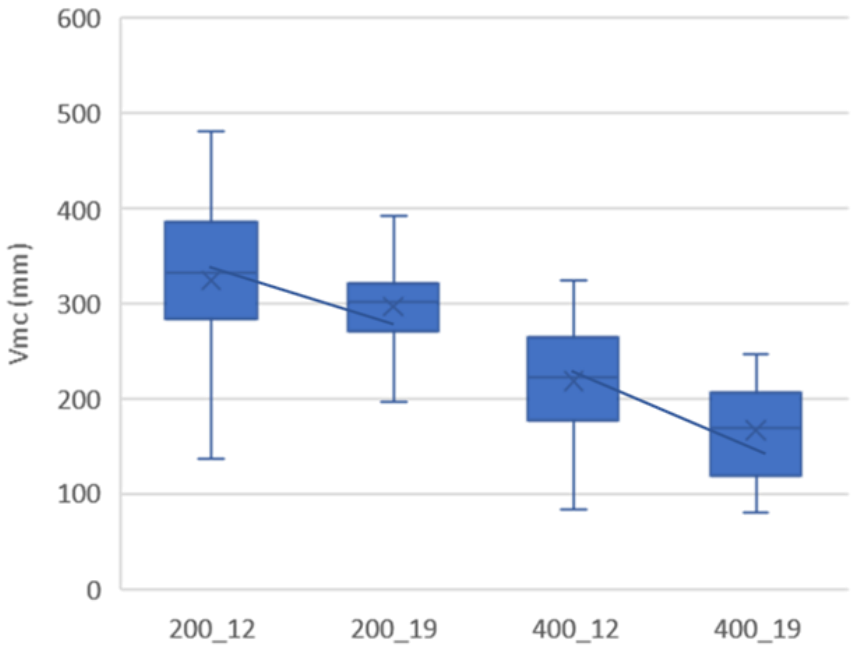

Figure 4.31 Maximum aggregate size effect on Vmc

In summary, the material volume parameters, namely Vm, Vmp, and Vmc, are significantly affected by factors such as cement dosage, water content, and maximum aggregate size. By comprehending these interconnections and their influence on material volume parameters, engineers can enhance mix designs and surface texture characteristics for diverse applications, considering aspects such as load-bearing capacity, durability, and sealing efficacy.

Feature Parameters

Peak Density (Spd) and Arithmetic mean peak curvature (Spc)

The maximum aggregate size, areal feature parameter Spd (Peak Density), and cement dosage all exhibited statistically significant relationships. There is an effect of these factors on Spd, as shown by the ANOVA results, which show a p-value of 0.0 for Spd concerning cement dosage and maximum aggregate size. Additionally, the p-value of 0.0429 for Spc (Arithmetic Mean Peak Curvature) suggested that the cement dosage, maximum aggregate size, water content, and gyration number interacted.

Spd decreased for a constant cement dosage as the maximum aggregate size increased (Figure 4.32a). The reason for this trend is that larger aggregates produce fewer peaks per unit area, resulting in a lower Spd value. Larger aggregates occupy more space in the mixture, thereby reducing the number of contact points with other objects and the number of peaks. As the size of the aggregates increased, there was a corresponding increase in both volume and surface area. This resulted in a decrease in the number of aggregate particles that could be accommodated within a given area.

The Spd decreased for higher cement dosages (Figure 4.32b). More cement paste in the mixture resulted from an increased cement dosage, which could produce a surface with fewer pronounced peaks. Cement paste can close the spaces between the aggregates, lowering the overall number of contact points and subsequently lowering Spd.

The interaction effect between the Cement Dosage, Dmax, Water Content, and Gyration Number is shown by the p-value of 0.0429 for the Spc. This implies that the level of each factor influences the impact of other factors on Spc. At different maximum aggregate sizes, water contents, and gyration numbers, the effect of the cement dosage on Spc might differ. The intricate interactions between these variables may cause different peak curvatures and affect the value of Spc.

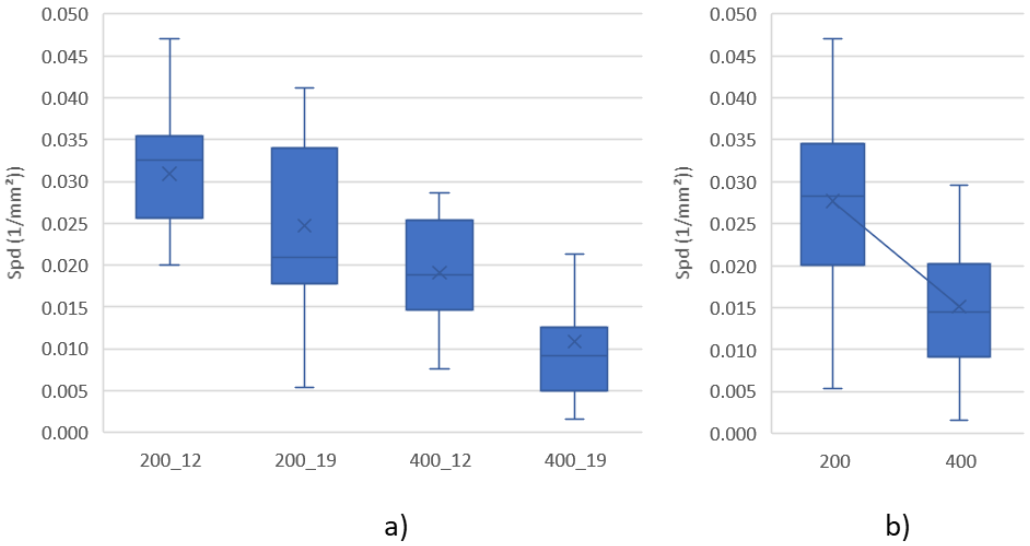

Figure 4.32 Spd values affected by a) Dmax b) Cement Dosage

In conclusion, the Spd and Spc values can be affected by the maximum aggregate size and cement dosage, based on their definitions and observed trends. Fewer peaks were produced by larger aggregate sizes, thus lowering the Spd value. By resulting in a smoother surface with fewer pronounced peaks, higher cement dosages may also lower the Spd. The interaction between the cement dosage, maximum aggregate size, water content, and gyration number on Spc demonstrates the complexity of these relationships and emphasizes the need to consider all variables when analyzing areal feature parameters on surfaces.

Five-point peak height (S5p), Five point pit height (S5v), and Ten point height (S10z)

The S5p, S5v, and S10z ANOVA results and trends showed that the cement dosage and maximum aggregate size had a significant impact on these parameters.

The average height of the five highest significant peaks within a defined area is known as S5p, the Five-Point Peak Height. This trend indicates that as the maximum aggregate size increases (Figure 4.33a), S5p decreases for a constant cement dosage, as well as when the cement dosage increases (Figure 4.33b).

Because there are fewer contact points and, consequently, fewer significant peaks, S5p decreases with larger aggregate sizes. Similarly, as the cement dosage increases, more cement paste surrounds the aggregates, producing a smoother surface with lower peak heights.

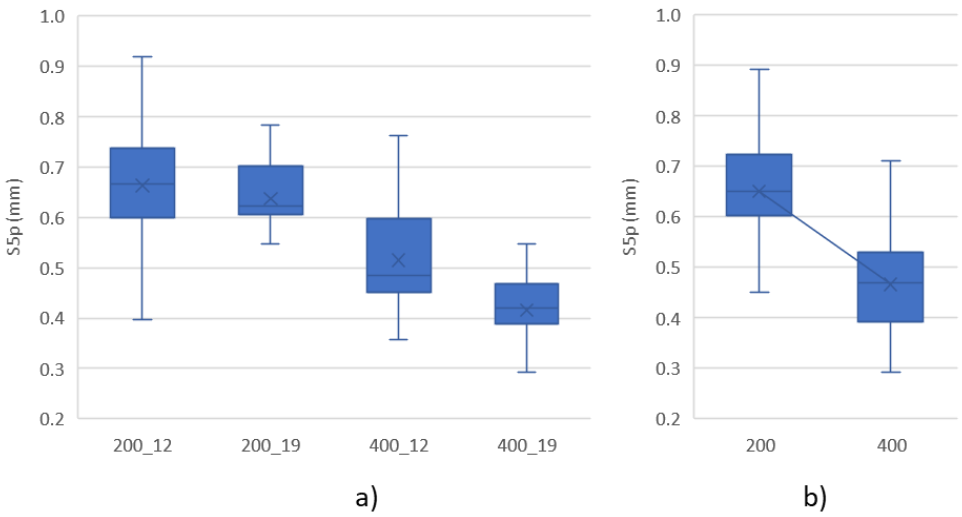

Figure 4.33 S5p change under the effect of a) Dmax b) Cement dosage

The average height (or depth) of the five lowest significant pits within the defined area was measured using S5v (five-point pit height). The trend shows that, as the maximum aggregate size increases (Figure 4.34a), S5v increases for a constant cement dosage and decreases with increasing cement dosage (Figure 4.34b).

The fact that larger aggregates can form deeper pits or valleys between them can explain why S5v increases with larger aggregate sizes. The depth of the pits can be decreased by increasing the dosage of cement, which can result in a higher proportion of cement paste filling the spaces between the aggregates.

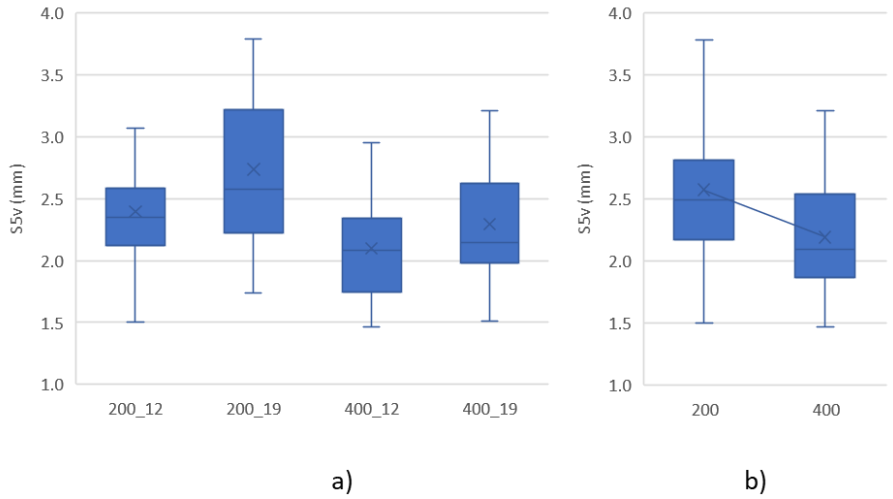

Figure 4.34 S5v change under the effect of a) Dmax b) Cement dosage

According to this trend, S10z increases for a constant cement dosage as the maximum aggregate size increases (Figure 4.35a) and decreases as the cement dosage increases (Figure 4.35b).

Larger aggregate sizes can result in higher peaks and deeper valleys, which improve the S10z value. This explains the increase in S10z for larger aggregate sizes. However, a lower S10z value can be obtained by increasing the cement dosage, which produces a smoother surface with lower peak heights and shallower valleys.

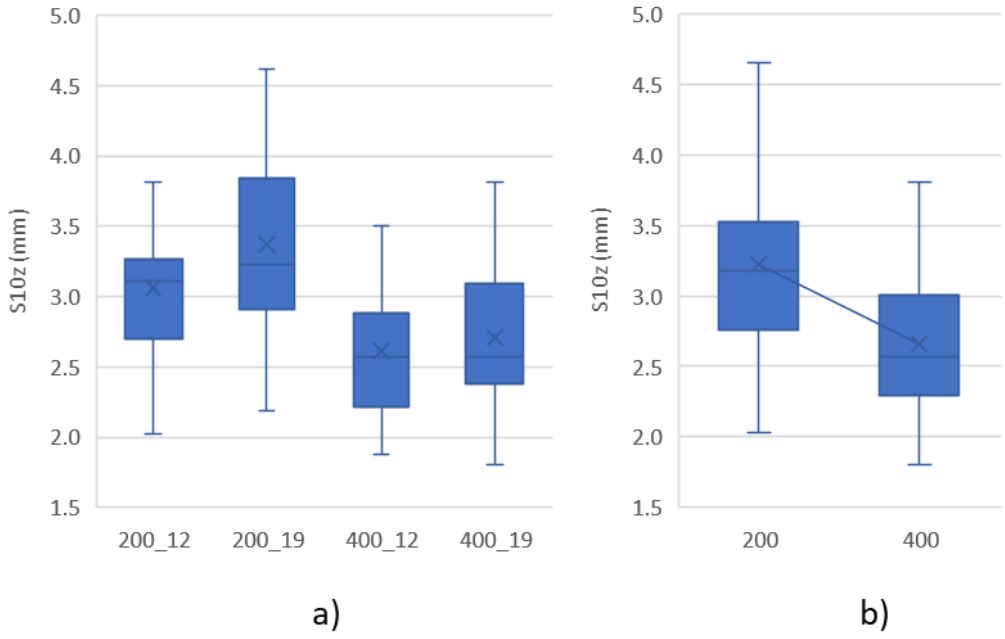

Figure 4.35 S10z change under the effect of a) Dmax b) Cement dosage

In conclusion, the trends in the S5p, S5v, and S10z parameters can be attributed to the impact of the aggregate distribution within the cement mixture and maximum aggregate size on the surface profile. The proportion of peaks to valleys shifts as the cement dosage and aggregate size change, thereby changing the values of the parameters. Characterizing the surface texture of a cement mixture, which directly affects its mechanical and functional properties, requires an understanding of these relationships.

Sda (Mean dale area) and Sha (Mean hill area)

Maximum aggregate size and water content have a significant impact on Sda (Mean dale area) and Sha (Mean hill area), according to the ANOVA results and trends for these parameters.

The average area of the dales connected to the edge at a particular height is denoted by the Mean Dale Area (Sda). This pattern indicates that for a constant cement dosage, Sda increases as the maximum aggregate size increases (Figure 4.36a).

Larger aggregates have the potential to produce dales that are more extensive and significant owing to the substantial spacing between the particles. The horizontal area of the dales projected onto the horizontal plane increased as the maximum aggregate size increased because the spaces between the aggregates widened and became more substantial. As the maximum aggregate size increased, Sda increased accordingly.

The term "Mean Hill Area" (or "Sha") refers to the typical area of hills that are joined to the edge at a specific height. The Sha and water content were significantly correlated, as shown by the ANOVA results, with a p-value of 0.0035. According to this trend (Figure 4.36b), Sha increased as the water content increased. A more fluid and workable cement mixture may have resulted from the addition of more water to the mix. Because of its improved workability, cement paste can flow more easily around aggregates, forming hills that are more pronounced as they fill the spaces between the aggregates. As a result, Sha increased as the horizontal area of the hills projected onto the horizontal plane expanded with increasing water content.

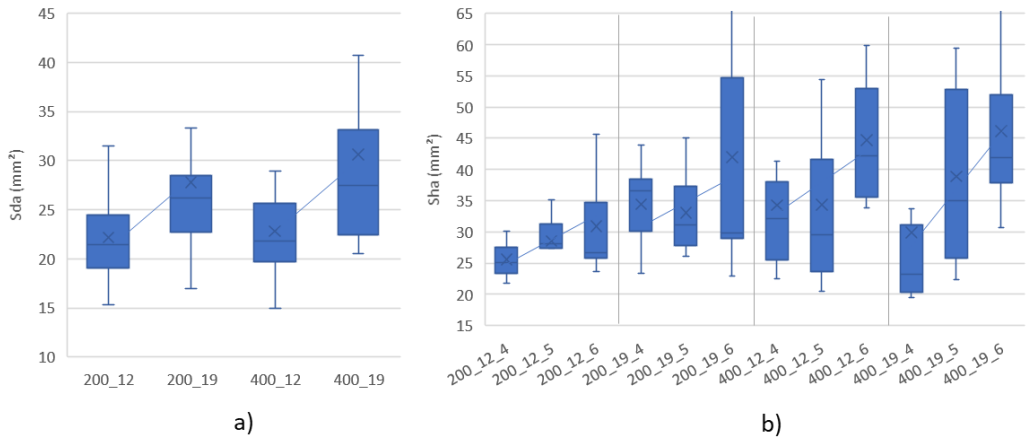

Figure 4.36 Box and whiskers plots for a) Sda b) Sha

In conclusion, the trends in the Sda and Sha parameters can be attributed to the effects of the maximum aggregate size and water content on the distribution of

aggregates within the cement mixture. The balance between the dales and hills shifts as the maximum aggregate size and water content change, thereby changing the values of the parameters.

Mean dale volume (Sdv) and Mean hill volume (Shv)

Max aggregate size and cement dosage have a sizable impact on these parameters, as shown by the ANOVA results and trends you provided for Sdv (Mean dale volume) and Shv (Mean hill volume).

The average volume of the dales connected to the edge at a specific height is represented by the Mean Dale Volume (Sdv). According to the trends, Sdv increases for a constant cement dosage as the maximum aggregate size increases and decreases as the cement dosage increases (Figure 4.37a and b). The spaces between the aggregates widened as the maximum aggregate size increased, resulting in denser dales with larger volumes. Additionally, a larger maximum aggregate size resulted in more significant voids for the cement paste to fill, which increased the volume of the dales. However, as the cement dosage increased, the overall volume of the cement paste increased, and the size of the voids between the aggregates decreased. As a result, the dales became smaller and had lower volumes, which lowered the Sdv value.

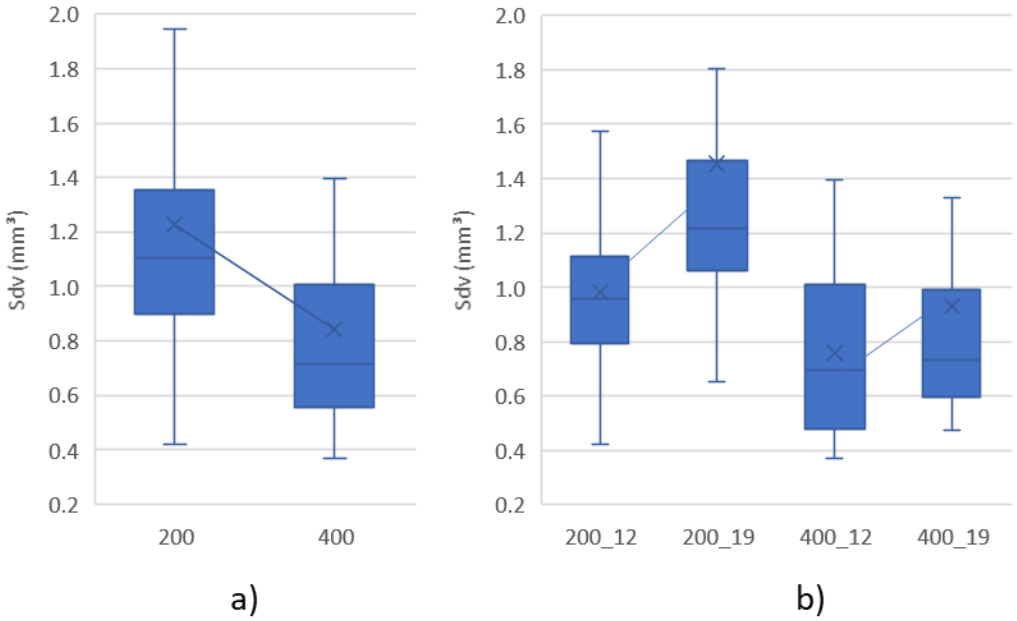

Figure 4.37 Sdv values under the effect of a) Cement dosage b) Dmax

The average volume of hills connected to the edge at a particular height is represented by the Mean Hill Volume (Shv). The patterns show that Shv increases with increasing maximum aggregate size for a constant cement dosage, and decreases with increasing cement dosage (Figure 4.38a and b).

When the maximum aggregate size was increased, the cement paste flowed around the larger aggregates, producing higher-volume hills that were more pronounced. As the maximum aggregate size increased, Shv increased. In contrast, as the cement dosage increased, the overall volume of the cement paste increased, thereby reducing the size of the voids between the aggregates. Smaller and less pronounced hills resulted from the reduction in void size, which ultimately caused a drop in Shv.

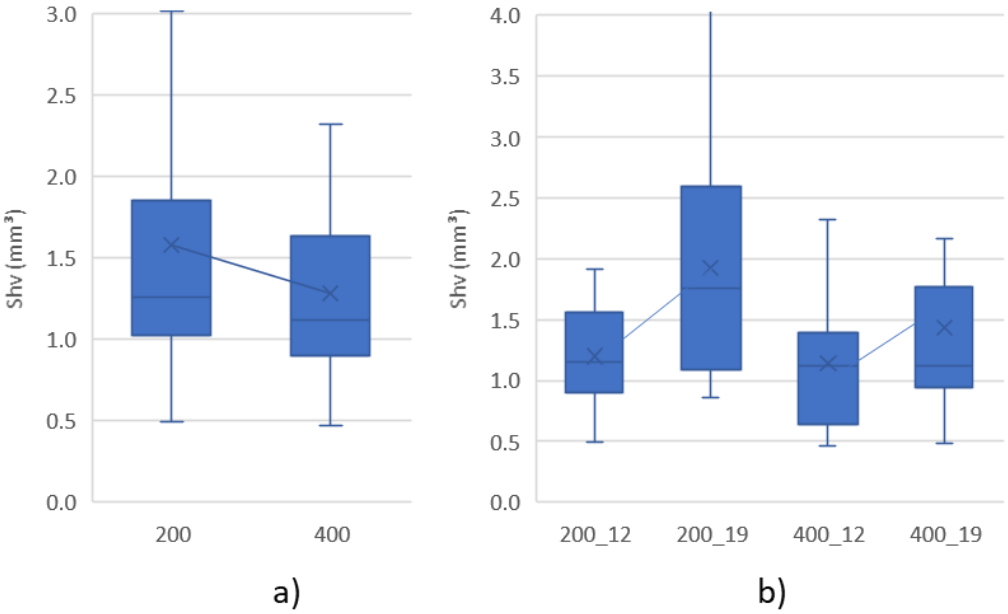

Figure 4.38 Shv values under the effect of a) Cement dosage b) Dmax

In conclusion, the trends in the Sdv and Shv parameters can be attributed to the effect of the maximum aggregate size and cement dosage on the distribution of aggregates within the cement mixture. The balance between the dales and hills shifted with the maximum aggregate size and cement dosage change, changing the values of the parameters.

4.2.2 Examination of surface parameter relation to macrotexture (MTD)

The relationships and associations between the surface parameters and macrotexture properties are analyzed in this section. R-squared (R2) and the Pearson correlation coefficient are two statistical measures used to analyze the relationships between variables.

The Pearson correlation coefficient measures the magnitude and direction of the linear relationship between two variables. It ranges from -1 to +1, with +1

representing a perfect positive linear relationship, 0 representing no linear relationship, and -1 a perfect negative linear relationship.

In a linear regression model, R-squared (R2) measures the proportion of variation in the dependent variable that can be accounted for by the independent variable. A value of 1 indicates that the independent variable completely explains the variation in the dependent variable, whereas a value of 0 indicates that the independent variable has no explanatory power over the variation in the dependent variable.

Although R2 and the Pearson correlation coefficient can be derived from each other, they are not interchangeable. In a linear regression model, the Pearson correlation coefficient measures the strength and direction of the linear relationship between two variables, whereas (R2) quantifies the proportion of variation in one variable that can be explained by another variable.

In the following graphs, instances in which the R-squared and Pearson correlation coefficients have values of 0.90, 0.80, and 0.70 or greater are examined. These values are of particular interest because strong correlations exist between them.

- An R-squared or Pearson correlation coefficient value greater than or equal to 0.9 indicates a very strong linear relationship, with the independent variable accounting for a substantial proportion of the variation in the dependent variable.
- A value greater than or equal to 0.8 indicates a strong linear relationship between the variables, with the independent variable exerting a significant influence over the dependent variable.
- A value greater than or equal to 0.7 denotes a moderately strong linear relationship in which the independent variable has a significant influence on the dependent variable.

Valuable insight is gained into the relationships between the variables and their respective strengths by analyzing these values in the graphs. The overall

relationships between MTD and roughness parameters are summarised in Figure 4.39 and are discussed in detail later in this chapter.

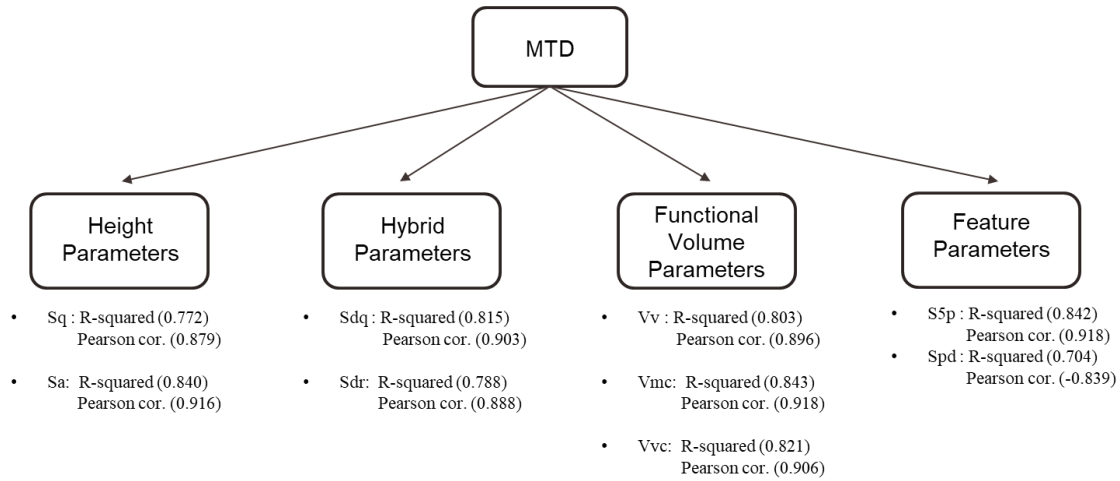

Figure 4.39 Summary of MTD and roughness parameters relation

The Figure 4.40a and b shows the relationship between the parameters of Mean Texture Depth (MTD), Arithmetical Mean Height (Sa), and Root Mean Square Height (Sq), according to their respective R-squared and Pearson correlation values.

There is a significant relationship between these parameters based on the R-squared values for Sq-MTD (0.772) and Sa-MTD (0.840), with Sa-MTD showing a marginally stronger relationship than Sq-MTD.

The strength and direction of the linear relationship between two variables are measured by the Pearson correlation coefficient, on the other hand. In this instance, the Sq-MTD and Sa-MTD had Pearson correlation values of 0.879 and 0.916, respectively. These favorable results indicate that the corresponding parameters exhibit a strong positive linear relationship.

The fact that these parameters are mathematically connected also explains their high correlation. The ordinates Z(x, y) within the evaluation area were used to calculate Sq and Sa, whereas the MTD was calculated using volumetric measurements of the surface macrotexture. These variables naturally depend on similar surface properties; therefore, so it makes sense that they exhibit a strong correlation.

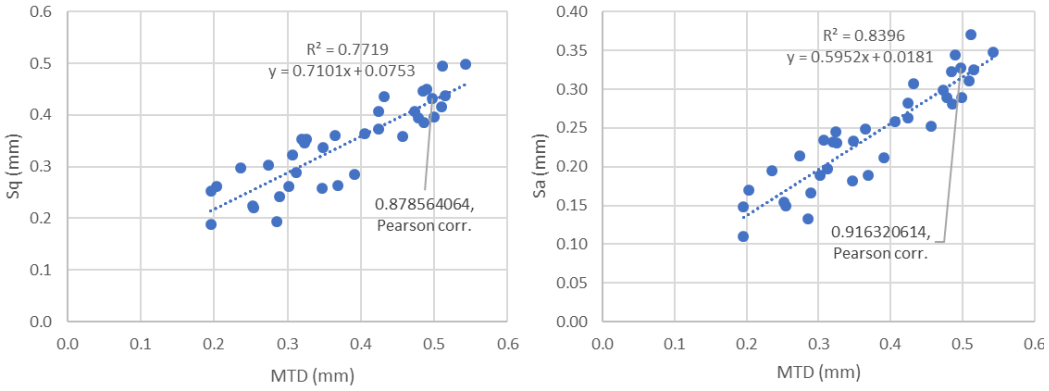

a) b)

Figure 4.40 Correlation between MTD and a) Sq b) Sa

The Figure 4.41a and b shows a correlation between the mean texture depth (MTD) of the pavement surfaces and the hybrid surface parameters Sdq (Root Mean Square Gradient) and Sdr (Developed Interfacial Area Ratio). With R-squared values of 0.815 and 0.788 and Pearson correlation values of 0.903 and 0.888 for the Sdq-MTD and Sdr-MTD, respectively, the correlation coefficients were quite high.

Because all three parameters are related to the surface texture characteristics of pavement surfaces, there is a strong correlation between Sdq and MTD, as well as between Sdr and MTD. The surface slopes in all directions were measured using the root-mean-square gradient (Sdq). Both the amplitude and spacing of the surface texture affected this parameter. A rougher surface is indicated by a higher Sdq value, which can increase friction and skid resistance. The developed interfacial area ratio, Sdr, measures the amount of extra surface area that a surface texture adds in comparison to an ideal plane with the same dimensions as the measurement region. Sdr is influenced by the amplitude and spacing of the surface texture and frequently increases as the spatial complexity of the texture increases.

The fact that both parameters capture information regarding the surface roughness and texture amplitude explains the strong correlation between Sdq and MTD (R-squared = 0.815, Pearson correlation = 0.903). Higher Sdq and MTD values were

produced by rougher surfaces with higher texture amplitudes. It is reasonable to anticipate a strong correlation between the two parameters because the texture amplitude and spacing affect both parameters.

The similar dependence of Sdr and MTD on surface texture properties also explains their high correlation (R-squared:0.788, Pearson correlation =0.888). Sdr typically increases as surface texture complexity increases, and a more complex surface texture may also have a higher MTD value. There is a strong correlation between Sdr and MTD owing to the interaction between the texture amplitude and spacing.

In conclusion, it can be said that the Sdq-MTD and Sdr-MTD have high correlation values because they both depend on the texture amplitude and spacing of the pavement surface.

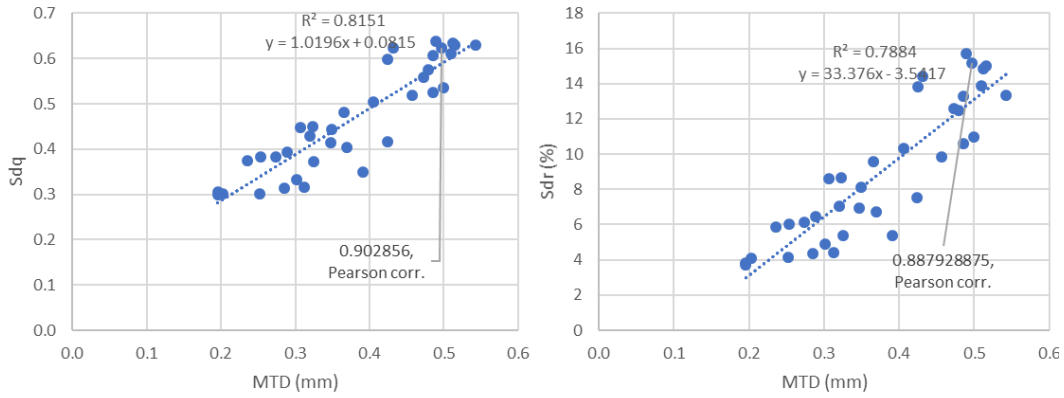

a) b)

Figure 4.41 Correlation between MTD and a) Sdq b) Sdr

Figure 4.42a, b, and c show the relationships between the three functional volume parameters (Vv, Vmc, and Vvc) and mean texture depth (MTD).

All three variables had strong correlations with MTD, proving their accuracy as MTD predictors. The potential causes for these high correlations can be discussed based on the definitions of the parameters and their connections to the MTD.

In direct relation to the porosity of the pavement surface, void volume (Vv) denotes the region of space bound by the surface texture. Because more space is available for

the sand particles to occupy during the sand patch test, a higher void volume would typically produce a larger MTD.

Vmc (Core Material Volume) represents the volume of material that makes up the texture between the heights corresponding to the material ratio values of "p" and "q." The amount of material in the pavement surface between the designated heights also increases as the core material volume increases, which may have a direct impact on the MTD.

The core void volume, or Vvc, is a representation of the volume of space bound by a texture at heights determined by the values of "p" and "q" in the material ratio. Similar to Vv, Vvc is also influenced by pavement porosity, and a higher core void volume typically translates into a higher MTD.

The fact that all three parameters are connected and represent different aspects of the pavement surface texture can be observed in the high correlations (R-squared and Pearson corr.) between the Vv-MTD, Vmc-MTD, and Vvc-MTD. Strong correlations between these parameters and the MTD suggest that the functional volume parameters, which represent the characteristics of the surface texture, are accurate predictors of the depth of the macrotexture, as determined by the sand patch method.

In conclusion, the strong correlations between the functional volume parameters and MTD can be attributed to their dependence on the pavement's surface porosity and texture.

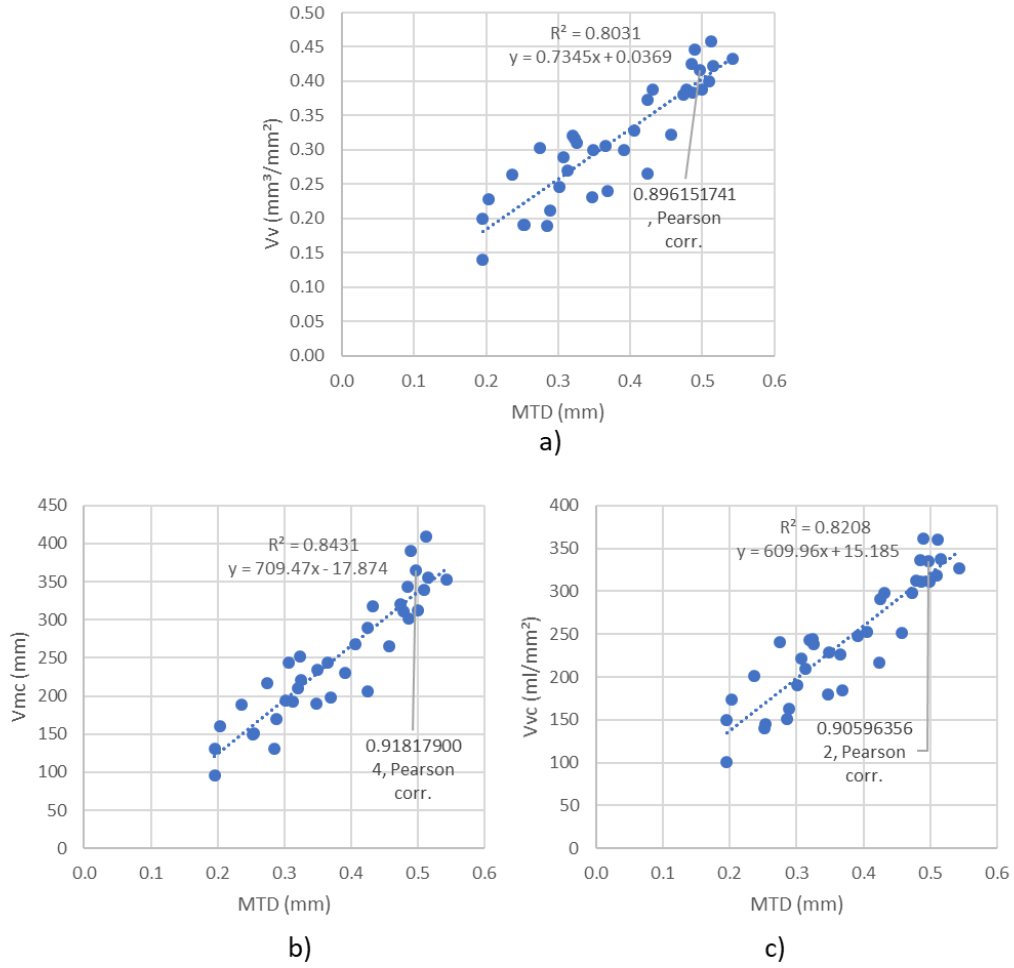

Figure 4.42 Correlation between MTD and a) Vv b) Vmc c) Vvc

The Five-point Peak Height (S5p) and Mean Texture Depth (MTD) showed a strong positive correlation with an R-squared value of 0.842 and a Pearson correlation value of 0.918 (Figure 4.43a).

The fact that S5p and MTD both deal with pavement surface texture and macrotexture is a potential reason for this high correlation. While the MTD assesses the depth of the surface texture, S5p measures the average height of the five highest peaks, which reflects the surface roughness. As S5p increases, implying a rougher surface, the MTD also tends to increase because of the greater texture depth. Another explanation is that the presence of larger peaks (S5p) on the surface might affect the outcomes of sand patch tests, which would then affect the MTD. The measured

diameter and calculated MTD can both increase with larger peaks because the sand will spread over a larger area.

The peak Density (Spd) and volume difference, extra sand measured during the sand patch test, were negatively correlated with each other in a moderately strong manner, as shown by the R-squared value of 0.704 and Pearson correlation value of -0.839 (Figure 4.43b). The Volume difference tended to decrease as Spd increased.

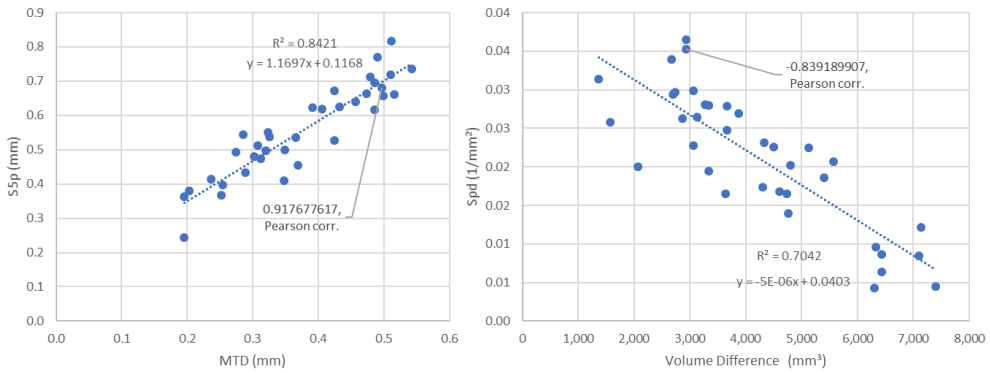

a) b)

Figure 4.43 Correlation between a) S5p and MTD b) Spd and Volume Difference

In conclusion, the shared relationship between the parameters' high correlation values and pavement surface texture and macrotexture can be used to explain the parameters' high correlation values, especially for the S5p-MTD and Spd-Volume difference. The lack of a significant direct correlation between Spd and MTD is explained by the indirect relationship between the two variables, which is mediated by volume difference.

4.2.3 Summary of the chapter

As a summary, the measured macrotexture properties of the RCC samples are directly corrected with the height, hybrid, volume, and feature parameters determined utilizing the proposed photogrammetric-based imaging method and experimental method.

In Table 4.6, a significant effect of the sources on the evaluated parameters is presented. Considering the obtained resolution of 0.003 mm, a correlation between the roughness parameters and the MTD was observed. However, no correlations were found with the BPN values, indicating that the resolution was not small enough to detect any correlation between them.

Table 4.6 ANOVA results of all the measured parameters

		Source												
		CD	Dmax	W(%)	GN	CD*Dmax	CD*W(%)	CD*GN	Dmax*W(%)	Dmax*GN	W(%)*GN	CD* Dmax* W(%)	Dmax* W(%) *GN	CD* Dmax *W(%) *GN
Height Parameters	Sq	+		+			+							
	Sa	+	+	+			+							
	Ssk	+	+			+			+					
	Sku	+	+			+			+	+				
Spatial Parameters	Sal	+		+					+			+		
	Str	+			+	+			+					
Hybrid Parameters	Sdq	+		+	+	+	+		+		+			
	Sdr	+	+	+	+		+		+		+			
Functional Volume Parameters	Vv	+		+										
	Vvv	+		+			+							
	Vvc	+		+										
	Vm	+												
	Vmp	+												
	Vmc	+	+	+										
	p-value													
	0.00-0.01	Strong evidence against the null hypothesis.												
	0.01-0.02	Strong evidence against the null hypothesis.												
	0.02-0.03	Moderate evidence against the null hypothesis.												
	0.03-0.04	Weak to moderate evidence against the null hypothesis.												
	0.04-0.05	Weak evidence against the null hypothesis.												

Table 4.7 ANOVA results of all the measured parameters (continued)

		Source												
		CD	Dmax	W(%)	GN	CD*Dmax	CD*W(%)	CD*GN	Dmax*W(%)	Dmax*GN	W(%)*GN	CD* Dmax* W(%)	Dmax* W(%) *GN	CD* Dmax *W(%) *GN
Feature Parameters	Spd	+	+											
	Spc													+
	S5p	+	+											
	S5v	+	+	+			+							
	S10z	+	+	+			+							
	Sda		+				+	+				+		
	Sha			+										
	Sdv	+	+				+	+						
	Shv	+	+											
BPN	Dry				+				+				+	
	Wet		+		+		+		+			+		+
MTD		+	+	+	+	+	+		+				+	

	p-value	
	0.00-0.01	Strong evidence against the null hypothesis.
	0.01-0.02	Strong evidence against the null hypothesis.
	0.02-0.03	Moderate evidence against the null hypothesis.
	0.03-0.04	Weak to moderate evidence against the null hypothesis.
	0.04-0.05	Weak evidence against the null hypothesis.

CHAPTER 5

CONCLUSIONS AND RECOMMENDATIONS

This chapter presents a summary of the principal outcomes derived from the assessment of diverse RCC mixture designs and an investigation of the impact of RCC mixing parameters on macrotexture and microtexture characteristics. The chapter stated the various constraints encountered during the study and provided suggestions for minimizing these challenges in subsequent research. Through the recognition of these constraints and the integration of recommended enhancements, the objective of this chapter is to facilitate the development of more resilient and comprehensive applications in the field of pavement engineering. This will ultimately augment the understanding of the intricate interdependence between the surface texture parameters and RCC mix design parameters.

5.1 Summary of Findings

In this study, 12 different mixes with two different cement dosages (200-400 kg/m3), two different aggregate gradations (Dmax 12-19 mm), and three different water contents (4%-5%-6%) were compacted with a Superpave Gyratory Compactor (SGC) at three different gyration numbers: 50, 60, and 75. Then the macro- and micro-surface properties of RCC pavements were assessed not only by the widely accepted standard techniques but also by using a novel 3D photogrammetry method that was developed. The standard techniques include the British pendulum test which was used to determine the microscale slip potential, and the sand patch test which was used to ascertain the pavement surface depth of the samples produced. The effects of the mixing parameters on the RCC surface texture were also studied by

conducting one-factor ANOVA analyses on the results obtained for the experimental data.

The findings obtained from experimental data (BPT and Sand Patch Test) can be briefly summarized as follows;

- For the 200- and 400-dose mixtures, the average surface depth was 0.46 mm and 0.29 mm, respectively. The 200-dose mixes were very close to the specification limits, even though these values were lower than those obtained for the Highways Technical Specification for Concrete Road, emphasizing the significance of traffic safety for RCC pavements used on urban and rural roads.
- The macrotexture of the RCC pavements was significantly affected by the addition of more cement to the mixes, which led to a significant reduction in the average surface depth. On the other hand, for high-dosage mixes, a larger aggregate size resulted in a lower average surface depth.
- The characteristics of the pavement surface are heavily influenced by the interaction between the water content and aggregate size. For both the smaller and larger aggregates, a water content of 5% resulted in the best macrotexture and skid resistance results, providing essential data for pavement designers.
- All the RCC mixtures had BPN values of 70 on the dry surface, 64 for approximately 200 dosages, and 62 for approximately 400 dosages on the wet surface. These BPN values highlight the need for additional measures, such as speed-limit reduction, to ensure road safety by emphasizing the high risk of slipping on RCC pavements.
- Wet surface measurements were used to determine the effect of cement dosage on BPN values. A decline in BPN was found to correlate with an increase in dosage.
- Road safety and performance can be further improved by monitoring and controlling environmental factors during pavement design and construction,

because the characteristics of the pavement surface can change depending on the environment, such as wet or dry surfaces.

- The number of gyrations significantly influenced the MTD and BPN values. By balancing the surface roughness and smoothness during pavement manufacturing, the gyration number can be optimized to enhance skid resistance and overall road safety.

Although there is great potential for the use of RCC pavements, it is necessary to determine and control their surface properties, especially in terms of road safety, and to take additional measures in practice when necessary. As can be seen from the findings summarized above, the mixing parameters (cement dosage, water ratio, and aggregate size) significantly affected the RCC surface properties. Therefore, road safety, in addition to pavement strength and durability, should be considered when selecting RCC mixture parameters.

A new 3D photogrammetry technique was developed to evaluate the obtained surfaces. ContextCapture was used to process photographs of the textures of the study samples. It was then edited using MeshLab. Python programming and DigitalSurf were used to analyze the obtained surfaces. In ISO 25178-2, the International Standard for Specification and Measurement of 3D Surface Texture defines more than 60 roughness properties. The parameters for each sample surface were then computed.

The following briefly summarizes the main conclusions drawn from the 3D photogrammetry method and the analysis of the surface parameters and macrotexture:

- Height Parameters: Greater cement dosage and water optimization at 5% resulted in smoother surface textures, with larger aggregate sizes resulting in more uniform mixtures. Mean Texture Depth (MTD), Arithmetical Mean Height (Sa), and Root Mean Square Height (Sq) were significantly correlated.

- Spatial Parameters: Adding more cement resulted in a surface texture that was longer, more uniform, and more anisotropic. The autocorrelation length was significantly influenced by water content, whereas the texture aspect ratio was influenced by the gyration number.
- Hybrid Parameters: Changes in the cement dosage and water content had an impact on the Sdq and Sdr values, with the ideal water content being essential for obtaining the desired surface characteristics. The Sdr-MTD and Sdq-MTD relationships were found to have high correlation values.
- Functional Volume Parameters: Parameters governing the void and material volume were influenced by intricate interactions between the cement dosage, water content, and aggregate size. The functional volume parameters (Vv, Vmc, and Vvc) and MTD were strongly correlated.
- Feature Parameters: Areal feature parameters were significantly affected by cement dosage, aggregate size, water content, and gyration number. S5p and MTD showed a strong positive correlation, while Spd and volume difference showed a moderately strong negative correlation.

To ensure traffic safety and to implement additional measures when necessary, it is critical to evaluate and regulate the properties of RCC pavement surfaces. The significant impact of mixing parameters on the surface properties of RCC is highlighted by analyzing the relationships between surface parameters and macrotexture, such as cement dosage, water content, and aggregate size.

5.2 Limitations and Recommendations

In this study, even though useful insights into the effects of mixing parameters on the surface characteristics of RCC pavements were offered, some limitations need to be acknowledged. One drawback is the compaction process utilized. It is well known that the laboratory-based SGC method accurately reflects the compaction conditions encountered in the field when the mechanical properties of the material are

considered. It is possible that this technique may not accurately simulate the surface texture conditions.

Moreover, the study did not consider other elements that might affect pavement performance, such as traffic loads, environmental conditions, or construction methods. By examining the long-term performance of RCC pavements, more precise and thorough data on RCC pavement surface characteristics may be produced.

REFERENCES

Aavik, A., Kaal, T., & Jentson, M. (2013, August). Use of pavement surface texture characteristics measurement results in Estonia. In *The XXVIII International Baltic Road Conference. Vilnius, Lithuania*.

Abou El-Atta, U. B. (1991). *Surface roughness assessment in three-dimensional machined surfaces for some manufacturing operations* (Doctoral dissertation, M. Sc. Thesis, Industrial Production Engineering Department, University of Mansoura, Egypt).

Adresi, M., & Lacidogna, G. (2021). Investigating the Micro/Macro-Texture Performance of Roller-Compacted Concrete Pavement under Simulated Traffic Abrasion. *Applied Sciences*, *11*(12), 5704.

Aghaeipour, A., & Madhkhan, M. (2020). Mechanical properties and durability of roller compacted concrete pavement (RCCP)–a review. *Road Materials and Pavement Design*, *21*(7), 1775-1798.

Ahammed, M. A., & Tighe, S. L. (2008). Concrete pavement surface textures and multivariables frictional performance analysis: a North American case study. *Canadian Journal of Civil Engineering*, *35*(7), 727-738.

American Society of Civil Engineers. (n.d.). First concrete pavement. ASCE. Retrieved from https://www.asce.org/about-civil-engineering/history-and-heritage/historic-landmarks/first-concrete-pavement

American Society of Mechanical Engineers. (2002). ANSI/ASME B46.1-2002: Surface Texture (Surface Roughness, Waviness and Lay). ASME.

ASTM, A. (2015). E965-15 Standard Test Method for Measuring Pavement Macrotexture Depth Using a Volumetric Technique. *Annual book of American society for testing materials. ASTM standards*.

ASTM, E. (1911). Standard Test Method for Measuring Surface Frictional Properties Using the Dynamic Friction Tester.

ASTM, E. (1996). 867 "Standard Terminology Relation to Traveled Surface Characteristics". *Defines friction resistance as "the ability of the traveled surface to prevent the loss of traction. US*.

ASTM, E. (2005). 2380. *Standard test method for measuring pavement texture drainage using an outflow meter, West Conshohocken (PA) ASTM International*.

Baddeley, A., Rubak, E., & Turner, R. (2015). *Spatial point patterns: methodology and applications with R*. CRC press.

Bentley System, 2019. ContextCapture User Guide

Bitelli, G., Simone, A., Girardi, F., & Lantieri, C. (2012). Laser scanning on road pavements: A new approach for characterizing surface texture. *Sensors*, *12*(7), 9110-9128.

BPI Consulting, LLC. (2023). BPI Consulting, LLC. https://www.spcforexcel.com/

Chamberlin, W. P., & Amsler, D. E. (1982). *Measuring surface texture by the sand-patch method* (No. STP 763).

Chappard, D., Degasne, I., Hure, G., Legrand, E., Audran, M., & Basle, M. F. (2003). Image analysis measurements of roughness by texture and fractal analysis correlate with contact profilometry. *Biomaterials*, *24*(8), 1399-1407.

Chhorn, C., Hong, S. J., & Lee, S. W. (2017). A study on performance of roller-compacted concrete for pavement. *Construction and Building Materials*, *153*, 535-543.

Cignoni, P., Callieri, M., Corsini, M., Dellepiane, M., Ganovelli, F., & Ranzuglia, G. (2008, July). Meshlab: an open-source mesh processing tool. In *Eurographics Italian chapter conference* (Vol. 2008, pp. 129-136).

Corrosionpedia. (n.d.). Laser profilometry. Retrieved from https://www.corrosionpedia.com/definition/4972/laser-profilometry#:~:text=What%20Does%20Laser%20Profilometry%20Mean,laser%20profilometer%20or%20laser%20mapper.

De Los Santos, L., & Gasca, C. (1978). Organization, Planning and Administration Of Road Maintenance. *Informacion Tecnica De Carreteras*.

Diggle, P. J. (2013). *Statistical analysis of spatial and spatio-temporal point patterns*. CRC press.

DONDI, G. D., SIMONE, A. S., LANTIERI, C. L., & VIGNALI, V. V. (2010). Context sensitive design and safety review of bike lanes.

Doty, R. N. (1975). *Study of the sand patch and outflow meter methods of pavement surface texture measurement* (No. Conf Paper). ASTM International.

Elunai, R., Chandran, V., & Mabukwa, P. (2010). Digital image processing techniques for pavement macro-texture analysis. In *Proceedings of the 24th ARRB Conference: Building on 50 Years of Road and Transport Research* (pp. 1-5). ARRB Group Ltd.

Flintsch, G. W., De León, E., McGhee, K. K., & AI-Qadi, I. L. (2003). Pavement surface macrotexture measurement and applications. *Transportation research record*, *1860*(1), 168-177.

GD&T Basics. (n.d.). What is a profilometer? https://www.gdandtbasics.com/what-is-a-profilometer/

Gierasimiuk, P., Wasilewska, M., & Gardziejczyk, W. (2021). A comparative study on skid resistance of concrete pavements differing in texturing technique. *Materials*, *14*(1), 178.

Guo, Z., Yang, Q., & Liu, B. (2009). Mixture design of pavement surface course considering the performance of skid resistance and disaster proof in road tunnels. *Journal of Materials in Civil Engineering*, *21*(4), 186-190.

Hall, J. W., Smith, K. L., Titus-Glover, L., Wambold, J. C., Yager, T. J., & Rado, Z. (2009). Guide for pavement friction. *Final Report for NCHRP Project*, *1*, 43.

Harrington, D., Abdo, F., Ceylan, H., Adaska, W., Hazaree, C., & Bektas, F. (2010). Guide for roller-compacted concrete pavements.

He, B., Ding, S., & Shi, Z. (2021). A comparison between profile and areal surface roughness parameters. *Metrology and Measurement Systems*, *28*(3), 413-438.

Hiti, M., & Ducman, V. (2014). Analysis of the slider force calibration procedure for the British Pendulum Skid Resistance Tester. *Measurement Science and Technology*, *25*(2), 025013.

Illian, J., Penttinen, A., Stoyan, H., & Stoyan, D. (2008). *Statistical analysis and modelling of spatial point patterns*. John Wiley & Sons.

International Organization for Standardization. (1996). ISO 13565-2:1996 - Geometrical product specifications (GPS) – Surface texture: Profile method; Surfaces having stratified functional properties – Part 2: Height characterization using the linear material ratio curve. ISO.

International Organization for Standardization. (1997). ISO 4287:1997 - Geometrical product specifications (GPS) – Surface texture: Profile method – Terms, definitions and surface texture parameters. ISO.

International Organization for Standardization. (2002). ISO 1302:2002 - Geometrical product specifications (GPS) - Indication of surface texture in technical product documentation. ISO.

International Organization for Standardization. (2009). ISO 25178-2:2009 - Geometrical product specifications (GPS) – Surface texture: Areal – Part 2: Terms, definitions and surface texture parameters. ISO.

International Organization for Standardization. (2009). ISO 25178-3:2009 - Geometrical product specifications (GPS) – Surface texture: Areal – Part 3: Specification operators. ISO.

International Organization for Standardization. (2012). ISO 25178-2:2012 - Geometrical product specifications (GPS) – Surface texture: Areal – Part 2: Terms, definitions and surface texture parameters. ISO.

Jalalkamali, R., Dibaee, M. M., Jalal Kamali, M. H., & Hassani, A. (2021). An investigation of the relationship among skid resistance, mean texture depth and abrasion resistance for different macrotextures of concrete pavements. *Civil Engineering Infrastructures Journal*, *54*(2), 301-317.

KAÇMAZ, B., TOPAL, A., ŞENGÖZ, B., & TANYEL, S. (2015). Farklı tip esnek kaplamaların yol yüzey özelliklerinin arazi ölçümleriyle değerlendirilmesi. *Teknik Dergi*, *26*(3), 7115-7137.

Keyence. (n.d.). Non-contact surface roughness measurement. Keyence Corporation. Retrieved from https://www.keyence.com/ss/products/microscope/roughness/equipment/non-contact-instruments.jsp

Keyence. (n.d.). Spd (density of peaks) - Surface analysis glossary. Keyence. Retrieved from https://www.keyence.com/ss/products/microscope/roughness/surface/spd-density-of-peaks.jsp

Kuemmel, D. A., Sonntag, R. C., Jaeckel, J. R., Crovetti, J. A., Becker, Y. Z., & Satanovsky, A. (2000). Using a road surface analyzer to explain noise characteristics of Portland cement concrete pavement surface texture. *Transportation research record*, *1716*(1), 144-153.

Lachambre, S., Lagarde, S., & Jover, C. (2017). Photogrammetry workflow. *Rapport Technique, Unity*.

Leach, R. (Ed.). (2013). *Characterisation of areal surface texture*. Springer Science & Business Media.

Mahyar, M. (2021). Texture Characterization Of Roller Compacted Concrete Pavements By An In-House Developed Optical Surface Profiler.

Mataei, B., Zakeri, H., Zahedi, M., & Nejad, F. M. (2016). Pavement friction and skid resistance measurement methods: A literature review. *Open Journal of Civil Engineering*, *6*(04), 537.

Michmet. (n.d.). Spatial glossary. Retrieved from https://michmet.com/glossary-term-category/spatial/

Mikhail, E. M., Bethel, J. S., & McGlone, J. C. (2001). *Introduction to modern photogrammetry*. John Wiley & Sons.

Miller, T., Swiertz, D., Tashman, L., Tabatabaee, N., & Bahia, H. U. (2012). Characterization of asphalt pavement surface texture. *Transportation research record*, *2295*(1), 19-26.

Pancewicz, T., & Mruk, I. (1996). Holographic contouring for determination of three-dimensional description of surface roughness. *Wear*, *199*(1), 127-131.

Pawlus, P., Graboń, W., & Reizer, R. (2013). Variation of areal parameters on machined surfaces. In *11th International Symposium on Measurement and Quality Control*.

Ripley, B. D. (1976). The second-order analysis of stationary point processes. *Journal of applied probability*, *13*(2), 255-266.

Rosén, B. G. (1993). Representation of three-dimensional surface topography in CAD-systems and image-processing software. *International Journal of Machine Tools and Manufacture*, *33*(3), 307-320.

Santero, N. J., Masanet, E., & Horvath, A. (2011). Life-cycle assessment of pavements Part II: Filling the research gaps. *Resources, Conservation and Recycling*, *55*(9-10), 810-818.

Sarsam, S. I., & Ali, A. M. (2015). Assessing pavement surface macrotexture using sand patch test and close range photogrammetric approaches. *Int. J. Mater. Chem. Physics, Public Sci. Fram. Am. Inst. Sci*, *1*(2), 124-131.

Schenk, T. (2005). Introduction to photogrammetry. *The Ohio State University, Columbus*, *106*, 2005.

Seewig, J. (2013). Areal filtering methods. *Characterisation of Areal Surface Texture*, 67-106.

Sengoz, B., Topal, A., & Tanyel, S. (2012). Comparison of pavement surface texture determination by sand patch test and 3D laser scanning. *Periodica Polytechnica Civil Engineering*, *56*(1), 73-78.

Şengün, E. (2019). Effects of mixture design parameters and compaction methods on the properties of roller compacted concrete pavements.

Shabani, R., Şengün, E., Öztürk, H. I., & Yaman, İ. (2021). Silindirle Sıkıştırılmış Beton (SSB) Kaplamaların Yüzey Özelliklerine Karışım Parametrelerinin Etkisi. *Teknik Dergi*, *32*(5), 11153-11174.

Snyder, M. B. (2019). *Concrete Pavement Texturing [techbrief]* (No. FHWA-HIF-17-011). United States. Federal Highway Administration. Office of Preconstruction, Construction, and Pavements.

SPC for Excel. (n.d.). SPC for Excel - Software for Quality Control and Statistical Process Control. Retrieved April 18, 2023, from http://www.spcforexcel.com/

Stout, K. J. (1997). Surface roughness measurement by contact profilometry. Measurement Science and Technology, 8(6), 981-995.

Tian, Y., Wang, J., Peng, Z., & Jiang, X. (2011). Numerical analysis of cartilage surfaces for osteoarthritis diagnosis using field and feature parameters. *Wear*, *271*(9-10), 2370-2378.

Topličić-Ćurčić, G., Grdić, D., Ristić, N., & Grdić, Z. (2015). Properties, materials and durability of rolled compacted concrete for pavements. *Zaštita materijala*, *56*(3), 345-353.

Van Dam, T. J., & Taylor, P. (2011). 5 Concrete Pavements. *Green Building with Concrete: Sustainable Design and Construction*, 109.

Van Dam, T., Taylor, P., Fick, G., Gress, D., VanGeem, M., & Lorenz, E. (2011). Sustainable concrete pavements: a manual of practice.

Wallman, C. G., & Åström, H. (2001). Friction measurement methods and the correlation between road friction and traffic safety: A literature review.

Wang, J., Jiang, X., Gurdak, E., Scott, P., Leach, R., Tomlins, P., & Blunt, L. (2011). Numerical characterisation of biomedical titanium surface texture using novel feature parameters. *Wear*, *271*(7-8), 1059-1065.

Wei, D., Li, B., Zhang, Z., Han, F., Zhang, X., Zhang, M., ... & Wang, Q. (2018). Influence of surface texture characteristics on the noise in grooving concrete pavement. *Applied Sciences*, *8*(11), 2141.

Yaacob, H., Hassan, N. A., Hainin, M. R., & Rosli, M. F. (2014). Comparison of sand patch test and multi laser profiler in pavement surface measurement. *Jurnal Teknologi*, *70*(4).

Yıldız, K. (2018). Şehir içi asfalt kaplamaların kayma potansiyelinin değerlendirilmesi-bir durum çalışması. *Politeknik Dergisi*, *21*(2), 513-518.

Zollinger, D. G. (2016). *Roller-Compacted Concrete Pavement: [techbrief]* (No. FHWA-HIF-16-003). United States. Federal Highway Administration.